

# **Research Plan for Spin Physics at RHIC**

## **Abstract**

In this report we present the research plan for the RHIC spin program. The report covers 1) the science of the RHIC spin program in a world-wide context; 2) the collider performance requirements for the RHIC spin program; 3) the detector upgrades required, including timelines; 4) time evolution of the spin program.

# 1 Executive Summary

An action item from the June 30-July 1, 2004 DOE Office of Nuclear Physics Science and Technology Review of the Brookhaven National Laboratory (BNL) Relativistic Heavy Ion Collider (RHIC) written Report, dated September 13, 2004, was that "*BNL should prepare a document that articulates its research plan for the RHIC spin physics program. A copy should be submitted to DOE by January 31, 2005.*" This document is submitted to the DOE Office of Nuclear Physics on behalf of the Laboratory, in response to that action item.

We provide here a plan that addresses: 1) the science of the RHIC spin program in a worldwide context; 2) the collider performance requirements for the RHIC spin program; 3) the detector upgrades required, including timelines; 4) time evolution of the spin program. The RHIC Spin Plan Group was charged to formulate the plan by Thomas Kirk, BNL Associate Director for High Energy and Nuclear Physics.

The importance of the study of nucleon spin to nuclear physics and its co-evolution with heavy ion physics in the RHIC facility is discussed in the first section of this report. Here, we note that, of all the basic properties of the nucleons (protons and neutrons), the intrinsic spin angular momentum aspects are least well known. In particular, the contribution of the gluons to the net spin of the nucleons, as well as the role of orbital angular momentum among the quarks and gluons is almost totally unmeasured. Our plan will argue that the RHIC facility will provide the most comprehensive and precise measurements possible in the present and foreseen worldwide program of spin physics and will be able to accomplish this in a proposed program of 10 weeks (on average) of data taking per year through the year 2012. This scenario is labeled "the technically limited BNL spin plan". If budgetary constraints on the spin program evolution are imposed, the program will be stretched out accordingly and the results will be available later and at higher total cost.

The RHIC 100-250 GeV colliding beams facility of highly polarized protons, with arbitrary spin orientation at two interaction points around the RHIC ring (at the PHENIX and STAR detectors), is unique in the world and likely to remain so for the foreseeable future. The maximum polarization in each beam is expected to rise from 45% to 70% in the 2005-2006 time frame. Exploiting this powerful accelerator and experimental detector capability, together with a steadily improving average luminosity at the interaction points, a unique and important program of spin physics measurements can be completed over the time period 2005-2012. Determination of the gluon's contribution to the proton spin will be an early achievement of the program, followed by the direct measurement of the quark and anti-quark contributions to the proton spin, sorted by quark flavor. These results will be achieved in a later phase of the spin physics program via W-boson production measurements. In the same time frame, the power of lattice gauge physics, carried out on BNL supercomputers, is expected to be able to relate the spin results to the predictions of Quantum Chromo-Dynamics, now believed to be the fundamental theory of the strong nuclear interactions.

We summarize our findings on the four areas in the charge:

**Science:** Gluon polarization will be measured at RHIC using several independent methods:  $\pi^0$ , jet, direct  $\gamma$  and  $\gamma$ +jet, and heavy quark production. Results from the different methods will overlap to allow us to test our understanding of the processes involved and expand the range

of momentum fraction for the measurements. We want to learn both the average contribution to the proton spin of the gluons as well as a detailed map. We use first the higher cross section processes,  $\pi^0$  and jet production and, as we reach higher luminosity and polarization, the clean but rarer process of direct  $\gamma$  production. We plan to emphasize these measurements for  $\sqrt{s}=200$  GeV collisions from 2005-2008. At that time, we expect to have reached a precision that can clearly distinguish between zero gluon polarization and a minimal ("standard") gluon polarization. A large gluon polarization, consistent with the gluon carrying most of the spin of the proton, would be precisely measured. In this period we will also pursue the question of the transverse spin structure. Gluons, massless spin 1 particles, cannot contribute to the transverse spin. Large transverse spin asymmetries have been seen for deeply inelastic scattering (DIS) and now for RHIC, so this topic is also a potential window into a new understanding of the structure of the nucleons.

Production of W bosons, the carrier of the weak interaction, has an inherent handedness. At RHIC we plan to use this "parity violation" signal to directly measure the polarization of the quark and anti-quark that form the W boson. To do this we will run at the top RHIC energy,  $\sqrt{s}=500$  GeV. This will provide the first direct measurements of anti-quark polarization in the proton, with excellent sensitivity. We plan to begin these measurements in 2009. The W measurements will require the prior completion of certain detector improvements for both PHENIX and STAR.

The RHIC spin results will provide precise measurements of gluon and anti-quark polarization. With these results we will also understand the role of the remaining contributor to the proton spin, orbital angular momentum. We will have also explored our understanding of the interconnected results from the different RHIC spin probes, and from the DIS measurements. The sensitivity at RHIC for gluon polarization is shown in Figure 1, where we also include the sensitivity for the ongoing DIS experiment at CERN, which measures gluon polarization by the production of hadrons. From the figure, we see that RHIC will provide precise results over a large range in momentum fraction, characterizing the gluon contribution to the proton spin.

Figure 1:  $\Delta G/G(x)$  vs.  $\log x$  with a model showing the  $x$  range for various RHIC processes with expected uncertainties; 200 and 500 GeV data are shown with experimental uncertainties in RHIC and COMPASS for  $Q^2 \geq 1$ .

The sensitivity of RHIC for anti-quark polarization is shown in Figure 2. We will measure the  $u$  and  $d$  quark polarizations to about 0.01, as well as  $\bar{u}$  and  $\bar{d}$  quark polarizations. The measurement is direct and very clean, using parity violating production of W bosons. DIS measurements also yield the anti-quark polarizations. The method has the disadvantage of theoretical uncertainties in modeling the fragmentation and the advantage that the method is accessible today. The RHIC and DIS methods probe the proton at very different distances, ( $Q^2$  range) where RHIC corresponds to X Fermi and DIS to Y Fermi, compared to the proton radius of 1 Fermi. The theory of QCD prescribes how to connect the results from different probing distances—the description of unpolarized DIS results over a very large distance range is one of the major successes of QCD. Both the anti-quark and the gluon results from RHIC and DIS test the QCD assumption of universality, namely that the physics for both proton and lepton processes can be described with the same underlying quark, anti-quark, and gluon distributions.

Figure 2:  $\Delta q/q(x)$  vs.  $\log x$  with a model for  $u$ ,  $d$ ,  $\bar{u}$  and  $\bar{d}$ ; with RHIC and DIS expected

uncertainties.

We emphasize that the planned RHIC program will make major contributions to our understanding of matter. Our results will complement the DIS measurements, completed and planned. We include in our report expectations from a next stage of DIS-colliding polarized electrons with polarized protons and neutrons which probes still further into the structure of matter. As we develop theoretical tools to apply QCD to understand this structure, these spin results will provide a deep test of our understanding of the fundamental building blocks of matter.

**Collider Performance Requirements:** The spin physics program requires RHIC beams with high polarization, and high integrated luminosity. For the sensitivities assumed above, we have used  $P=0.7$  and luminosity  $300 \text{ pb}^{-1}$  at  $\sqrt{s}=200 \text{ GeV}$  and  $800 \text{ pb}^{-1}$  at  $\sqrt{s}=500 \text{ GeV}$ . (Note that this refers to "delivered" luminosity, while the sensitivities in this report use the luminosity expected to be recorded by each experiment.)

The polarization level is presently  $P=0.45$  and is expected to reach 70% polarization by 2006. This improvement is expected using new Siberian Snake Magnets installed in the AGS in 2004 and 2005. The average luminosity at store must be increased by a factor 15 to reach the integrated luminosity goals for three years of running at 10 physics weeks per year. To achieve this level of performance will require completion of the planned vacuum improvements in RHIC, expected for 2007. The luminosity increase then comes from reaching a bunch intensity of  $2 \times 10^{11}$ . A limit will be caused by beam-beam interactions that change and broaden the betatron tune of the machine, moving part of the beam into a beam resonance region where beam is then lost. Work in 2004 discovered a new betatron tune for RHIC that greatly improves losses from the beam-beam interaction. RHIC at our luminosity goal will operate near or above previously achieved beam-beam parameters, and will be the first hadron collider in the strong-strong beam-beam regime.

Reaching these goals requires "learning by doing". We plan to study limits and develop approaches to improve the polarization and luminosity during physics runs by including beam studies for one shift per day. It is also important that a sustained period of running and development be followed, if possible each year. It is this approach that has led to the major improvements for heavy ion luminosity and to our improvements to this date in polarization and proton luminosity.

**Experimental Detector Capabilities:** The PHENIX and STAR detectors are complete for the gluon polarization program. Improvements to both detectors are required to carry out the W physics program. Both experiments also plan upgrades that benefit both the heavy ion and spin programs, significantly extending the range of physics probes for spin.

*W Program Upgrades–PHENIX* The present online event selection for muons, the channel used for W physics, will need to be improved for the W luminosity. New resistive plate chambers (RPC) are being proposed to provide the tighter event selection, along with electronics changes to the muon tracking readout. The RPC proposal was submitted to NSF in January 2005, with a cost estimate of \$1.8M. The tracking readout proposal has been submitted to the Japan Society for the Physical Sciences, with a cost of \$1.0M. The planned timeline is to complete both for the 2008 run.

*W Program Upgrades–STAR* New tracking for forward electrons from W decay is necessary for the W program. It is planned to propose this upgrade in 2006 to DOE, with an estimated cost of \$5M, although research and development on the technology (GEM detectors) is proceeding

and the cost estimate is rough at this time. The forward tracking detector is to be completed for the 2010 run, with part of the detector in place earlier.

*Heavy-Ion/Spin Program Upgrades* PHENIX plans a barrel micro vertex detector that provides access to heavy quark states and to jet physics based on tracking. The heavy quark data will add a new probe for gluon polarization at lower momentum fraction (shown on Fig. 1). The jet information will be used in correlated ( $\gamma$ +jet) measurements, which better determine the sub-process kinematics for gluon polarization measurement. A second upgrade being planned is to change the brass "nose cones", used as a filter for the muon arms, to active calorimeters that will measure photons,  $\pi^0$  and jet energy. The nose cone calorimeters would provide a larger momentum fraction range for the gluon polarization measurements. Both are important upgrades for the heavy ion physics program. The vertex detector is planned for the 2008 run, and the nose cone calorimeter proposal is being developed now.

STAR has proposed expanded forward calorimeters to NSF in January 2005. The calorimeters will measure the gluon density for proton-gold collisions and will also provide very significant spin measurements. With the calorimeters, forward  $\pi^0$ , direct  $\gamma$ , and jet events can be observed, yielding sensitivity to gluon polarization at lower momentum fraction, as shown on Fig. 1. A second upgrade driven by the heavy ion program, a barrel inner tracker, will give access to heavy quark measurements for spin. The forward calorimeters are to be in place for the 2007 run. The barrel inner tracker is to be completed for the 2010 run.

**Time Evolution:** In order to indicate the pace of spin program evolution under different budget assumptions, we provide two examples with an average of 10 weeks and 5 weeks of spin physics data taking per year. We note that the actual running plan will continue to be developed, year-by-year, from the experiment beam-use proposals. The time evolution cases provided here indicate paths for reaching the spin program's strategic goals under two example scenarios.

We show in Fig. 3, the impact of 10 and 5 averaged spin physics weeks per year. The "technically-driven schedule" represents the luminosity used for the sensitivities shown in the figures above. With 10 weeks per year, we achieve the  $\sqrt{s}=200$  GeV target in 3 years, assuming that we successfully climb the accelerator learning curve to reach the target store luminosity. The 500 GeV running target is also expected to be achieved in 3 years (there is a natural luminosity improvement for 500 GeV of a factor of 2.5 over 200 GeV from the smaller cross section beams).

With 10 averaged spin physics weeks per year, technically driven, our proposed target sensitivities can be reached running at  $\sqrt{s}=200$  GeV from 2005-2008, and at  $\sqrt{s}=500$  GeV from 2009-2012. We have assumed that 2009 will be an engineering run for W physics (new detector systems and higher luminosity), with a full detector in place for PHENIX and a partial detector for STAR. 2010-2012 will provide full-functionality W physics runs at high luminosity for both detectors. This is the preferred scenario from BNL.

As can be seen in Fig. 3, running 5 averaged spin physics weeks per year (we have interpreted this as running 10 spin physics weeks every two years to reduce end effects), each program, 200 GeV and 500 GeV, takes more than 6 years. Under this scenario RHIC would run roughly 25% of the year and both the heavy ion and spin programs would be stretched a factor of greater than two in calendar time. We hope that such a slow and relatively inefficient program can be avoided.

Fig. 3: pp luminosity projections for 10 and 5 physics weeks per year ( $5=10/2$ ).

## 2 The science case for RHIC Spin

Spin is one of the most fundamental concepts in physics, deeply rooted in Poincaré invariance and hence in the structure of space-time itself. All elementary particles we know today carry spin, among them the particles that are subject to the strong interactions, the spin-1/2 quarks and the spin-1 gluons. Spin, therefore, plays a central role also in our theory of the strong interactions, *Quantum Chromodynamics (QCD)*, and to understand spin phenomena in QCD will help to understand QCD itself. To contribute to this understanding is the primary goal of the spin physics program at RHIC.

It is a remarkable property of QCD, known as *confinement*, that quarks and gluons are not seen in isolation, but only bound to singlet states of the strong “color” charge they carry. At the heart of investigating confinement in QCD is the study of the inner structure of strongly-interacting particles in nature that are composed of quarks and gluons. Among these, the proton and neutron are clearly special as they make up all nuclei and hence most of the visible mass in the universe. Their detailed study is therefore of fundamental interest. The proton and neutron also carry spin-1/2, which immediately brings the central role of spin in nucleon structure to the fore. It is worth recalling that the discovery of the fact that the proton has structure— and hence really the birth of strong interaction physics— was due to spin, through the measurement of a very unexpected “anomalous” magnetic moment of the proton by O. Stern and collaborators in 1933 [1]. Today, after decades of ever more detailed studies of nucleon structure, a prime question is how the proton spin-1/2 is composed of the average spins and orbital angular momenta of quarks and gluons inside the proton. Polarization has become an essential tool in the investigation of the strong interactions through nucleon structure.

Quarks were originally introduced simply based on symmetry considerations [2], in an attempt to bring order into the large array of strongly-interacting particles observed in experiment. In order to satisfy the Pauli exclusion principle for baryons such as the  $\Delta^{++}$  or the  $\Omega^-$  which are made up of three quarks of the same flavor, the spin-1/2 quarks had to carry a new quantum number [3], later termed “color”. A modern rendition of Rutherford’s experiment has shown us that quarks are real. This experiment is the deeply-inelastic scattering (DIS) of electrons (or, later, muons) off the nucleon, a program that was started in the late 1960’s at SLAC [4]. A high-energy electron interacts with the nucleon, via exchange of a highly virtual photon. For virtuality of  $\sqrt{Q^2} > 1$  GeV distances  $< 0.2$  fm are probed in the proton. The proton breaks up in the course of the interaction. The early DIS results compelled an interpretation as elastic scattering of the electron off pointlike, spin-1/2, constituents of the nucleon [5, 6], carrying fractional electric charge. These constituents, called “partons” were subsequently identified with the quarks. The existence of gluons was proved indirectly from a missing  $\sim 50\%$  contribution [7] to the proton momentum not accounted for by the quarks. Later on, direct evidence for gluons was found in three-”jet” production in electron-positron annihilation [8]. From observed angular distributions of the jets it became clear that gluons have spin one [9].

The so successful parton interpretation of DIS assumed that partons are practically free (i.e., non-interacting) on the short time scales set by the high virtuality of the exchanged photon. This

implied that the underlying theory of the strong interactions must actually be relatively weak on short time or, equivalently, distance scales [10]. In a groundbreaking development, Gross, Wilczek and Politzer showed in 1973 that the non-abelian theory “QCD” of quarks and gluons, which had just been developed a few months earlier [11], possessed this remarkable feature of “asymptotic freedom” [12], a discovery for which they were awarded the 2004 Nobel Prize for Physics. The interactions of partons at short distances, while weak in QCD, were then predicted to lead to visible effects in the experimentally measured DIS structure functions known as “scaling violations” [13]. These essentially describe the response of the partonic structure of the proton to the resolving power of the virtual photon, set by its virtuality  $Q^2$ . It has arguably been *the* triumph of QCD that the predicted scaling violations have been observed experimentally and verified with great precision. Deeply-inelastic scattering thus paved the way for our theory of the strong interactions, QCD.

Over the following two decades or so, studies of nucleon structure became ever more detailed and precise. Partly this was due to increased luminosities and energies of lepton machines, culminating in the HERA ep collider. Also, hadron colliders entered the scene. It was realized that, again thanks to asymptotic freedom, the partonic structure of the nucleon seen in DIS is universal in the sense that it can also be studied in very inelastic reactions in proton-proton scattering [14, 15, 16]. This offered the possibility to learn about other aspects of nucleon structure (and hence, QCD), for instance about its gluon content which is not primarily accessed in DIS. Being known with more precision, nucleon structure also became a tool in the search of new physics, the outstanding example perhaps being the discovery of the  $W^\pm$  and  $Z$  bosons at CERN’s Sp $\bar{p}$ S collider [17]. The Tevatron collider today and LHC in the near future are continuations of this theme.

A further milestone in the study of the nucleon was the advent of *polarized* electron beams in the early seventies [18]. This later on allowed to perform DIS measurements with *polarized* lepton beam and nucleon target [19], offering for the first time the possibility to study whether for example quarks and antiquarks have on average preferred spin directions inside a spin-polarized nucleon. The program of polarized DIS has been continuing ever since and has been an enormously successful branch of particle physics. Its single most important result is the finding that quark and antiquark spins provide very little – only about  $\sim 20\%$  – of the proton spin [20]. In parallel, starting from the mid 1970’s, there also was a very important line of research on polarization phenomena in hadron-hadron reactions in fixed-target kinematics. In particular, unexpectedly large single-transverse spin asymmetries were seen [21] which, as will be discussed later, may tell us about further fundamental spin-related properties of the nucleon, but have defied a complete understanding in QCD so far.

In the context of the exploration of nucleon structure achieved so far, it is clear that the RHIC spin program is the logical continuation. Very much in the spirit of the unpolarized hadron colliders in the 1980’s, RHIC enters the field to start from where polarized DIS has taken us so far. Here, too, asymptotic freedom of QCD, accessible because of the high energy of RHIC’s polarized beams, is the tool to investigate the partonic structure of the proton. Experiments with polarization at RHIC will probe the proton spin in new profound ways [22], complementary to polarized DIS. We will learn about the polarization of gluons in the proton and about details of the flavor structure of the polarized quark and antiquark distributions. RHIC will probe the structure of transversely polarized protons, and it will unravel the origin of the transverse-spin asymmetries mentioned above. RHIC will also investigate polarization phenomena in high-energy *elastic*

scattering of protons, an equally uncharted area of QCD. Finally, if circumstances are very favorable, knowledge gathered about the spin structure of the proton could conceivably be used to turn RHIC into a discovery machine for New Physics, or a machine that probes the *chiral* structure, inaccessible in unpolarized pp collisions, of new interactions possibly to be found at the LHC.

The field of nucleon structure thrives on the complementarity of information obtained in lepton-nucleon and nucleon-nucleon scattering. We shall see examples of this throughout this report. We see a collider with polarized electrons and protons as the next logical step after RHIC in our quest to explore the spin structure of the nucleon and spin phenomena in QCD.

After a brief review of where we currently stand in this field, the subsequent sections will address the most exciting aspects of the RHIC spin physics program in more detail.

## 2.1 Synopsis of the results from polarized DIS

Spin physics at RHIC has been motivated by the exciting results from the experimental program on polarized DIS over the last  $\sim 30$  years. Most of the DIS measurements were performed with longitudinal polarization of the lepton beam and the nucleon target. The difference of cross sections for the case where lepton and nucleon have aligned spins or opposite spins then gives access to the spin-dependent structure function  $g_1(x, Q^2)$  of the nucleon. Here  $Q^2$  is as before the virtuality of the exchanged photon, and  $x$  is the Bjorken variable,  $x = Q^2/(2P \cdot q)$  with  $P$  and  $q$  the nucleon and photon momenta, respectively. The left part of Fig. 1 shows a recent compilation [23] of the world data on  $g_1(x, Q^2)$ . Information from both proton and neutron targets is available. The importance of  $g_1$  lies in the fact that it has a simple interpretation in the parton model, equivalent to considering the lepton-nucleon interaction as a scattering of polarized leptons off polarized free partons. In the parton model, and including the dominant part of the QCD scaling violations mentioned above,  $g_1$  may be written as

$$g_1(x, Q^2) = \frac{1}{2} \sum_q e_q^2 [\Delta q(x, Q^2) + \Delta \bar{q}(x, Q^2)] . \quad (1)$$

Here the  $\Delta q$ ,  $\Delta \bar{q}$  are the helicity distribution functions of quarks and antiquarks in the nucleon. For example,

$$\Delta q(x, Q^2) = q^+(x, Q^2) - q^-(x, Q^2) \quad (2)$$

counts the number densities of quarks with the same helicity as the nucleon, minus opposite. It contains information on the *spin* structure of the proton. The kinematic Bjorken variable  $x$  is identified with the proton momentum fraction carried by the struck quark. The  $Q^2$ -dependence of the parton distributions is precisely the dependence on the “resolving power” mentioned earlier, quantitatively predictable in QCD perturbation theory, thanks to asymptotic freedom. It is also known as  $Q^2$ -“evolution” of the parton distributions. Physically, it expresses the fact that as  $Q^2$  increases one has higher resolution of the partons, so that it is more likely that a struck quark has radiated one or more gluons so that it is effectively resolved into several partons, each with lower momentum fraction. Similarly, a struck quark may have originated from a gluon splitting into a quark-antiquark pair. This picture explains another remarkable feature of the DIS scaling violations: the  $Q^2$ -dependence of the quark densities, and hence of the structure function  $g_1(x, Q^2)$ , is partly driven by the gluon density in the proton, despite the fact that the gluon



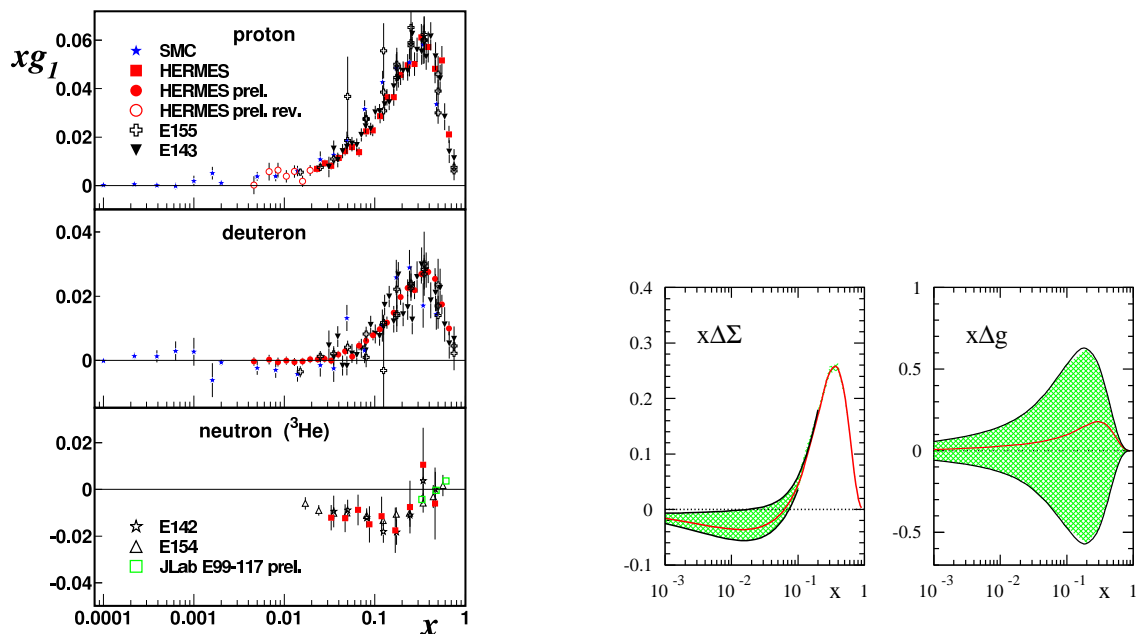


Figure 1: Left: data on the spin structure function  $g_1$ , as compiled and shown in [23]. Right: results from an analysis [?] of polarized DIS in terms of spin-dependent nucleon parton densities  $\Delta\Sigma(x, Q^2)$  and  $\Delta g(x, Q^2)$  at  $Q^2 = 1 \text{ GeV}^2$ .  $\Delta\Sigma$  is the total quark and antiquark helicity distribution (see Eq. (4)) and  $\Delta g$  the gluon helicity distribution defined in Eq. (3). The shaded bands present typical current uncertainties in our knowledge of the distributions.

density does not appear in Eq. (1). The polarized “helicity” gluon density is defined in analogy with Eq. (2) as

$$\Delta g(x, Q^2) = g^+(x, Q^2) - g^-(x, Q^2). \quad (3)$$

Thus scaling violations in polarized DIS allow, in principle, to determine not only the  $\Delta q + \Delta\bar{q}$  combinations for various flavors, but also  $\Delta g$ .

Extensive analyses of polarized-DIS data in terms of the polarized parton distributions have been performed by several groups, taking into account a “state-of-the-art” theoretical framework that includes additional non-leading (“higher-order”) corrections to the framework described above. A typical result, taken from [?], is shown in the right part of Fig. 1. The results refer to a  $Q^2$  scale of  $1 \text{ GeV}^2$ , which is a typical scale from which perturbative evolution as described above could be used to calculate the distributions at higher  $Q^2$ . The first panel shows the sum of all polarized quark and antiquark distributions distribution,

$$\Delta\Sigma = \Delta u + \Delta\bar{u} + \Delta d + \Delta\bar{d} + \Delta s + \Delta\bar{s} \quad (4)$$

as a function of  $x$ . As can be seen, it is known to a fair accuracy, except at the lower  $x$ , where we have shown a typical present uncertainty by a shaded band. The right-hand plot displays the polarized gluon density  $\Delta g$ . Evidently, we know very little, if anything, about gluon polarization in the nucleon. The latter result is not surprising: as we pointed out earlier, the only information on  $\Delta g$  from polarized DIS comes from scaling violations. Since all experiments performed so far have been with fixed targets, the available energy, and hence the reach in  $Q^2$ , have been very limited, resulting in a virtually unconstrained  $\Delta g$ .

It has been possible to extrapolate the results shown in Fig. 1 to  $x \rightarrow 0$ . There are important insights into nucleon structure that could be gained from this. First of all, there is a venerable

sum rule by Bjorken [?] – that actually predates QCD – which remarkably relates the integrals over all  $x$  of the high- $Q^2$  DIS polarized structure functions for the proton and the neutron to the decay constant  $g_A \approx 1.273$  in low-energy neutron  $\beta$ -decay:

$$\int_0^1 dx (g_1^p(x, Q^2) - g_1^n(x, Q^2)) = \frac{1}{6}g_A + \mathcal{O}(\alpha_s(Q^2)) , \quad (5)$$

where we have indicated that there are perturbative-QCD corrections to the relation, known to very high accuracy. This sum rule, which was the original motivation for performing measurements in polarized DIS, has been verified experimentally at the 10% level [?].

Using further information from baryon  $\beta$ -decays, it was also possible to determine the  $x$ -integral over the combination  $\Delta\Sigma$  shown in Fig. 1. This has resulted in one of the most renowned – and debated – results in recent Nuclear and Particle Physics. The importance of the integral of  $\Delta\Sigma$ , also known as the nucleon “axial charge”, lies in the fact that it yields the average of all *quark and antiquark helicity contributions to the proton helicity*:

$$\langle S_q \rangle = \frac{1}{2} \int_0^1 \Delta\Sigma(x, Q^2) dx . \quad (6)$$

This follows from the definition of the spin-dependent quark distribution functions in Eq. (2); the factor 1/2 is because quarks carry spin-1/2. Experimentally,

$$\langle S_q \rangle \approx 0.1 , \quad (7)$$

with an error of about 50%. Despite its large error, the fact that  $\langle S_q \rangle \ll 0.5$  implies that very little of the proton spin is carried by that of the quarks. This result is in striking contrast with predictions from constituent quark models and has therefore been dubbed “proton spin crisis”. Even though the identification of nucleon with parton helicity is not a prediction of QCD, such models have enjoyed success in describing hadron magnetic moments and spectroscopy. In any case, polarized DIS teaches us that we must look elsewhere for the proton spin!

## 2.2 Compelling questions in spin physics

The results from polarized inclusive DIS clearly called for further investigation of the nucleon spin. What are first of all the other candidates for carrying the nucleon spin? An examination of angular momentum in QCD equates the spin-1/2 of the proton by contributions from quark spins, gluon spins, and quark and gluon orbital angular momenta:

$$\frac{1}{2} = \langle S_q \rangle + \langle S_g \rangle + \langle L_q \rangle + \langle L_g \rangle . \quad (8)$$

We have suppressed a dependence of each of the terms on the resolution scale  $Q^2$ . The gluon spin contribution is directly obtained from the gluon helicity distribution in Eq. (3):

$$\langle S_g \rangle(Q^2) = \int_0^1 \Delta g(x, Q^2) dx . \quad (9)$$

Equation (8) motivates a substantial part not only of RHIC spin physics, but of virtually all major current activities in the field of high-energy spin physics. More specifically, the compelling questions are:

**How do gluons contribute to the proton spin?** There are a number of reasons to be interested in  $\Delta g(x, Q^2)$ . First of all, its integral could well be a major contributor to the proton spin. In fact, it is a remarkable feature of QCD that at momentum scales relevant to RHIC physics  $\langle S_g \rangle(Q^2)$  may well *be* significant, perhaps even large compared to the “1/2” on the right-hand-side of Eq. (8). The reason is that the integral of  $\Delta g(x, Q^2)$  evolves as  $1/\alpha_s(Q^2)$ , that is, rises logarithmically. This peculiar evolution pattern is a very deep prediction of QCD, related to its so-called axial anomaly. It has inspired ideas that a reason for the smallness of the quark spin contribution should be sought in a “shielding” of the quark spins due to a particular perturbative part of the DIS process  $\gamma^* g \rightarrow q\bar{q}$ . The associated contributions arise only at order  $\alpha_s(Q^2)$ ; however, the peculiar evolution of  $\langle S_g \rangle(Q^2)$  would compensate this suppression. To be of any practical relevance, such models would require a large positive gluon spin contribution,  $\langle S_g \rangle > 1$ , even at low “hadronic” scales of a GeV or so. A very large polarization of the confining fields inside a nucleon, even though suggested by some nucleon models, would be a very puzzling phenomenon and would once again challenge our picture of the nucleon. Subsection 2.4.1 will discuss in detail the efforts being made at RHIC to address the questions related to  $\Delta g$ , and the prospects for the planned measurements.

**What are the patterns of up, down, and strange quark and antiquark polarizations?** As is evident from Eq. (1), polarized DIS has given us access to the combinations  $\Delta q + \Delta \bar{q}$ . We have already discussed one particularly interesting combination of these,  $\Delta \Sigma$ . To really understand the proton helicity structure in detail, one needs to learn about the various quark and antiquark densities,  $\Delta u, \Delta \bar{u}, \Delta d, \Delta \bar{d}, \Delta s, \Delta \bar{s}$ , individually. This also provides an important additional test of the smallness of the quark spin contribution, independent of the additional input from baryon  $\beta$ -decays necessary so far. It is also important for models of nucleon structure which generally make clear qualitative predictions about, for example, the flavor asymmetry  $\Delta \bar{u} - \Delta \bar{d}$  in the proton sea. These predictions are often related to fundamental concepts such as the Pauli principle: since the proton has two valence- $u$  quarks which primarily spin along with the proton spin direction,  $u\bar{u}$  pairs in the sea will tend to have the  $u$  quark polarized opposite to the proton. Hence, if such pairs are in a spin singlet, one expects  $\Delta \bar{u} > 0$  and, by the same reasoning,  $\Delta \bar{d} < 0$ . Such questions become all the more exciting due to the fact that rather large *unpolarized* asymmetries  $\bar{u} - \bar{d} \neq 0$  have been observed in DIS and Drell-Yan measurements. Further fundamental questions concern the strange quark polarization. The polarized DIS measurements point to a sizable negative polarization of strange quarks, in line with other observations of significant strange quark effects in nucleon structure. Recently, in the unpolarized case the asymmetry between strange and antistrange distributions has attracted much attention, due to its interest for nucleon models, but also due to its possible implications for an explanation of the  $\sim 3\sigma$  “anomaly” in the NuTeV measurement of the Weinberg angle. A measurement of the difference between strange and antistrange polarizations, while probably lying in the future, might give further insights. In subsection 2.4.2 we present the possibilities RHIC offers for disentangling the various flavor polarizations in the nucleon.

**What orbital angular momenta do partons carry?** Equation (8) shows that quark and gluon orbital angular momenta are the other candidates for the carriers of the proton spin. Consequently, theoretical work focused also on these in the years following the discovery of the “spin crisis”. A conceptual breakthrough was made in the mid 1990s when it was realized that a particular class of “off-forward” nucleon matrix elements, in which the nucleon in the initial and final state has different momentum, measure total parton angular momentum. Put simply, orbital angular momentum is  $\vec{r} \times \vec{p}$ , with  $\vec{r}$  a derivative with respect to momentum transfer in

Quantum Mechanics. Thus, in analogy with the measurement of the Pauli form factor it takes a finite momentum transfer on the nucleon to access matrix elements with operators containing a factor  $\vec{r}$ . It was also shown how these “off-forward” distributions, really generalizations of the ordinary parton distributions, may be experimentally determined from certain rare exclusive processes in lepton-nucleon scattering, the prime example being “Deeply-Virtual Compton Scattering (DVCS)”  $\gamma^*p \rightarrow \gamma p$ . A major emphasis in current and future experimental activities in lepton scattering is on the DVCS and related reactions. There are other observables that are related to orbital angular momentum of nucleon constituents. The Pauli form factor is one of them. Another, accessible in proton-proton scattering, may contribute to spin asymmetries measured with a single transversely polarized proton and an unpolarized one. This brings us to the next compelling question.

**What is the role of transverse spin in QCD?** So far, we have only considered the helicity structure of the nucleon, that is, the partonic structure we find when we probe the nucleon when its spin is aligned with its momentum. High-energy protons may also be studied when *transversely* polarized, and it has been known for a long time now that very interesting spin effects are associated with this in QCD. Partly this is known from theoretical studies which revealed that besides the helicity distributions  $\Delta f$  discussed above, for transverse polarization there is a new set of parton densities, called “transversity”. They are defined analogously to Eq. (2), but now for transversely polarized partons polarized along or opposite to the transversely polarized proton. Nothing is known so far experimentally about the transversity densities. Their measurement is highly desirable, for a number of reasons. Not only does transversity complete the set of nucleon parton distributions. Differences between the helicity and transversity densities give information about relativistic effects in the nucleon. The transversity densities also give the nucleon tensor charge, which is equally fundamental as its axial charge mentioned earlier. Finally, transversity also plays a role in predictions for the neutron electric dipole moment. We will discuss transversity in more detail in subsection ??, and prospects for its measurement at RHIC later in section ??.

The other reason why transverse spin has captured the attention of researchers in QCD for a long time is related to experimental observations of very large single-transverse spin asymmetries in pp scattering, where really none were expected. Related azimuthal asymmetries were seen in lepton scattering. Often, when simple expectations are refuted experimentally, new insights emerge, and this has been no different in this case. With time it was realized that single-spin asymmetries may tell us many more things about QCD and the nucleon than anticipated. Particularly interesting examples are parton orbital angular momenta and the color Lorentz force inside a polarized nucleon. We are, however, still far from a complete understanding of all mechanisms that may be involved in single-spin asymmetries. We will show in more detail in section ?? that RHIC is poised to provide answers.

We now turn in more detail to the various physics topics relevant at RHIC. We start by a brief description of the theoretical underpinnings for the theoretical description of “deeply inelastic” hadronic reactions, considering unpolarized scattering for simplicity. We then discuss how polarized pp scattering at RHIC addresses the compelling questions in spin physics raised above. We will also describe other exciting physics opportunities the RHIC spin program offers.

## 2.3 Unpolarized pp scattering

The basic concept that underlies most of RHIC spin physics is the factorization theorem [16]. It states that large momentum-transfer reactions may be factorized into long and short-distance contributions. The long-distance pieces contain information on the structure of the nucleon in terms of its distributions of constituents, “partons”. The short-distance parts describe the hard interactions of these partons and can be calculated from first principles in QCD perturbation theory. While the parton distributions describe universal properties of the nucleon, that is, are the same in each reaction, the short-distance parts carry the process-dependence and have to be calculated for each reaction considered.

As an explicit example, we consider the cross section for the reaction  $pp \rightarrow \pi(p_\perp)X$ , where the pion is at high transverse momentum  $p_\perp$ , ensuring large momentum transfer.  $X$  denotes an arbitrary hadronic final state. The statement of the factorization theorem is then:

$$d\sigma = \sum_{a,b,c} \int dx_a \int dx_b \int dz_c f_a(x_a, \mu) f_b(x_b, \mu) D_c^\pi(z_c, \mu) \times d\hat{\sigma}_{ab}^c(x_a P_A, x_b P_B, P_\pi/z_c, \mu) , \quad (10)$$

where the sum is over all contributing partonic channels  $a + b \rightarrow c + X$ , with  $d\hat{\sigma}_{ab}^c$  the associated partonic cross section. The  $f_{a,b}$  describe the distributions of partons in the nucleon \*. Any factorization of a physical quantity into contributions associated with different length scales will rely on a “factorization” scale that defines the boundary between what is referred to as “short-distance” and “long-distance”. In the present case this scale is represented by  $\mu$  in Eq. (10).  $\mu$  is essentially arbitrary, so the dependence of the calculated cross section on  $\mu$  represents an uncertainty in the theoretical predictions. However, the actual dependence on the value of  $\mu$  decreases order by order in perturbation theory. This is a reason why knowledge of higher orders in the perturbative expansion of the partonic cross sections is important. We also note that Eq. (10) is of course not an exact statement. There are corrections to Eq. (10) that are down by inverse powers of the momentum transfer, the so-called “power corrections”. These corrections may become relevant towards lower  $p_T$ . As we shall see in Figs. 3 and ?? below, comparisons of RHIC data for unpolarized cross sections with theoretical calculations based on Eq. (10) do not suggest that power corrections play a very significant role in the RHIC kinematic regime, even down to fairly low  $p_T$ .

Figure 2 offers a graphic illustration of QCD factorization. Thanks to factorization, one can study nucleon structure, represented by the parton densities  $f_{a,b}(x, \mu)$ , through a measurement of  $d\sigma$ , hand in hand with a theoretical calculation of  $d\hat{\sigma}$ . The partonic cross sections may be evaluated in perturbation theory. Schematically, they can be expanded as

$$d\hat{\sigma}_{ab}^c = d\hat{\sigma}_{ab}^{c,(0)} + \frac{\alpha_s}{\pi} d\hat{\sigma}_{ab}^{c,(1)} + \dots . \quad (11)$$

$d\hat{\sigma}_{ab}^{c,(0)}$  is the leading-order (LO) approximation to the partonic cross section. The lowest order can generally only serve to give a rough description of the reaction under study. It merely captures the

---

\*In this particular example, the fact that we are observing a specific hadron in the reaction requires the introduction of additional long-distance functions, the parton-to-pion fragmentation functions  $D_c^\pi$ . These functions have been determined with some accuracy by observing leading pions in  $e^+e^-$  collisions and in DIS [24].

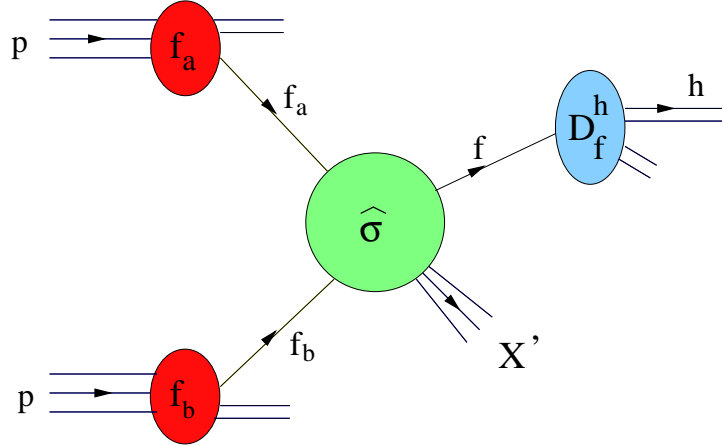


Figure 2: Factorization in terms of parton densities, partonic hard-scattering cross sections, and fragmentation functions.

main features, but does not usually provide a quantitative understanding. The first-order (“next-to-leading order” [NLO]) corrections are generally indispensable in order to arrive at a firmer theoretical prediction for hadronic cross sections.

There have already been results from RHIC that demonstrate that the NLO framework outlined above is very successful. Figure 3 shows comparisons of data from Phenix and STAR for inclusive-pion production  $pp \rightarrow \pi^0 X$  with NLO calculations. As can be seen, the agreement is excellent at central and forward rapidities, and down even to  $p_\perp$  values as low as  $p_\perp \gtrsim 1$  GeV. In Fig. 4 we decompose the  $\pi^0$  cross sections of Fig. 3 into the contributions from the various two-parton initial states. It is evident that in both cases, central and forward, processes with initial gluons dominate by far for the pion transverse momenta accessed so far. This implies that  $pp \rightarrow \pi^0 X$  provides an excellent probe of gluons in the nucleon.

A similar comparison is shown for prompt-photon production  $pp \rightarrow \gamma X$  in Fig. 5. The left part presents the recent result of a measurement by Phenix [?], along with the NLO calculation. Again, very good agreement is found. On the right, we show the decomposition of the NLO prompt-photon cross section into the contributions from the initial partonic states. The quark-gluon “Compton process” dominates at a level of 75%.

We note that an agreement between data and NLO calculations like the one seen in Figs. 3 and 5 was not found in previous comparisons made in the fixed-target regime. The good agreement of the pion and photon spectra with NLO QCD at RHIC’s  $\sqrt{s}$ , and the good precision of the RHIC data provide a solid basis to extend this type of analysis to polarized reactions. The clear sensitivity to gluons in the initial state further makes the reactions very promising probes of gluon polarization. We will now turn to polarized pp collisions at RHIC.

## 2.4 Probing the spin structure of the nucleon in polarized pp collisions

The measured quantities in spin physics experiments at RHIC are *spin asymmetries*. As an example, for collisions of longitudinally polarized proton beams, one defines a double-spin asymmetry

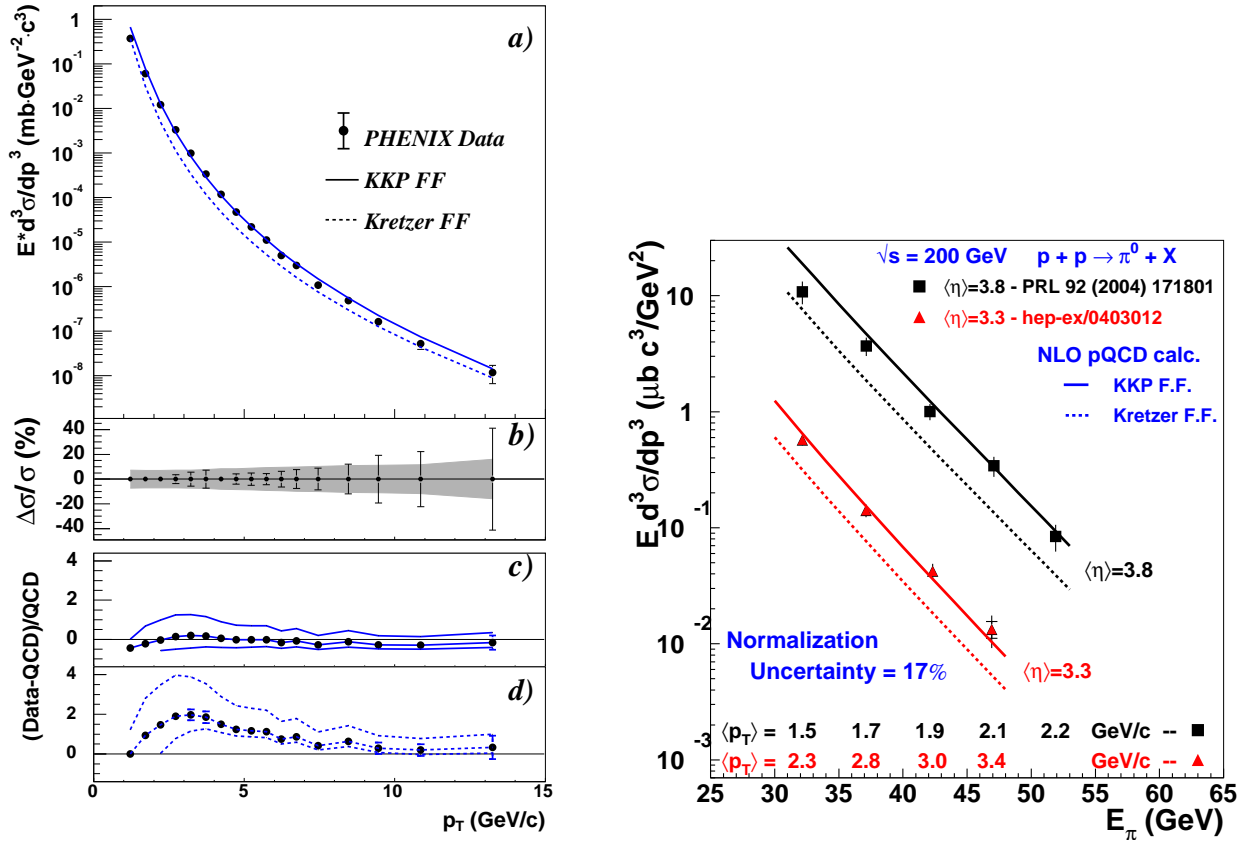


Figure 3: Data from Phenix (left, [?]) and STAR (right, [?]) for the cross section for inclusive  $\pi^0$  production  $pp \rightarrow \pi^0 X$  at  $\sqrt{s} = 200$  GeV. The lines show the results of the next-to-leading order calculation [?].

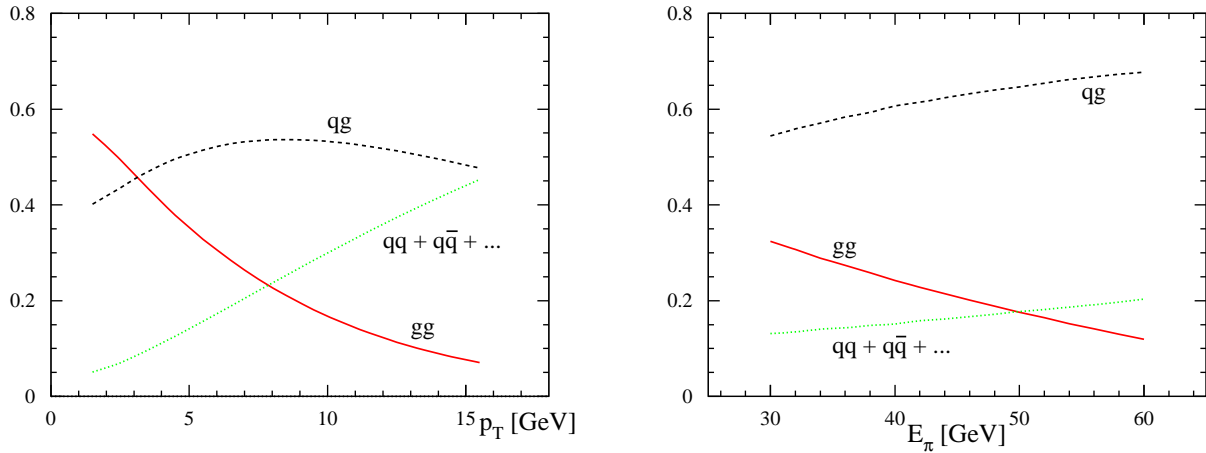


Figure 4: Decomposition of the above NLO cross sections for  $pp \rightarrow \pi^0 X$  collisions shown in Fig. 3 into the contributions from initial  $gg$ ,  $qg$ , and  $qq$  states.

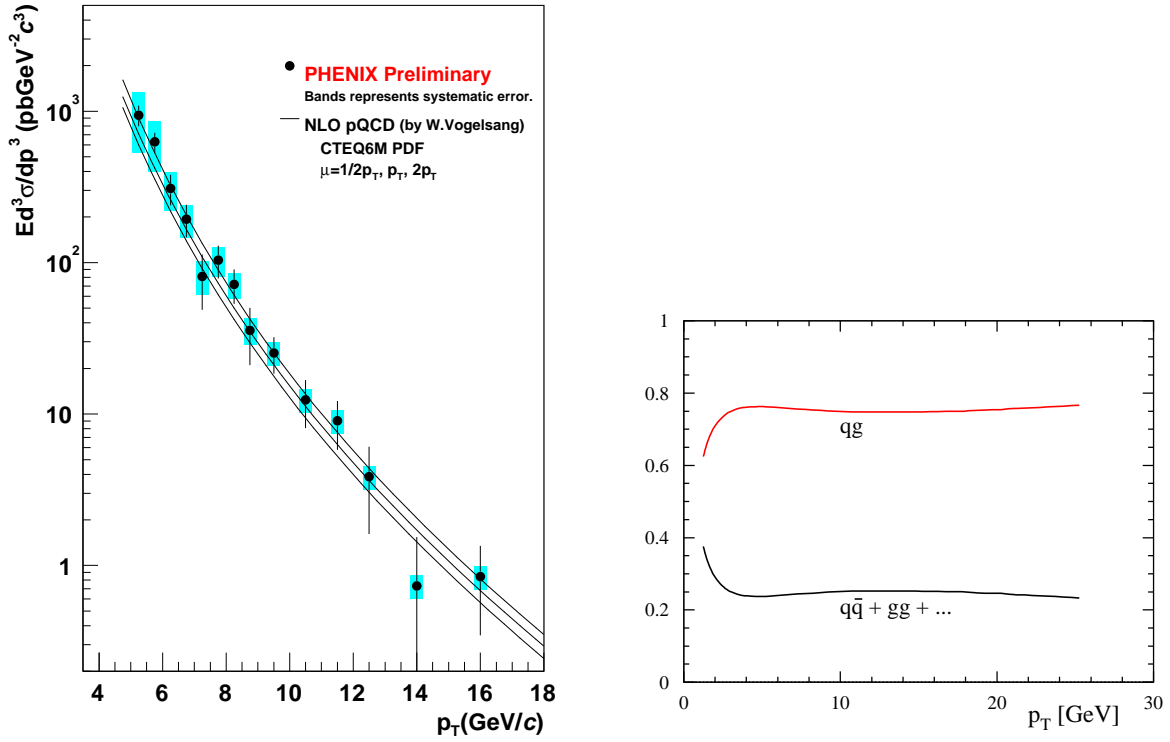


Figure 5: Left: Phenix data [?] for inclusive prompt-photon production,  $pp \rightarrow \gamma X$ , compared to the NLO calculation [?]. Right: Decomposition of the NLO cross section into the contributions from initial  $qg$  and  $q\bar{q}$ +other states.

for a given process by

$$A_{LL} = \frac{d\sigma(++) - d\sigma(+-)}{d\sigma(++) + d\sigma(+-)} \equiv \frac{d\Delta\sigma}{d\sigma}, \quad (12)$$

where the signs indicate the helicities of the incident protons. The basic concepts laid out so far for unpolarized inelastic  $pp$  scattering carry over to the case of polarized collisions: spin-dependent inelastic  $pp$  cross sections factorize into “products” of polarized parton distribution functions of the proton and hard-scattering cross sections describing spin-dependent interactions of partons. As in the unpolarized case, the latter are calculable in QCD perturbation theory since they are characterized by large momentum transfer. Schematically, one has for the numerator of the spin asymmetry:

$$d\Delta\sigma = \sum_{a,b=q,\bar{q},g} \Delta a \otimes \Delta b \otimes d\Delta\hat{\sigma}_{ab}, \quad (13)$$

where  $\otimes$  denotes a convolution and where the sum is over all contributing partonic channels  $a + b \rightarrow c + X$  producing the desired high- $p_T$  or large-invariant mass final state.  $d\Delta\hat{\sigma}_{ab}$  is the associated perturbative spin-dependent partonic cross section, defined as

$$d\Delta\hat{\sigma}_{ab} = d\hat{\sigma}_{ab}(++) - d\hat{\sigma}_{ab}(+-), \quad (14)$$

the signs denoting the helicities of the initial partons  $a, b$ . The sensitivity with which one can probe the polarized parton densities will foremost depend on the weights with which they enter



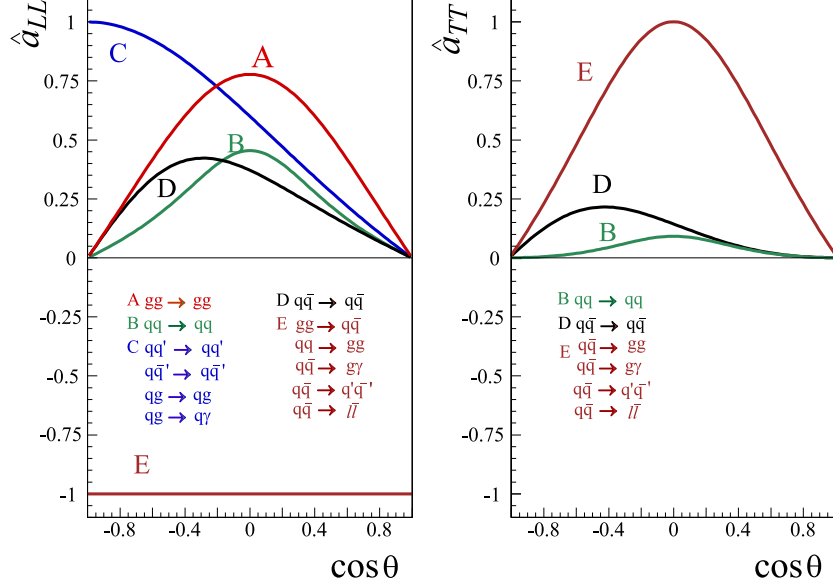


Figure 6: Spin asymmetries for the most important partonic reactions at RHIC at lowest order in QCD. Left: helicity dependence, right: transverse polarization.

the cross section. Good measures for this are the so-called partonic analyzing powers. The latter are just the spin asymmetries

$$\hat{a}_{LL} = \frac{d\hat{\sigma}_{ab}(++) - d\hat{\sigma}_{ab}(+-)}{d\hat{\sigma}_{ab}(++) + d\hat{\sigma}_{ab}(+-)} \quad (15)$$

for the individual partonic subprocesses. Figure 6 shows these analyzing powers at LO for all partonic reactions. One can see that they are usually very substantial. For future reference, we also give the subprocess asymmetries for *transverse* polarization. Here, Eq. (13) applies as well. The parton densities are then the transversity distributions, to be discussed in more detail below, and the partonic cross sections are defined as in Eq.(14), but for transverse initial polarization. One customarily uses a small  $\delta$  to designate transversely polarized quantities. In this section, we will focus on the longitudinal case; we will return to transverse polarization in the next section.

Since the partonic cross sections are calculable from first principles in QCD, Eq. (13) may be used to determine the polarized parton distribution functions from measurements of the spin-dependent pp cross section on the left-hand side. A crucial point here is that the parton distributions are universal, that is, they are the same in all inelastic processes, not only in pp scattering, but also for example in deeply-inelastic lepton nucleon scattering which up to now has mostly been used to learn about nucleon spin structure. This means that inelastic processes with polarization have the very attractive feature that they probe fundamental and universal spin structure of the nucleon. In effect, we are using the asymptotically free regime of QCD to probe the deep structure of the nucleon.

At RHIC, there are a number of sensitive and measurable processes at our disposal. The key ones, some of which will be discussed in detail in the following, are listed in Table 1, where we also give the dominant underlying partonic reactions and the aspect of nucleon spin structure they probe. We emphasize that, even though we have only shown LO results in Fig. 6, the NLO corrections are available for each process relevant for RHIC-Spin, thanks to considerable efforts

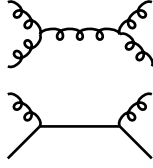
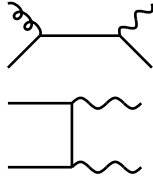
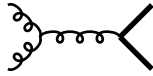
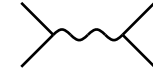
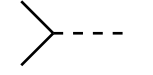
Reaction	Dom. partonic process	probes	LO Feynman diagram
$\vec{p}\vec{p} \rightarrow \pi + X$ [?, ?]	$\vec{g}\vec{g} \rightarrow gg$ $\vec{q}\vec{g} \rightarrow qg$	$\Delta g$	
$\vec{p}\vec{p} \rightarrow \text{jet}(s) + X$ [?]	$\vec{g}\vec{g} \rightarrow gg$ $\vec{q}\vec{g} \rightarrow qg$	$\Delta g$	(as above)
$\vec{p}\vec{p} \rightarrow \gamma + X$ $\vec{p}\vec{p} \rightarrow \gamma + \text{jet} + X$ $\vec{p}\vec{p} \rightarrow \gamma\gamma + X$ [?, ?, ?, ?, ?]	$\vec{q}\vec{g} \rightarrow \gamma q$ $\vec{q}\vec{g} \rightarrow \gamma q$ $\vec{q}\vec{q} \rightarrow \gamma\gamma$	$\Delta g$ $\Delta g$ $\Delta q, \Delta\bar{q}$	
$\vec{p}\vec{p} \rightarrow DX, BX$ [?]	$\vec{g}\vec{g} \rightarrow c\bar{c}, b\bar{b}$	$\Delta g$	
$\vec{p}\vec{p} \rightarrow \mu^+\mu^- X$ (Drell-Yan) [?, ?, ?, ?]	$\vec{q}\vec{q} \rightarrow \gamma^* \rightarrow \mu^+\mu^-$	$\Delta q, \Delta\bar{q}$	
$\vec{p}\vec{p} \rightarrow (Z^0, W^\pm)X$ $p\vec{p} \rightarrow (Z^0, W^\pm)X$ [?, ?, ?]	$\vec{q}\vec{q} \rightarrow (Z^0, W^\pm)$	$\Delta q, \Delta\bar{q}$	

Table 1: Key processes at RHIC for the determination of the parton distributions of the longitudinally polarized proton, along with the dominant contributing subprocesses, the parton distribution predominantly probed, and representative leading-order Feynman diagrams. The references given in the left column are for the corresponding next-to-leading order calculation.

made over the past decade or so. We give reference to the corresponding work in the first column of Table 1. These calculations bring the theoretical calculations for RHIC-Spin to the same level that has been so successful in the unpolarized case, as demonstrated by Figs. 3 and 5. For each of the processes in Table 1 the parton densities enter with different weights, so that each has its own role in helping to determine the polarized parton distributions. Some will allow a clean determination of gluon polarizations, others are more sensitive to quarks and antiquarks. Eventually, when data from RHIC will become available for most or all processes, a “global” analysis of the data, along with information from lepton scattering, will be performed which then determines the  $\Delta q, \Delta\bar{q}, \Delta g$ .

We will now address some of the most important processes in more detail, summarizing theoretical predictions and experimental plans and prospects at RHIC. We will start with those that are sensitive to gluon polarization in the proton, and then discuss  $W$  production which will give information about the quark and antiquark polarizations.

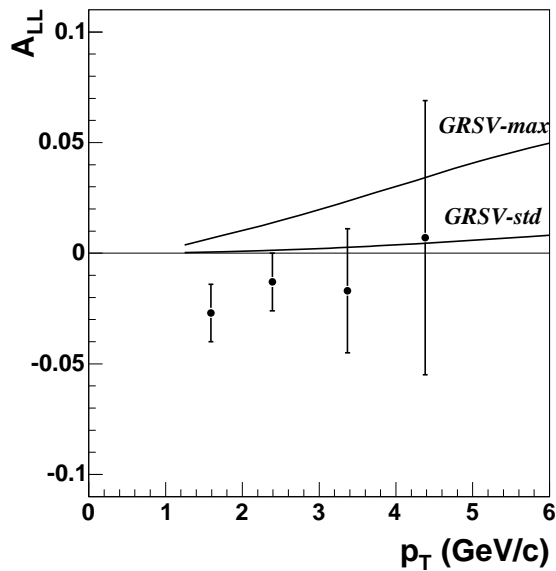


Figure 7: Phenix measurement [?] for the double-spin asymmetry  $A_{LL}^{\pi^0}$  at central rapidities.

### 2.4.1 Mapping gluon helicity preferences

As follows from Table 1 and Fig. 6, gluon polarization can be probed in several sensitive ways at RHIC. All of the approaches discussed in this subsection have the distinct advantage over deep inelastic lepton scattering that the gluons are directly involved at leading order, via partonic processes marked by large gluon spin sensitivity in measured two-spin helicity asymmetries  $A_{LL}$ . This direct sensitivity promises to allow substantial improvements over DIS analyses in both the statistical and systematic uncertainties in the extraction of  $\Delta g(x)$ . Access to a number of alternative reaction channels, with distinct experimental and interpretational challenges outlined below, is especially important to demonstrate the robustness and systematic uncertainty reduction of gluon polarizations extracted at RHIC. Other tests of robustness involve comparison of results for a given Bjorken  $x$  range of the participating gluons, probed at different QCD scales (*i.e.*, different  $p_T$  values) and with different constraints on the flavor and  $x$ -range of the colliding partner partons. In addition, it will be important to compare quark polarizations extracted from RHIC spin analyses to those from DIS. The need for these cross-checks strongly influences our estimates below of target requirements on running time and beam performance: we aim to improve the statistical precision in gluon helicity preferences over current DIS analyses by at least a factor  $\approx 3$ , even for the weakest (but cleanest) of the pp channels used to probe the gluons.

As the proton collision luminosity and beam polarization steadily improve over the coming few years, STAR and PHENIX will address the gluon polarization with a progression of probes. The earliest measurements will exploit the abundant channels for inclusive pion and jet production. The large cross sections for these processes, and the solid NLO understanding of the  $\pi^0$  production cross sections measured by PHENIX and STAR even down to  $p_T < 2$  GeV/c (see Fig. 3), promise statistically and systematically significant sensitivity to  $\Delta g(x)$  even at lower integrated luminosities. Indeed, PHENIX has already published [?] first  $A_{LL}$  data for  $\pi^0$  production from the 2003 RHIC (see Fig. 7), where integrated luminosities of only a few hundred

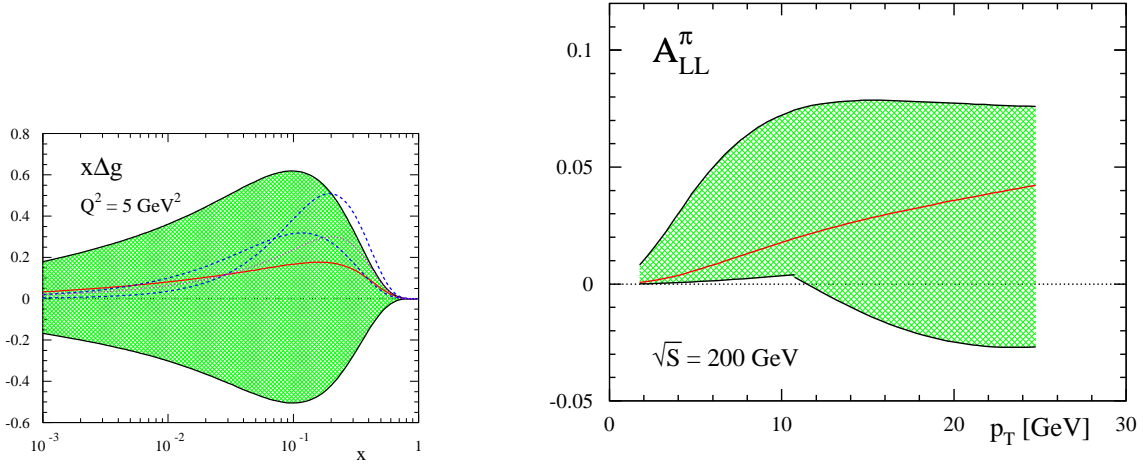


Figure 8: Left: typical current uncertainty in  $\Delta g(x)$  from polarized DIS, as already shown in Fig. 1. We also show the gluon densities resulting from the analyses in [?, ?]. Right: range of spin asymmetries  $A_{LL}$  for  $pp \rightarrow \pi^0 X$  at  $\sqrt{s} = 200$  GeV and central rapidities, corresponding to the uncertainty shown on the left.

$\text{nb}^{-1}$  and beam polarizations  $\approx 30\%$  already provided statistical sensitivity to gluon polarization approaching that of the existing DIS database. The improved luminosity and beam polarization anticipated for the 2005 run should provide an order of magnitude decrease in statistical uncertainties, as reflected in the projections of PHENIX data for pion production (Fig. 8) and STAR data for inclusive jet production (Fig. 9), with still greater improvements anticipated in subsequent years. The projected uncertainties in these figures are based on measurements already made, and hence they incorporate realistic  $\pi^0$  and jet triggering/reconstruction efficiencies ( $\sim xx\%$  and  $yy\%$ , respectively). Even the data anticipated from the 2005 run alone would allow a significant reduction from the  $\Delta g(x)$  uncertainties characterizing current DIS analyses, as represented by the error bands on the theoretical calculations shown in Figs. 8 and 9.

The disadvantages of the inclusive hadron and jet production channels arise from the  $p_T$ -dependent competition among  $gg$ ,  $qg$ , and  $qq$  partonic scattering subprocesses (see Fig. 4). The first two of these provide quadratic and linear sensitivity, respectively, to  $\Delta g(x)$ , while the  $qq$  contribution dilutes the sensitivity. The competition depends on parton fragmentation functions, including at high momentum fractions ( $z \gtrsim 0.8$ ) where they are not well measured. This is true even for jet detection, because the possible bias of various jet triggers in favoring one partonic subprocess over another depends on the fragmentation details. Furthermore, the inclusive yields involve a convolution over a substantial range of partonic  $x$ -values (see Fig. XX), and for the hadron production, over a significant range of partonic  $p_T$  values and hence QCD scales. While the quantitative implications of these complications for systematic uncertainties in extracted gluon polarizations are under study, it is important as well to supplement the inclusive pion and jet measurements with investigations of more selective channels.

One way of varying the partonic subprocess sensitivities in a controlled manner is to measure  $A_{LL}$  for coincident detection of hadron or jet pairs, as a function both of  $p_T$  and the angles and

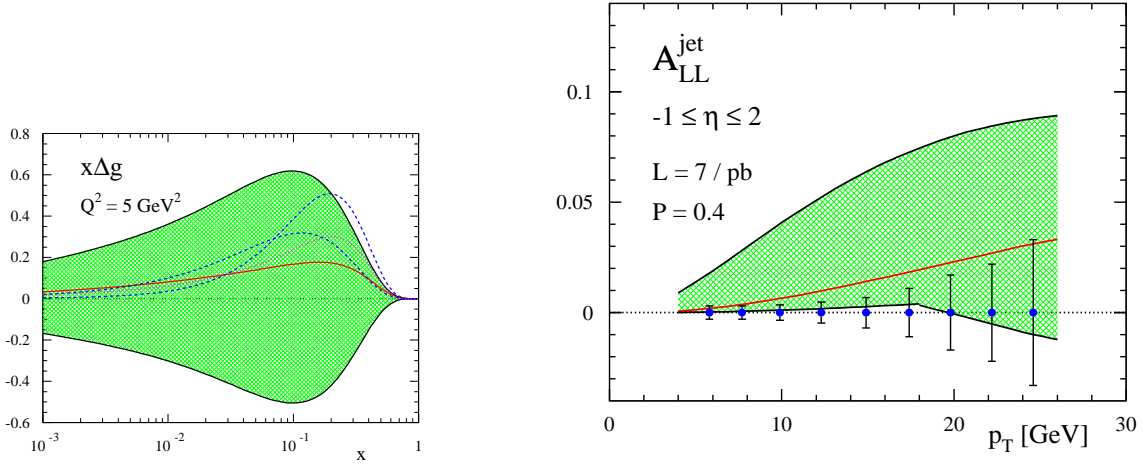


Figure 9: Same as Fig. 9, but for  $pp \rightarrow \text{jet}X$  at rapidities  $1 \leq \eta \leq 2$ . DESCRIBE ERROR BARS.

angle differences between the detected particles. For example, dijets of substantial  $p_T$  that are azimuthally back-to-back ( $\Delta\phi \approx \pi$ ), but both at forward rapidity ( $\eta_1 \approx \eta_2 \neq 0$ ), arise preferentially from quite asymmetric partonic collisions, where the unpolarized pdf's in the nucleon favor  $qg$  scattering. This kinematic correlation is illustrated by PYTHIA simulations in Fig. XX, which show, for a detected hadron pair at fixed  $p_T$  with one particle at forward angles, that the lower parton  $x$ -value probed decreases rapidly with decreasing magnitude  $|\Delta\eta|$  of the pseudorapidity interval between the two hadrons, with a consequent variation of the parton subprocess parentage. Thus, for example,  $A_{LL}$  measurements for forward pion pairs should be especially sensitive to the polarization of low- $x$  gluons. The correlation also implies that di-hadron or di-jet measurements can be made to emphasize  $qq$  scattering, and sensitivity to quark (for comparison to DIS results) over gluon polarization, by concentrating on sizable  $p_T$  and large  $|\Delta\eta|$ .

Still cleaner subprocess selection can be made with the rarer, semi-electromagnetic process of direct photon production:  $pp \rightarrow \gamma X$  or  $pp \rightarrow \gamma + \text{jet} + X$ . In RHIC kinematics, this channel is dominated (at the  $\sim 75\%$  level) by QCD Compton scattering,  $qg \rightarrow q\gamma$ , providing strong, linear and nearly undiluted sensitivity to  $\Delta g(x)$ . While there have been difficulties in understanding direct photon cross sections measured in earlier fixed-target experiments [?] quantitatively in a pQCD context, the NLO theory provides a good description of the unpolarized  $pp \rightarrow \gamma X$  cross section already measured at RHIC (see Fig. 5), giving confidence that analogous predictions for  $A_{LL}$  should be realistic. Another advantage of this channel is that measurement of the isolated photon's  $p_T$  in an electromagnetic calorimeter determines the transverse momentum of the dominant partonic process, hence the QCD scale at which the gluon polarization is being probed, modulo small ambiguities associated with intrinsic transverse momentum of the partons before they collide.

Figures 10 and 11 show such theoretical NLO calculations of  $A_{LL}^\gamma$  for inclusive photon production at RHIC, for both  $\sqrt{s}=200$  and 500 GeV. The calculations include an isolation cut on the photon, as will have to be imposed experimentally to suppress contributions from jets that have

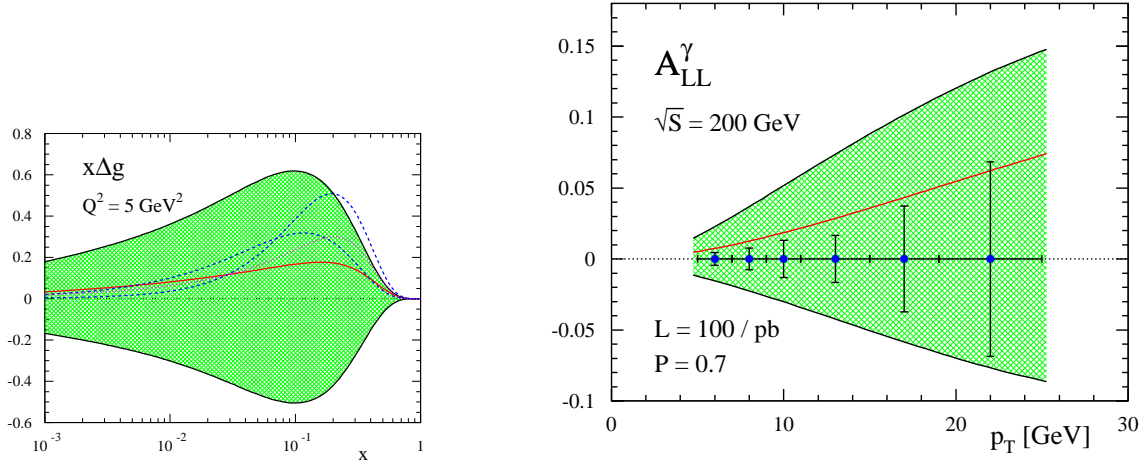


Figure 10: Same as Fig. 8, but for the case of prompt photon production at  $\sqrt{s} = 200$  GeV.

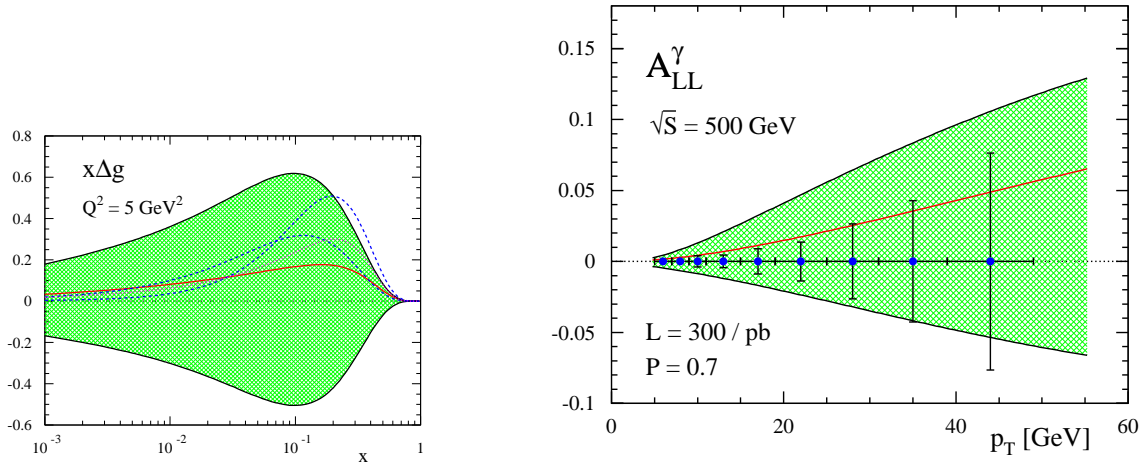


Figure 11: Same as Fig. 10, but for  $\sqrt{s} = 500$  GeV.

an energetic photon, or a decaying  $\pi^0$  that cannot be adequately discriminated from a single photon, as one of the fragments of a scattered quark or gluon [?]. The projected experimental error bars in Figs. 10 and 11 represent statistical and background subtraction errors with realistic  $p_T$  cuts, achievable at RHIC with beam polarizations of 0.7 and integrated luminosities recorded at STAR or PHENIX of  $100 \text{ pb}^{-1}$  at 200 GeV and  $300 \text{ pb}^{-1}$  at 500 GeV. Comparison of these error bars with the present theoretical uncertainty band shows that, despite the small cross section for prompt photon production, one can substantially improve upon present uncertainties in the gluon polarization in realistic RHIC running times. If the interpretation of the results in terms of gluon polarization turns out to be consistent with that from the higher statistics channels discussed above, this will place meaningful constraints on interpretation uncertainties within pQCD.

Inclusive direct photon asymmetries at given measured photon  $p_T$  probe gluon polarizations

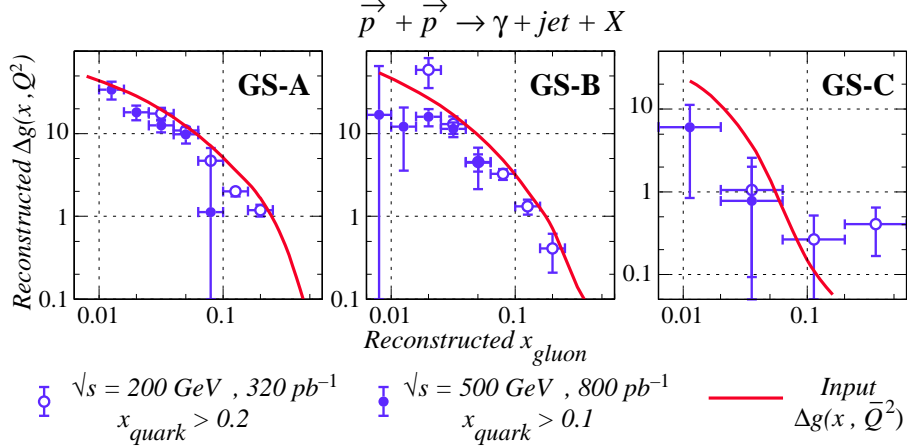


Figure 12: Possibilities for gluon reconstruction from measurements of the spin asymmetry in  $pp \rightarrow \gamma jet X$  at  $\sqrt{s} = 200$  and  $500$  GeV.

over a narrow partonic momentum transfer scale, but still involve a convolution over a broad range of gluon  $x$ -values. An effective way to provide an experimental map of the so far unconstrained shape of  $\Delta g(x)$  is to measure coincidences between the photon and the jet or leading hadron that emerges from the away-side quark from Compton scattering. Such coincidence measurements permit significant event-by-event constraints on the colliding parton kinematics. These constraints, in turn, allow important tests of the robustness of the interpretation, by seeing if measured asymmetries exhibit the predicted variations as one changes the  $x$ -value (hence, the polarization) of the colliding quark, the momentum transfer for fixed  $x$ , etc. Since a jet accompanies each direct photon, and with sufficient detector acceptance the jets can be reconstructed with good efficiency, one does not have to sacrifice significant statistical sensitivity in comparison to the inclusive measurements [?].

The possibilities with  $pp \rightarrow \gamma + jet + X$  measurements are illustrated by STAR simulations in Fig. 12. Here, a LO analysis of the parton kinematics from the detected photon and jet properties has been used to determine the quark and gluon  $x$ -values event by event. Conservative cuts requiring  $p_T \geq 10$  GeV/c and  $x_{greater} \geq 0.2$  (the latter to select the quarks with highest polarization) have been imposed on the events included in Fig. 12. The simulations illustrate both the  $A_{LL}$  values predicted for one particular parameterization of gluon polarization, and the statistical uncertainties achievable in  $x\Delta g(x)$  for three different parameterizations consistent with the DIS database. Under the minimal RHIC spin luminosity scenarios defined herein, one can distinguish readily among such distinct parameterizations. The ultimate analysis of such coincidence data will, of course, be performed within the same global NLO framework as used for the inclusive channels, but the LO simulations of Fig. 12 provide insight into the sensitivities.

One final set of channels that will be used at RHIC to probe gluon polarization involves the production of particles with open charm or bottom quarks. These proceed predominantly via gluon-gluon fusion,  $g + g \rightarrow q + \bar{q}$  (see Table 1), providing quadratic sensitivity to  $\Delta g(x)$ . The decay of heavy-flavor mesons dominates the inclusive production of leptons in the  $\sim 2 - 10$  GeV/c range, so that the highest statistics measurements of heavy flavor production will be made via the inclusive electron or muon spectra. Forward lepton detection would provide access to gluons at low  $x$ . Figure 13 shows PHENIX projections of  $A_{LL}$  uncertainties attainable via inclusive



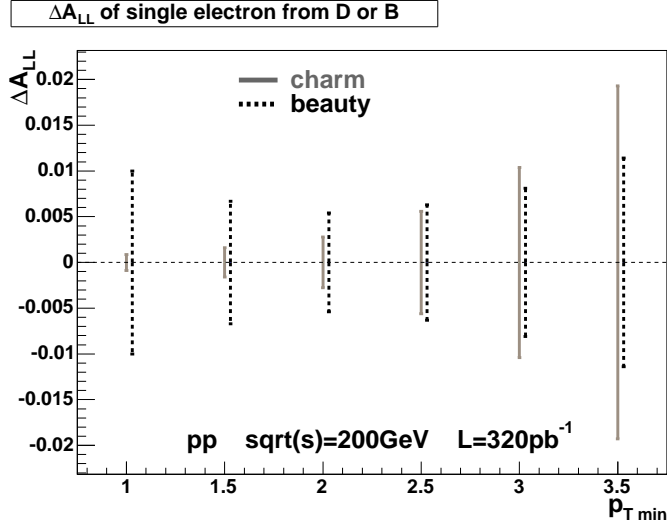


Figure 13: Projected uncertainties in the spin asymmetry for heavy flavor production for Phenix measurements.

electron detection at mid-rapidity. The experimental identification of weakly decaying heavy flavor mesons, discrimination between  $c$  and  $b$  production, and suppression of other charged hadron backgrounds could be significantly improved with upgraded inner vertex detectors by demanding a displaced vertex between the detected lepton and a daughter hadron. Other coincidence measurements can provide clean identification, at the expense of reduced branching ratios, for specific decay branches such as  $D \rightarrow K\pi$  or  $c\bar{c}/b\bar{b} \rightarrow e\mu$ . RHIC measurements of heavy flavor production, including hidden flavor in  $J/\psi$  production, will help to test the quantitative level of understanding of these channels and the assumption of gluon fusion dominance.

For all of the channels discussed above, it will be critical to achieve good statistical precision at two collision energies,  $\sqrt{s} = 200$  and  $500$  GeV. The lower energy will provide essential access to gluon  $x \gtrsim 0.1$ , a range overlapping that of ongoing studies of photon-gluon fusion in the COMPASS experiment, where DIS analyses still allow relatively large values of the gluon polarization. However, one of the most significant promises of the RHIC spin program is also to constrain the integral of  $\Delta g(x)$ , which measures the net gluon contribution to the proton spin. For this purpose, as can be seen from the simulations in Fig. 12, it is critical to extend the measurements down to  $x_{gluon} \approx 0.01$ , well below the anticipated peak in  $x\Delta g(x)$ . While this extension could be accomplished, in principle, by extending measurements at  $200$  GeV to low  $p_T$ , this approach might push the boundaries of pQCD applicability, besides running into experimental difficulties, *e.g.* in distinguishing single photons from a far more abundant  $\pi^0$  background. A more robust probe of the lowest  $x$ -values should be attainable at  $500$  GeV. Furthermore, the comparison of measurements at the same  $x$ -values but substantially different scales, reachable, for example, at  $\sqrt{s} = 200$  GeV and  $p_T \approx 4$  GeV/c vs.  $500$  GeV and  $10$  GeV/c, will test both the robustness of the pQCD treatment and our understanding of the QCD evolution of polarized gluon distributions.



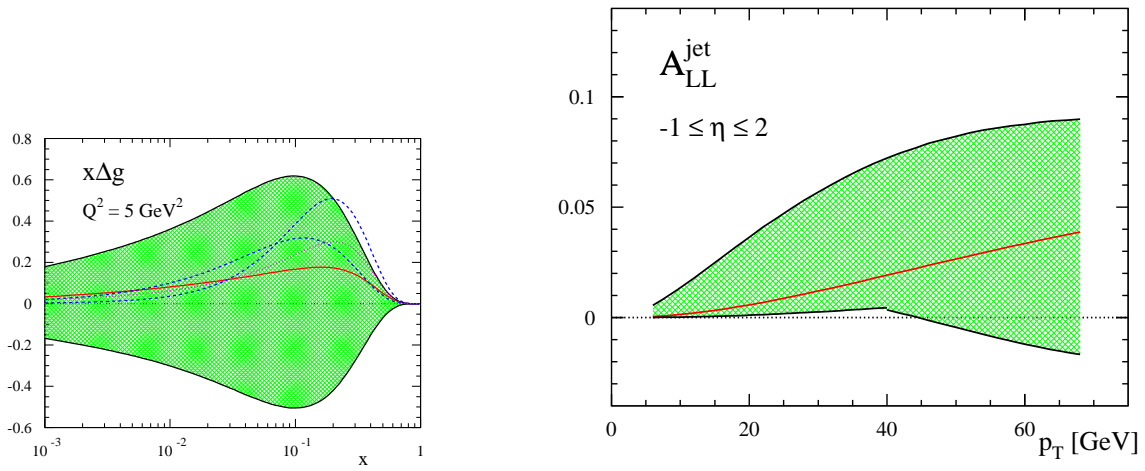


Figure 14: Same as Fig. 9, but for  $\sqrt{s} = 500$  GeV. ARE WE GOING TO USE THIS?

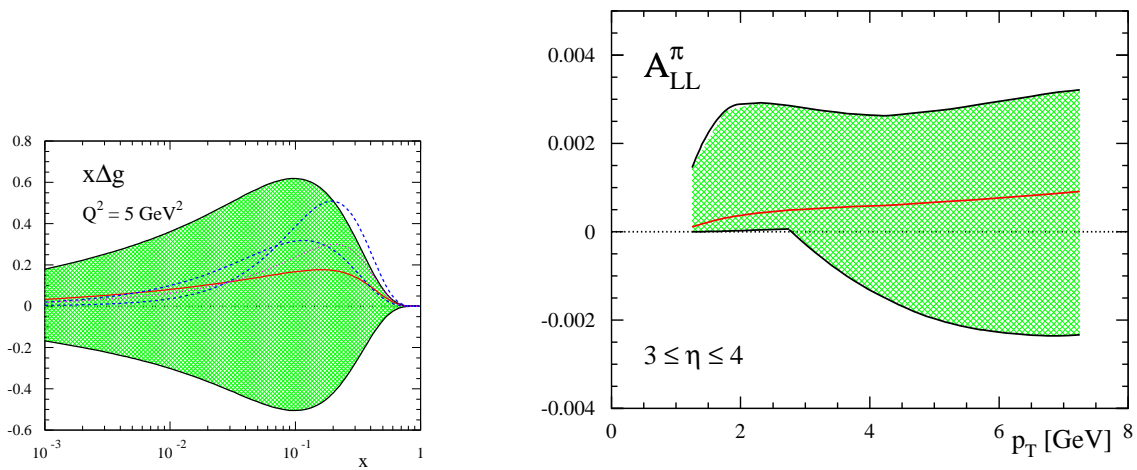


Figure 15: Same as Fig. 8, but for very forward rapidities  $3 \leq \eta \leq 4$ . ARE WE GOING TO USE THIS?

#### 2.4.2 (Anti)quarks from $W$ production (Bernd)

1. Naive pQCD picture/expectation of generation of QCD sea to be flavor symmetric ( $g - \bar{q} q$ )
2. Unpolarized result on u/d: flavor asymmetry in unpolarized sector

3. Non-perturbative QCD approach to account for this effect and discuss expectation for polarized case
4. Means to probe the flavor structure in the polarized sector:
  - a. DIS (e.g. SMC): Discuss limitations
  - b. RHIC SPIN case through W production (Figure 1: Feynman graph)
5. Discuss reconstruction of W with RHIC detectors (non-hermetic) and argue for leptonic asymmetries (RHICBOS) besides reconstruction of W rapidity. Stress forward direction
6. Show expectation for STAR (Figure 2) / PHENIX (Figure 3)
7. Summarize importance of this measurement in QCD: QCD sea production mechanism

## 2.5 Transverse spin structure

With the proton spin transversely polarized with respect to its momentum or the collision axis, a novel helicity flip *chiral-odd* twist-2 quark distribution - known as the transversity distribution,  $\delta q(x)$ , is theoretically allowed [77, 78]. Relation between the leading twist quark distribution,  $q(x)$ , helicity distribution,  $\Delta q(x)$ , and the transversity distribution,  $\delta q(x)$ , is best represented in terms of a (double) density matrix notation [79]

$$\mathcal{F}(x) = \frac{1}{2}q(x) I \otimes I + \frac{1}{2}\Delta q(x) \sigma_3 \otimes \sigma_3 + \frac{1}{2}\delta q(x) (\sigma_+ \otimes \sigma_- + \sigma_- \otimes \sigma_+) , \quad (16)$$

for the quark distribution function  $\mathcal{F}(x)$  of a nucleon. In Eq. (17), the first matrix in the direct product is in the nucleon helicity space and the second in the quark helicity space. Transversity distribution  $\delta q(x)$  is as fundamental as  $q(x)$  and  $\Delta q(x)$  in QCD, and has its unique factorization scale dependence [80, 81, 82] and angular momentum sum rule [83]. But, it is not completely independent because of the Soffer's Inequality [84],

$$|2 \delta q(x)| \leq q(x) + \Delta q(x) ,$$

which is valid for each quark flavor  $q$ . Independent measurements of  $q(x)$ ,  $\Delta q(x)$ , and  $\delta q(x)$  and their factorization scale dependence can provide a direct test of QCD dynamics and help putting limits on each other.

There is no leading twist gluon transversity distribution because it would require two units of helicity flip that the nucleon density matrix cannot provide.

Unlike the  $q(x)$  and  $\Delta q(x)$ , transversity distribution does not have the probability interpretation because the operator defining  $\delta q(x)$  represents an interference between two different quark helicity amplitudes, and can only be measured in terms of transverse spin asymmetries. Since perturbative hard processes conserve helicity, chiral-odd distributions must appear in pairs. Although transversity distribution can be in principle extracted from the measurements of *double* transverse spin asymmetries,  $A_{TT} \propto \delta q(x) \otimes \delta q'(x')$ , the asymmetries are often too small to be useful because of the dominance of gluonic contribution to the unpolarized cross sections. Therefore,  $\delta q(x)$  is better determined from observables dominated by quark-initiated partonic processes,

like  $A_{TT}$  of Drell-Yan [77, 78], or *single* transverse spin asymmetries (SSA),  $A_N \propto \delta q(x)$  with an aid of another chiral-odd unpolarized non-perturbative functions, like the Collins' function [85].

Single longitudinal-spin asymmetries for single particle inclusive production vanish due to parity and time-reversal invariance. Because of Lorentz invariance of QCD, we need at least four vectors including the spin vector to construct a physically observed SSA. With a proton spin vector  $S$  not parallel to its momentum, a hadron level SSA can be constructed to be proportional to  $\epsilon_{\mu\nu\alpha\beta} S^\mu P_A^\nu P_B^\alpha p^\beta$  with beam momenta,  $P_A$  and  $P_B$ , and observed particle momentum  $p$  in single hadron inclusive production,  $P_A(\mathbf{S}) + P_B \rightarrow h(p_T) + X$ . Significant single transverse-spin asymmetries,  $A_N$ , of ten or more percent of the unpolarized cross sections, were recorded by Fermilab E704 experiment in the beam fragmentation region of hadronic  $\pi$  production at  $p_T$  as large as GeV [86]. Since then, nonvanishing single transverse-spin asymmetries have been observed in lower energy hadronic collisions [87] and semi-inclusive lepton-hadron deeply inelastic scattering (SIDIS) [88, 89], as well as, in much higher energy  $pp$  collisions at RHIC [90].

However, theoretically, it was pointed out long time ago [91] that perturbative QCD calculation at leading power in collinear factorization formalism predicts vanishing single transverse-spin asymmetries,  $A_N \propto \alpha_s m_q / p_T$ , in inclusive single hadron production at large  $p_T$ . This is because the SSA requires a hadron-level helicity flip and is proportional to a T-odd combination of the vectors,  $A_N \propto \mathbf{S} \cdot (\mathbf{P}_A \text{ (or } \mathbf{P}_B) \times \mathbf{p}_T)$ . Within the leading twist collinear factorization formalism, the hadron helicity flip requires a quark helicity flip, which leads to the  $m_q$  dependence, while the suppression of a power of  $\alpha_s$  is due to the T-odd combination which requires a phase (or an imaginary part) from one of the two amplitudes.

Major theoretical progress has been made in last decade in understanding the “unexpected”, but, observed large SSA [?]. It is believed that SSA is a unique and excellent probe for studying parton's transverse motion and strength of color Lorentz force inside a bound nucleon.

Within the collinear factorization formalism, the parton-level helicity flip can be achieved from the interference between an amplitude of a spin (1/2) quark state and a spin (-1/2) quark-gluon composite state without requiring a quark helicity flip and the quark mass [92, 93]. The required phase for the SSA can be generated from a partonic pole, which corresponds to the non-local feature of the composite quark-gluon state and leads to a natural growth of the SSA into the fragmentation region [93, 94]. Because of the coherent interference of a single parton state and a two-parton composite state, corresponding nonperturbative matrix elements, known as high twist matrix elements, do not have probability interpretations. Since parton's transverse momentum  $k_T$  is integrated over in defining the matrix elements, quark-gluon correlation functions in collinear factorization formalism provide *averaged* (or integrated) information on partons' transverse motion, like averaged color Lorentz force experienced by the quarks [93]. These correlation functions are new physical observables for probing nonperturbative QCD dynamics.

If we go beyond the collinear factorization formalism, the necessary hadron-level helicity flip for SSA can be achieved without requiring a parton-level helicity flip because of parton's transverse motion or orbital angular momentum. A  $k_T$ -dependent (or un-integrated) parton distribution provides a direct information on both longitudinal and transverse motion of a parton inside a bound nucleon. As pointed out by Sivers [154], a  $k_T$ -dependent quark distribution of a

transversely polarized nucleon, could have both symmetric and antisymmetric terms when nucleon spin  $\mathbf{S} \rightarrow -\mathbf{S}$ . The antisymmetric term, known as the Sivers function, could be a source of nonvanishing single transverse spin asymmetries. Similarly, the Sivers mechanism can apply to the un-integrated gluon distribution to define a gluonic Sivers function [96]. The Sivers functions should be directly related to parton's transverse motion and orbital angular momentum.

Much of the predictive power of QCD is provided by the universality of nonperturbative parton distributions and/or fragmentation functions in factorization theorems for hadronic processes. In order to quantify and measure the parton's transverse motion inside a polarized nucleon, it is necessary to have a gauge invariant definition of  $k_T$ -dependent parton distributions and/or fragmentation functions, from which Sivers functions and/or Collins functions can be better defined [98, 99, 100, 101]. To extract the  $k_T$ -dependent distributions, so as Sivers and Collins functions, from physical observables, a factorization formalism in terms of these universal distributions is required. Since Sivers functions and Collins functions are sensitive to the transverse motion of partons at relatively low parton transverse momentum  $k_T$ , which is nonperturbative, another large physical scale,  $Q \gg k_T$ , is needed to ensure the  $k_T$ -dependent factorization [102]. For example, Drell-Yan pair of invariant mass  $Q$  at low transverse momentum  $q_T \sim k_T$  is a good probe of  $k_T$ -dependent quark distribution while the large  $Q$  ensures the factorization [102]. Sivers functions could also be measured in terms of asymmetric di-jet correlations at RHIC [97].

The  $k_T$ -factorization formalism was used to calculate the SSA in hadronic pion production,  $A_N$ , in terms of contributions of Sivers functions [103] and/or a combination of transversity and Collins functions [104]. Although the  $k_T$ -factorization for the inclusive pion production in hadronic collisions has not been formally proved, the calculated  $A_N$ , with  $x_F$  dependence mainly determined by the extracted Sivers and/or Collins functions from fitting low energy data, are consistent with new RHIC data at  $\sqrt{S} = 200$  GeV [106]. When pion's  $p_T$  is much larger than the typical  $k_T$  of parton's transverse motion in a nucleon,  $p_T \gg \langle k_T \rangle$ , the  $k_T$  factorization formalism used in these calculations is not expected to be valid. On the other hand, the proved collinear factorization formalism at twist-3 for hadronic  $A_N$  should be a good approximation [93]. Measurements of the SSA and its transition from the low  $p_T$  region where  $A_N \propto p_T / \langle k_T \rangle \sim k_T / \langle k_T \rangle$ , which is sensitive to the parton's transverse motion  $k_T$ , to the high  $p_T$  region where  $A_N \propto \langle k_T \rangle / p_T$ , which probes to the *averaged* transverse momentum or *averaged* color Lorentz force [93], should provide excellent information on parton's transverse motion.

With the ability to measure correlations of two hadrons (or jets) at RHIC, it is possible to separate Sivers effect, parton's transverse motion in initial-state hadron wave functions, from Collins effect, parton's spin effect in final-state hadronization. Sivers functions, Collins functions, transversity distribution and quark-gluon correlations all provide information on nucleon's spin structure that cannot be reached by measurements of longitudinal spin asymmetries. Single transverse spin asymmetry,  $A_N$ , opens a unique window to see partons' transverse motion inside a polarized nucleon.

The quark distribution function  $\mathcal{F}$  at leading-twist is expressed as[?]

$$\mathcal{F} = \frac{1}{2}q(x) I \otimes I + \frac{1}{2}\Delta q(x) \sigma_3 \otimes \sigma_3 + \frac{1}{2}\delta q(x) (\sigma_+ \otimes \sigma_- + \sigma_- \otimes \sigma_+) , \quad (17)$$

where the first matrix in the direct product is in the nucleon helicity space and the second in the quark helicity space. Here  $q(x)$ ,  $\Delta q(x)$ , and  $\delta q(x)$  are the spin average, spin, and transversity distribution functions, respectively, and their dependence on  $Q^2$  has been suppressed. Parton

distributions  $f(x)$  and corresponding helicity distributions  $\Delta f(x)$  provide excellent microscopic information on parton helicity structure inside a proton. However, complete parton helicity structure requires our knowledge of a novel helicity flip chiral-odd quark distribution - known as the transversity distribution  $\delta q(x)$ , which can only be measured in terms of transverse spin asymmetries because of its helicity flip nature. Transversity distribution  $\delta q(x)$  is as fundamental as  $f(x)$  and  $\Delta f(x)$  in QCD. But, it is not completely independent because of the Soffer's Inequality,

$$|2 \delta q(x)| \leq q(x) + \Delta q(x),$$

which is valid for each quark flavor  $q$ . Independent measurements of  $\delta q(x)$  and  $\Delta q(x)$  can help putting limits on each other. The size of  $\delta q(x)$  is crucial in generating double transverse-spin asymmetries,  $A_{TT}$ , as well as single transverse-spin asymmetries,  $A_N$ .

(Suggestion of addition by Akio)

- why it is different from longitudinal (**Jianwei**)
- Why delta-q and transversity need not to be the same
- transverse spin sum rule recently found (hep-ph/0406139 v2)
- why no gluon spin contribution in transverse case
- lattice found around 0.6 (recovery of EJ sum rule?)
- $Q^2$  evolution of transversity and difference from delta-q/delta-g
- any ideas on flavor separation of transversity? • Connections from Sivers function to parton motion/orbital angular momentum and GPD (for example Burkardt's recent works, or Jis work)
- Sivers function vanish if parton is only in s-state.
- We still lack the direct connection from (integral of?) Sivers function to the (transverse) spin sum rule. Need theoretical developments
- importance of FSI/gauge links and "modified" universality

With the proton spin ( $S$ ) transversely polarized with respect to its momentum ( $P$ ) or the collision axis, new asymmetries, in particular, the single spin asymmetries (SSA), which are otherwise forbidden in QCD, are theoretically allowed. Measurements of transverse spin asymmetries can not only provide additional information on parton's helicity distributions inside a proton, but also probe the proton structure that can never be reached by the observable of longitudinal spin asymmetries.

Single longitudinal-spin asymmetries for single particle inclusive production vanish because of parity and time-reversal invariance. However, significant single transverse-spin asymmetries,  $A_N$ , of ten or more percent of the unpolarized cross sections, were recorded by Fermilab E704 experiment in the beam fragmentation region of hadronic  $\pi$  production at  $p_T$  as large as GeV [86]. Since then, non-vanishing single transverse-spin asymmetries have been observed in lower energy hadronic collisions [87] and semi-inclusive lepton-hadron deeply inelastic scattering (SIDIS) [88, 89], as well as, in much high energy  $pp$  collisions at RHIC [90, ?].

Theoretically, on the other hand, it was pointed out long ago [91] that perturbative QCD calculation at leading power in collinear factorization formalism predicts vanishing single transverse-spin asymmetries,  $A_N$ , in single hadron inclusive production at high  $p_T$ . Because of Lorentz invariance of QCD, we need at least four vectors including the spin vector to construct a physically observed SSA. With a proton spin vector  $S$  not parallel to its momentum, a hadron level SSA can be constructed to be proportional to  $\epsilon_{\mu\nu\alpha\beta} S^\mu P_A^\nu P_B^\alpha p^\beta$  with beam momenta,  $P_A$  and  $P_B$ ,

and observed particle momentum  $p$ . However, inclusive production of a high  $p_T$  single parton in collision between two massless collinear partons does not have enough vectors to construct a parton level SSA. Additional transverse direction from parton's  $k_T$  or physical polarization of an extra gluon is necessary to connect to the spin vector  $S$  for generating the SSA. Therefore, measuring single transverse-spin asymmetries in hard collisions directly probe partons' transverse motion as well as multi-parton correlations inside a hadron. Single transverse-spin asymmetries generated by parton's transverse motion in a transversely polarized hadron is characterized by the Sivers function [107]. Single transverse-spin asymmetries can be also generated by the Collins' fragmentation function from a polarized parton [85, ?]. Within the collinear factorization formalism, single transverse-spin asymmetries are consequences of coherent multi-parton interactions characterized by high twist matrix elements, and the rising  $x_F$  dependence of the asymmetries is a natural result of the short distance dynamics [108, 94].

QCD factorization is necessary for reliable calculations of single transverse-spin asymmetries in hadronic collisions. For extracting Sivers function and Collins function, which are sensitive to the information of partons' intrinsic transverse momenta, a  $k_T$  factorization formalism is required [100]. Since dynamics at parton's typical intrinsic  $k_T$  is non-perturbative, additional hard scale, such as  $Q^2$  in SIDIS, is necessary for reliable perturbative QCD calculations of single transverse-spin asymmetries at  $p_T \sim \mathcal{O}(k_T)$  [?]. Since  $p_T$  is only large momentum scale in inclusive single hadron production in hadronic collisions and QCD factorization fails when  $p_T \sim \mathcal{O}(k_T)$ , single transverse-spin asymmetries at large enough  $p_T$  are probes of multi-parton correlations (or high twist matrix elements), which are as fundamental as parton helicity distributions [108]. The leading twist-3 quark gluon correlation function responsible for the high  $p_T$  and  $x_F$  single transverse-spin asymmetries gives a measurement of typical size of color Lorentz force inside polarized hadron [108]. When  $p_T$  decreases, non-perturbative physics at the scale of intrinsic  $k_T$  becomes more relevant the asymmetries should be roughly proportional to the dimensionless coefficient:  $p_T M_1 / (p_T^2 + M_2^2)$  where  $M_1 \sim M_2$  are typical non-perturbative hadronic scales (e.g., gluon condensate scale, or diquark mass in Ref. [?]). Measurement of single transverse-spin asymmetries as a function of  $p_T$  is an excellent probe of both perturbative and non-perturbative QCD dynamics.

- history, previous  $A_N$  measurements

In perturbative QCD at leading twist with collinear factorization,  $A_N$  is expected to be very small, on the order of  $\propto \alpha_S m_q / Q^2$  [91]. Contrary to this naive expectation, the transverse single spin asymmetry ( $A_N$ ) for  $p_\uparrow + p \rightarrow \pi + X$  was found to be 20 – 40% at large Feynman- $x$  ( $x_F$ ) at  $\sqrt{s} \leq 20$  GeV [86]. More recently, polarized p+p experiments[87] as well as semi-inclusive deep-inelastic lepton scattering experiments[88, 89] have reported measurements of transverse single-spin asymmetries (SSA) which are significantly different from zero. The intrigue surrounding the results has sparked a wave of experiments to explore the unexpectedly large signals. For example, the deep-inelastic scattering experiment HERMES has devoted a significant fraction of beam time with a transversely polarized target to study SSA in detail. At RHIC,  $A_N$  for pion production has been measured at  $\sqrt{s} = 200$  GeV over a large rapidity range[90, ?]. At forward rapidity, the large value of  $A_N$  was found to persist, even at collision energies a factor of 10 larger than earlier experiments.

The transverse SSA results from DIS experiments and RHIC, together with the observation

that the unpolarized yield at  $\sqrt{s} = 200$  GeV is well described with fixed order pQCD calculations, has inspired extraordinary theoretical progress towards understanding of transverse spin effects within the partonic scattering picture. If one takes a step beyond the collinear approach and allows partons to have transverse momentum ( $k_T$ ), there are 3 terms which can contribute to the asymmetry.

The first candidate is called the Sivers effect[107], which is an initial state correlation of the form  $\mathbf{S}_T \cdot (\mathbf{P} \times \mathbf{k}_T)$ , where  $\mathbf{S}_T$  is the transverse spin vector,  $\mathbf{P}$  is the nucleon momentum and  $\mathbf{k}_T$  is the parton transverse momentum in the nucleon. If the Sivers function were found to be non-zero, this would be the first direct evidence that the partons in the nucleons have non-zero orbital angular momentum. However, more theoretical work is required to quantitatively relate Sivers functions to parton orbital angular momentum and spin sum rules. Tremendous theoretical progress has been made in this direction recently, including ... (more about Sivers function, cite some of M. Burkardt's work? "modified" universality? etc? Depends on how much is covered by Jianwei)

The second candidate is the quark transversity distribution together with the Collins-Heppelmann effect[85, ?]. Since transversity is a chiral-odd function, measurements of transversity require another chiral-odd function. This can be another transversity distribution, or it could be a polarized chiral-odd fragmentation function (FF) which acts as an analyzer of the transversely polarized quark, called the Collins FF[85, ?].

The Collins FF displays itself as a correlation of the form  $\mathbf{S}_T \cdot (\mathbf{P}_{jet} \times \mathbf{k}_T)$  where  $\mathbf{S}_T$  is the transverse spin vector,  $\mathbf{P}_{jet}$  is the jet axis and  $\mathbf{k}_T$  is the transverse momentum of the hadron with respect to the fragmenting quark. This FF depends not only on the momentum fraction of the hadron with respect to the parton  $z = E_h/E_{parton}$ , but also on  $k_T$ . Early on it was realized that the measurement of two hadrons ( $h_1$  and  $h_2$ ) within a jet would also be sensitive to the Collins effect in a form  $\mathbf{S}_T \cdot (\mathbf{P}_{h_1} \times \mathbf{P}_{h_2})$  [?]. It was pointed out specifically that interference between s-wave and p-wave mesons can play a role[114], and so has been dubbed the "Interference FF." The Interference FF has an advantage in that the theory can work within a collinear approximation, free from gluon radiation effects which can modify the asymmetry. The Interference FF will depend on invariant mass of the two hadrons and total momentum fraction  $z = z_{h_1} + z_{h_2}$ . A model calculation[114] suggests that there will be sign change around the  $\rho$  mass for fragmentation into  $\pi^+ + \pi^-$ . A recent study[111] expects the Collins effect to be suppressed due to cancellations in quantum phases, and cannot explain very large  $A_N$  on its own.

The third involves a correlation between  $k_T$  and quark spin within the unpolarized nucleon, which is believed to be very small[100].

Besides the  $k_T$  factorization approach, theoretical calculations of twist-3 contributions in collinear factorization[108, 94] are done, resulting in three terms very similar to the three terms in the  $k_T$  factorization approach. Note that all of these mechanisms may simultaneously contribute, and have been used to explain the large  $A_N$  [109, 110, 108, 94] at  $\sqrt{s} = 20$  GeV. The mechanisms were extrapolated to  $\sqrt{s} = 200$  GeV and predicted  $A_N$  to be large, in agreement with data.

- planned measurements

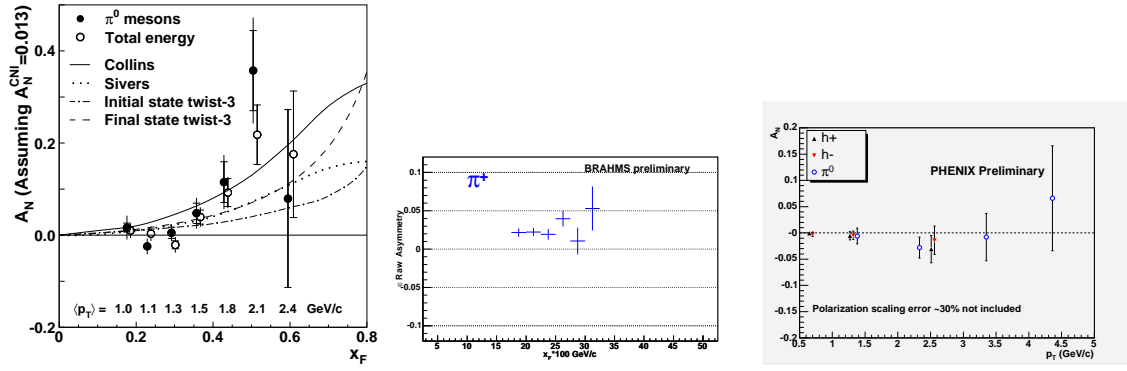


Figure 16: Single Spin asymmetry  $A_N$  for  $\pi^0$  production at STAR[90](left),  $\pi^-$  production at BRAHMS (middle) as function of  $x_F$  at forward rapidity.  $A_N$  for  $\pi^\pm$  production from PHENIX (right) as function of  $p_T$  at mid-rapidity.

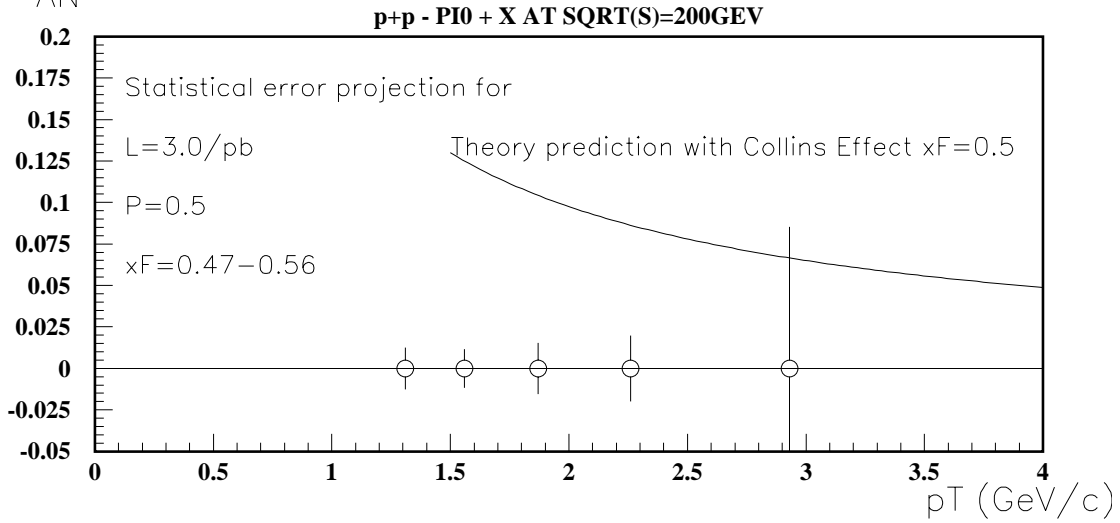


Figure 17: Statistical error projection for  $A_N$  as function of  $p_T$  for  $\pi^0$  production at STAR. A theory prediction for Collins effect (need citation!) for  $x_F = 0.5$  is also shown.

- mapping  $A_N$  in  $x_F$  and  $p_T$  plane

Higher precision measurements of  $A_N$  over a wide range of  $x_F$ ,  $p_T$ , and  $\sqrt{s}$  are necessary to understand the physics behind  $A_N$ .

The STAR experiment has reported preliminary  $A_N$  results at  $x_F < 0$  which are consistent with zero within the current experimental accuracy[?]. According to a recent study[111], the large negative  $x_F$  region is dominated by gluon Sivers effects. While the preliminary STAR data may already exclude a saturated gluon Sivers function, more data are required to establish its size. The data for Figure16 was taken with integrated luminosity of  $0.4pb^{-1}$  and polarization of 0.3. With  $3pb^{-1}$  and  $P = 0.5$ , the statistical precision will be improved by a factor of 5.

Measuring the  $p_T$  dependence of  $A_N$  test these pQCD based models, as they all predict a  $1/p_T$  dependence. Figure 17 shows the statistical error projection for  $A_N$  as function of  $p_T$  at fixed  $x_F = 0.5$  for  $\pi^0$  production at STAR.



Obtaining precise data for at very large  $x_F$  is interesting in order to test the expectation of  $A_N$  to turn over[112], due to the Soffer inequality [84] bounding the transversity distribution function.

(global fits with pp data and SIDIS too?).

- BBC[?] and ZDC asymmetries?
- Lambda and sigma polarization transfer?
  
- Away side di-jet/hadron for Sivers

To disentangle these different mechanisms behind  $A_N$ , it is required to go beyond inclusive measurements and measure either 2 final state particles or jet. For example,  $A_N$  for a jet, not a hadron, will only be sensitive to Sivers effect and Collins effects will not contribute. At forward rapidity,  $A_N$  is found to be small below  $x_F \sim 0.3$  and increase as  $x_F$  increases. If Siver's effect are responsible for the positive  $A_N$  at large  $x_F$ , it is expect to see the same positive  $A_N$  with near side two hadrons each with moderate  $x_F$  but sum  $x_{F1} + x_{F2}$  above 0.3. This measurement at forward rapidity may give the first hint on which effect dominate the  $A_N$ .

There is a class of observables for which the  $k_T$ -dependent distributions or fragmentation functions appears at leading-power, and are directly sensitive to a small measured transverse momentum[85, ?, 113]. A goal of the transverse spin program at RHIC is to disentangle the potential contributions to  $A_N$  by directly measuring the intrinsic  $k_T$  of partons in nucleon or transverse momentum in fragmentation process.

Back-to-back di-jet production in unpolarized and transversely polarized pp collisions can be used to measure the Sivers function[113]. Deviation of azimuthal angle difference  $\delta\phi = \phi_{jet1} - \phi_{jet2} + \pi$  from zero directly measure the  $k_T$  of the partons. When the jet production plane is close to the spin of the nucleon, the  $k_T$  imbalance of the parton will affect  $\delta\phi$  distribution and can give spin asymmetry  $A_N(\delta\phi) = \frac{\sigma^\uparrow(\delta\phi) - \sigma^\downarrow(\delta\phi)}{\sigma^\uparrow(\delta\phi) + \sigma^\downarrow(\delta\phi)}$ . At mid rapidity, this asymmetry may reach a few percent or more and could provide access to the gluon Sivers function, as shown in figure 18. The error bars shown in the plot (not yet here, coming) are estimated statistical uncertainty in STAR acceptance with  $3 \text{ pb}^{-1}$  and beam polarization of 0.4.

- Near side di-hadron for Collins

Measurements at RHIC are planned to study the Collins FF for jets and the Interference FF for two particles within a jet with unpolarized and transversely polarized pp collisions. Figure 19 shows.... (Matthias should write about PHENIX measurement here and some details on his plot).

By increasing the coverage of electromagnetic calorimetry in the forward direction, spin-dependent particle correlation studies are enabled in the rapidity range where large transverse single spin effects have already been observed. With calorimetry that spans  $2.5 < \eta < 4.0$ , coincident  $\pi^0 - \pi^0$  pairs can be observed at large rapidity. Near-side correlations ( $|\Delta\phi| = |\phi_{\pi,1} - \phi_{\pi,2} + \pi| \approx 0$ ) can be used to identify di-hadron fragments from a jet produced at large rapidity. In general, di-hadron fragmentation functions are not well constrained. Nonetheless, their rate

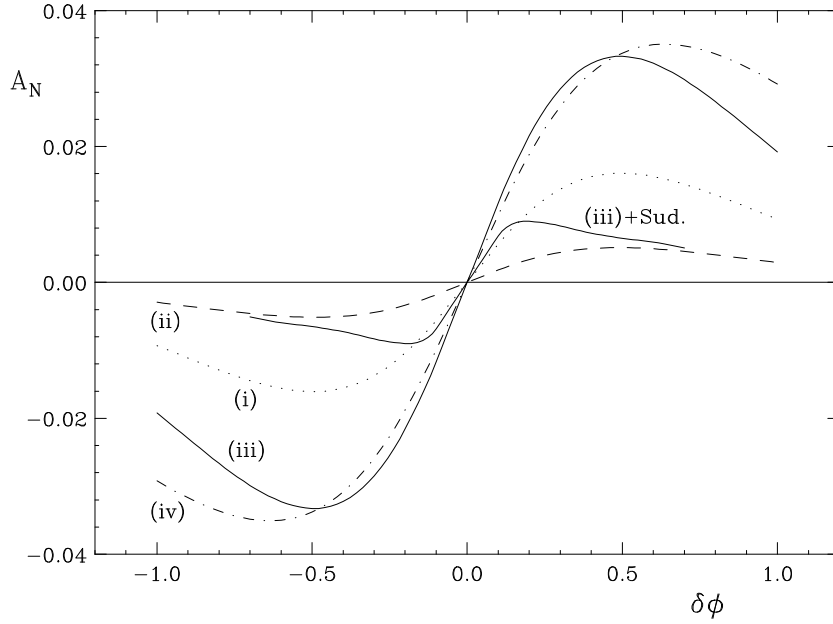


Figure 18: Predictions for the spin asymmetry  $A_N$  for back-to-back di-jet production at  $\sqrt{s} = 200$  GeV, for various different models for the gluon Sivers function. The solid line marked as “(iii)+Sud” shows the impact of leading logarithmic Sudakov effects on the asymmetry for model (iii)[113]. Error bars shown (not yet here, coming) is estimated statistical uncertainty in STAR acceptance with  $3 \text{ pb}^{-1}$  and  $P=0.4$ .

can be estimated by the Lund string model, as implemented in PYTHIA 6.222 [?].

There are two interesting scenarios to consider, each involving azimuthally correlated  $\pi^0 - \pi^0$  pairs indicative of di-hadron fragmentation of a forward jet.

In the Sivers picture  $A_N$  should be associated with the forward jet. We should therefore expect that the large  $A_N$  observed for a single  $\pi^0$  with  $x_{F1} > 0.4$  produced at  $\eta_1 \approx 3.8$  would also be present for forward jets that fragment into forward  $\pi^0 - \pi^0$  pairs having  $x_{F,1} + x_{F,2} > 0.4$ . From PYTHIA, we expect  $\approx 1.5 \times 10^4$   $\pi^0 - \pi^0$  events with  $x_{F1} > 0.25$  and  $x_{F2} > 0.15$  in the near-side jet-like peak in  $\Delta\phi$  for  $1 \text{ pb}^{-1}$  of integrated luminosity for p+p collisions at  $\sqrt{s}=200$  GeV. PYTHIA predicts the near-side  $\Delta\phi$  peak sits atop a uniform background. The signal to background ratio is approximately 1 : 1. With corrections for background, an accuracy of  $\delta A_N \approx 0.01$  could be achieved with  $3 \text{ pb}^{-1}$  of integrated luminosity and 70% beam polarization.

The Collins mechanism attributes  $A_N$  to the correlation  $(\vec{p}_1 \times \vec{p}_2) \cdot \vec{S}$  involving the momenta of two hadronic fragments of a jet and the proton spin vector. The transverse momentum associated with jet fragmentation that produces a  $\pi^0$  with  $x_{F1} > 0.4$  and  $3 < \eta_1 < 4$  can be determined by detecting a second forward  $\pi^0$  with  $x_{F2} > 0.15$  and by requiring the  $\pi^0 - \pi^0$  pair have  $|\eta_1 - \eta_2| < 0.5$ . Again, PYTHIA predicts the  $\Delta\phi$  correlation has a jet-like near-side correlation peak sitting atop a uniform background. For these kinematics, we expect  $2 \times 10^3$   $\pi^0 - \pi^0$  pairs in the near-side correlation peak for  $1 \text{ pb}^{-1}$  of integrated luminosity. If a non-zero Collins effect is observed, then larger integrated luminosity samples would be required to map out the  $x$  dependence of the transversity structure function.

In addition, Collins and Interference FF's are being measured at  $e^+ + e^-$  colliders[115] such

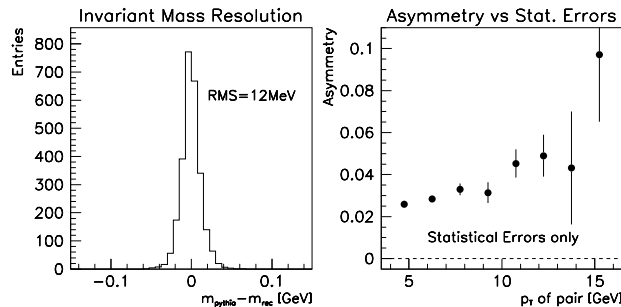


Figure 19: A statistical error projection for Collins asymmetry measurement at PHENIX with Soffer bound saturated transversity and interference FF model[114] at  $30 \text{ pb}^{-1}$  and  $P = 0.5$

as Belle, where analysis is currently ongoing[116]. Once these FF's are known, measurements at RHIC can be used to access the transversity distribution function.

- $A_{TT}(\text{jet, photon, DY})$

As stated earlier, transversity measurement always need the two chiral-odd functions, and both can be transversity. Transverse double-spin asymmetries  $A_{TT}$  for jet or tarfpdhigh-UT particle productions will be sensitive to product of 2 transversity functions. The advantage of this is that it does not require any knowledge of polarized fragmentation functions and directly access to the transversity. One the other hand, this asymmetry is highly suppressed because there is no gluon transversity, as well as double chirality flip process are color suppressed. It is important that  $A_{TT}$  measurement is done at a kinematical region where gluon contribution is small, and it requires full luminosity of the RHIC. There are other ideas to access the transversity such as production of J/psi[119] and D mesons[120]. One of cleanest way to measure the transversity is Drell-Yon process[118], but this may require the RHIC luminosity upgrade to have sufficient sensitivity.

- assess what requirements would be for key measurements here, and how they would compare to longitudinal running.

Table 2: Physics cases with transverse spin and its luminosity and polarization requirements

Channel	Luminosity [ $\text{pb}^{-1}$ ]	Polarization
Inclusive $A_N$	0.4	0.2
Mapping $A_N$ in $x_F$ and $p_T$ space	3	0.4
Sivers from di-jet	10	0.5
Transversity from di-hadron correlations within a jet	30	0.5
$A_{TT}$ of jet or high- $p_T$ particle	100	0.7
DY	1000	0.7

Table 2 is a summary of physics channels with transverse spin and its luminosity and polarization requirement.

(Do we need this part? : It is very difficult to estimate the luminosity and polarization requirement, since some of observable are multiple of two unknown functions each may be rapid-

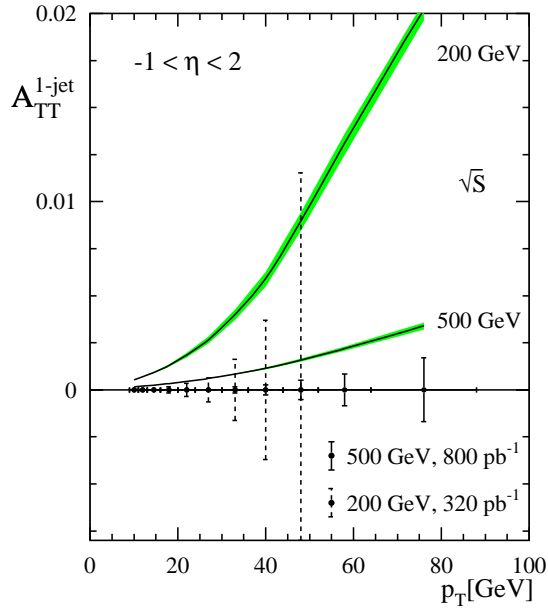


Figure 20: Maximally possible  $A_{TT}$  for single-inclusive jet production at  $\sqrt{s} = 200$  and  $500$  GeV as a function of  $p_T$ . Jet rapidities are integrated over  $-1 < \eta < 2$ . The shaded bands represent the theoretical uncertainty in  $A_{TT}$  estimated by varying scale by factor 2. Also indicated as error bars is the expected statistical accuracy with design luminosity of the RHIC [117].

ity changing, and highly differential. Also it depends on where in the kinematic regions we find non-zero asymmetries. The estimate was done here is with maximum effect allowed, or some relays on a specific model.)

There are achievable goals with a very low luminosity and polarization requirements, and we have produced physics results already. As luminosity and polarization increases, more channels will be made accessible. It is reasonable to expect we will have a chance to have both measurement of Sivers function and Transversity with  $\sim 20 pb^{-1}$  with polarization of 0.5. To archive this goal, and minimize the impact on the longitudinal spin physics cases, we will devote about 1/3 to 1/4 of beam time for the transverse spin physics. It is important to note that PHENIX and STAR have separate spin rotators, two experiments can choose longitudinal and transverse spin independently with minimum overhead to re-tune the beam with difference configuration,

Most of transverse spin measurement prefers the  $\sqrt{s} = 200$  GeV for larger asymmetries (transverse run at 2010-2012 need discussion here).

## 2.6 “What else is going on in the world”

- briefly discuss current efforts in DIS and their expected results & timelines (**Ernst, Akio**)

## 2.7 Elastic Scattering of polarized high energy protons (combined–L. True-man+Prospects)

The previous sections discuss the physics of hard scattering at RHIC with polarized protons, which can be understood as collisions of polarized quarks and gluons. The scattering is so energetic that we can use perturbative QCD to describe the interactions of the quarks and gluons, and, thus, probe the spin structure of the proton at very small distances. For example, scattering at  $Q^2=(80 \text{ GeV})^2$  probes wave lengths of 0.003 fermi. Small-angle scattering, from total cross section to  $t = -1 \text{ (GeV}/c)^2$ , probes the static proton properties and constituent quark structure of the proton, covering distances from 4 fermi [ $-t = 0.003 \text{ (GeV}/c)^2$  in the Coulomb nuclear interference (CNI) region] to a distance of  $\approx 0.2$  fermi. Unpolarized scattering shows striking behavior in this region, from the surprise that total cross sections rise at high energy, to observed dips in elastic cross sections around  $-t = 1 \text{ (GeV}/c)^2$ . Both polarimetry at RHIC and the PP2PP experiment explore this region for spin-dependent cross sections, for  $\sqrt{s}=7\text{-}500 \text{ GeV}$ , for the first time.

In the very forward region, the nuclear and electromagnetic amplitudes are of comparable magnitude, and the interference between them results in a small but significant maximum in the single transverse spin asymmetry  $A_N$  making elastic scattering in the CNI region useful for polarimetry [?]. Important results have already been obtained in the RHIC spin program in this region. There have been measurements made near RHIC injection energy (24 GeV/c) using a carbon micro-ribbon target both at the AGS (E950) and in RHIC; there have been measurements made with a 100 GeV/c beam on a carbon target and independently on a gas jet target. In addition, a measurement in the colliding beam mode has been carried out (pp2pp).

CNI scattering produces an asymmetry from the scattering of an unpolarized particle, a proton in one RHIC beam or a carbon nucleus in a fixed target, from the anomalous magnetic moment of a polarized proton, with a maximum of  $A_N = 0.04$  at  $-t = 0.003 \text{ (GeV}/c)^2$ . However, a hadronic spin-flip term can also contribute to the maximum, and this term is sensitive to the static constituent quark structure of the proton. The authors of Reference [?] remark that the helicity flip probes the shortest interquark distance in the proton, and that the helicity nonflip is sensitive to the largest quark separation in the proton due to color screening. The helicity-flip term, if present, can indicate an isoscalar anomalous magnetic moment of the nucleons [?], an anomalous color-magnetic moment causing helicity nonconservation at the constituent quark-gluon vertex [?], and/or a compact quark pair in the proton [?, ?].

The results from scattering 100 GeV/c polarized protons on carbon [?] are shown on the left side of Fig. 2.8.1. An asymmetry reaching 0.02 is observed, with a  $t$ -dependence quite different from pure electro-magnetic spin flip (the top curve in the figure). The curves use a standard CNI form [?], with the lower curve including hadronic spin flip. Results from scattering 100 GeV/c protons on a highly polarized hydrogen jet target [?] are shown on the right side of Fig. 2.8.1. In this figure, the solid line is the prediction with only electromagnetic spin flip. For pp scattering at this energy ( $\sqrt{s}=14 \text{ GeV}$ ), no hadronic spin flip is observed. Further, the preliminary measurement from the pp2pp experiment with colliding beams at RHIC is also shown on the right side of the figure. For  $\sqrt{s}=200 \text{ GeV}$ , the asymmetry is somewhat larger than the CNI curve without hadronic spin flip, but, including present uncertainty on the beam polarization (the measurement was made in 2003 before the jet provided more precise polarization results), the

result is consistent also with no hadronic spin flip for  $pp$  scattering.

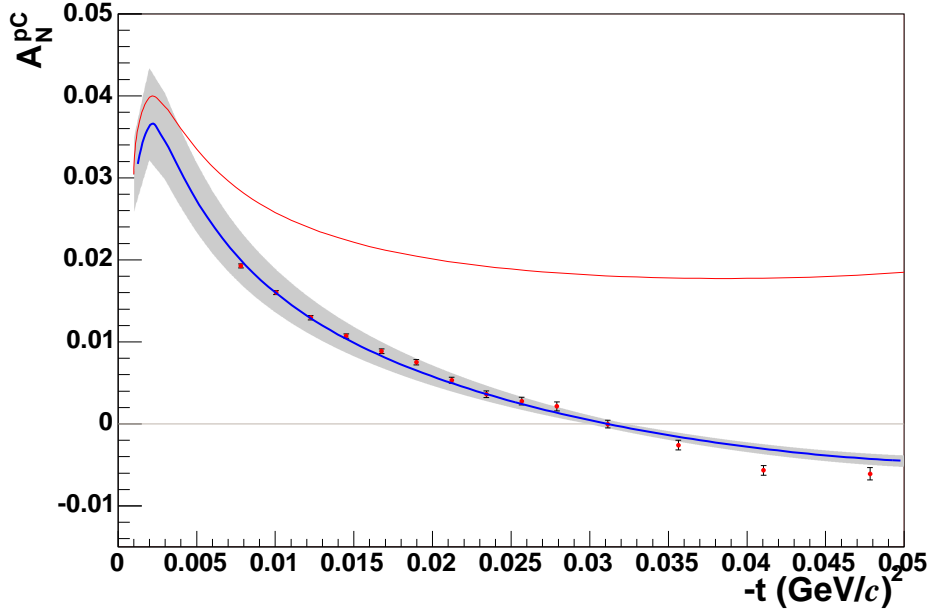


Figure 21:  $A_N(t)$  for  $pC$  elastic scattering at 100 GeV, left side [?]. The shaded band represents the systematic uncertainties of the measurement. The solid line in the band is a fit to the data including a significant hadronic spin-flip contribution (see text). The result is significantly different from the no hadronic spin-flip prediction (top curve). The right side shows preliminary measurements (solid points) of proton-proton elastic scattering with 100 GeV protons incident on a highly polarized atomic hydrogen jet target [?]. The open squares are data from E704 at Fermilab [?]. In this case, the curve with no hadronic spin flip describes the data well. The closed box is the preliminary result from the colliding beam experiment  $pp2pp$ ,  $\sqrt{s}=200$  GeV [?]. A 20% systematic uncertainty for the beam polarization is not shown. The dashed curve is the pure CNI prediction for this energy. Again, no hadronic spin flip appears to be required.

Small-angle scattering at high energy is presently understood in a Regge picture as being dominated by Pomeron exchange [?]. The Pomeron, which has the vacuum quantum numbers with charge-conjugation  $C = +1$ , can be interpreted as a two-gluon exchange. These results for  $A_N$  for carbon and proton targets imply that the isospin 0 Reggeons (which include the Pomeron) have a significant spin flip coupling for the carbon target. The  $I = 1$  Regge poles for the proton target scattering must be sufficiently strong to nearly cancel the  $I = 0$  contribution at this energy. The couplings required have been determined and indicate that asymptotically the Pomeron will contribute about 10% spin-flip; i.e. the cancellation leading to no spin-flip in  $pp$  at 100 GeV/c will go away as the energy increases [?].

Many other measurements can be made at RHIC, for elastic scattering and also for diffractive scattering with rapidity gap measurements. The two-spin transverse asymmetry in the CNI region, for example, is sensitive to a C-parity odd exchange, referred to as the Odderon [?]. For larger  $t$ , a steep exponential fall with momentum transfer, characteristic of pomeron exchange matches on to an approximate  $t^{-8}$  dependence at larger  $-t$  in the unpolarized cross sections. The latter has a natural interpretation in terms of three vector exchanges between pairs of valence quarks. Whether these individual scatterings should be thought of as single gluons, or as (at least in part) perturbative exchanges in color-singlet configurations remains to be seen. This profile is fairly stable with energy, even as the details of its shape change. The observation of a stable

profile in polarized elastic scattering at RHIC would surely initiate a new class of theoretical investigations. Lastly, the dramatic spin dependence of proton-proton elastic scattering at moderate  $-t$  observed in the Argonne and BNL experiments of twenty years ago remains an outstanding puzzle [?]. This could also be explored at RHIC.

At higher energy, such as at the LHC, the CNI region becomes inaccessible. The minimum  $-t$  reachable with colliding beams depends on scattering the protons out of the beams. For fixed  $-t$ , the scattering angle falls as  $1/p_{\text{beam}}$ , whereas the beam size falls more slowly as  $1/\sqrt{p_{\text{beam}}}$ . Roughly, this limits an experiment at the LHC to  $-t > 0.01$  (GeV/c)<sup>2</sup>.

## 2.8 Physics beyond the Standard Model

Single beam helicity asymmetries violate parity and give access to searches for potential physics beyond the Standard Model, for example for quark substructure, new neutral gauge bosons present in some supersymmetric models, and supersymmetric particle production. In general, parity violation searches can compete with the sensitivity of much higher energy unpolarized colliders, and a parity violation signal beyond known electo-weak effects would be a decisive signal for new physics. Furthermore, if a new interaction is discovered for example at the LHC, and lower-lying masses are accessible at RHIC, RHIC will be able to explore the chiral structure of the new interaction. We discuss the potential new particles and mass ranges where RHIC can contribute in this section. For sensitivities we generally consider the target luminosity for  $\sqrt{s}=500$  GeV of  $\sim 1$  fb<sup>-1</sup> and a large acceptance detector, for example STAR with high luminosity capability. However, a suggested new detector[?] and an order of magnitude higher luminosity from a RHIC II can also be considered. Fig. 22 shows the single beam helicity asymmetry  $A_L$  for single jet production versus the transverse energy of the jet, for the Standard Model and for extensions of the Standard Model (SM). The SM predicts a parity violating asymmetry, around  $E_T = M_W/2$  for  $W \rightarrow 2 \text{ jet}$  production, and from QCD-electroweak interference. Indeed, the data in the peak provides a calibration for the SM effects. The figure uses the top RHIC energy, our target luminosity for this energy, and the acceptance of the STAR detector [126]. The sensitivities shown do not include detector efficiency. Two extensions of the SM are considered: quark compositeness, and new neutral gauge bosons that appear in several string-derived models [131](non-supersymmetric models may be also constructed [132]).

The quark compositeness curves in the figure use a compositeness scale  $\Lambda=2$  GeV and maximal parity violation  $\eta = \pm 1$ . Composite models of quarks and leptons [122] generally violate parity, since the scale of compositeness  $\Lambda_c \gg M_W$ . The present limit from unpolarized collisions, at the Tevatron, is [123]  $\Lambda \cong 1.6$  TeV. Due to the direct sensitivity to parity violation, RHIC can compete with the much higher energy Tevatron. Further, if an anomalous parity violation signal is observed, it would be a definitive observation of new physics. The limits of sensitivity for  $\Lambda$  in the contact model of quark compositeness [126] are tabulated in Table 3 for RHIC, the Tevatron and the LHC, with  $L \sim 1$  fb<sup>-1</sup> integrated luminosity the RHIC spin target for  $\sqrt{s}=500$  GeV, and  $L \sim 10$  fb<sup>-1</sup> a potential target for RHIC II.

Also shown in Fig. 22 are  $Z'$  curves. In the framework of supersymmetric models with an additional Abelian  $U(1)'$  gauge, it has been shown [133] that the  $Z'$  boson could appear with a relatively low mass ( $M_Z \leq M_{Z'} \leq 1$  TeV) and a mixing angle with the standard  $Z$  close to zero. The effects of different representative models are also shown in Fig. 22 (see Ref. [127])

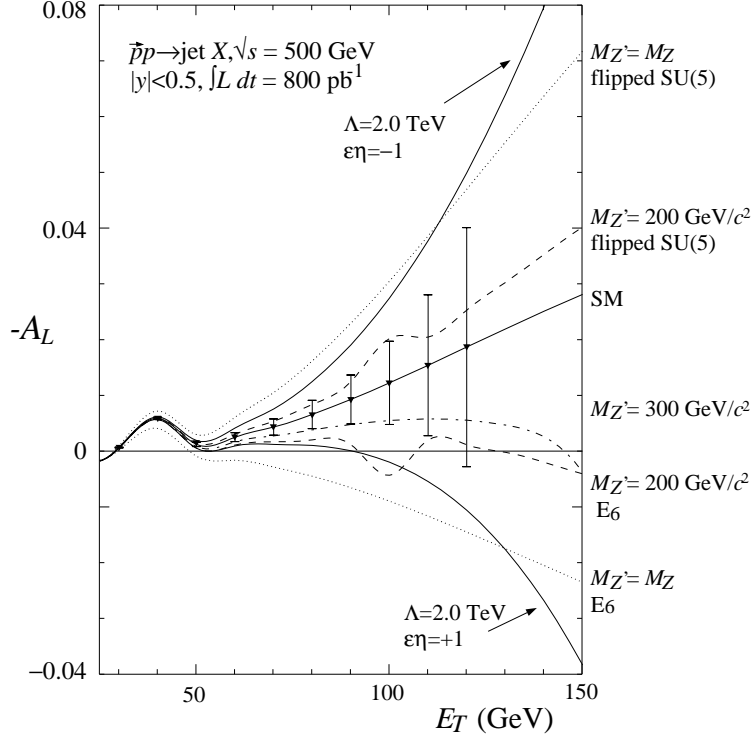


Figure 22:  $A_L$ , for one-jet inclusive production in  $\vec{p}p$  collisions versus transverse energy, for  $\sqrt{s} = 500 \text{ GeV}$ . The solid curve with error bars represents the SM expectations. The error bars show the sensitivity at RHIC for  $800 \text{ pb}^{-1}$ , for the STAR detector. The other solid curves, labeled by the product of  $\epsilon\eta$ , correspond to the contact interaction at  $\Lambda = 2 \text{ TeV}$  [126]. The dashed and dotted curves correspond to different leptophobic  $Z'$  models. The calculations are at leading order.

for details). RHIC covers some regions of parameters space of the different models that are unconstrained by present and forthcoming experiments, and RHIC would also uniquely obtain information on the chiral structure of the new interaction. In Ref. [128], it has been suggested to extend this study to the collisions of polarized neutrons, which could be performed with colliding at RHIC polarized  ${}^3\text{He}$  nuclei [134]. The authors argue that, in case of a discovery, a compilation of the information coming from both polarized  $\vec{p}\vec{p}$  and  $\vec{n}\vec{n}$  collisions should constrain the number of Higgs doublets and the presence or absence of trilinear fermion mass terms in the underlying model of new physics.

There are also a number of other examples. Using the RHIC target luminosity ( $1 \text{ fb}^{-1}$ ) at  $\sqrt{s}=500 \text{ GeV}$ , parity violating asymmetry in the production of  $XX$  from supersymmetric sparticles with mass to  $75 \text{ GeV}$  would be observable [135]. Another example is to search for a transverse asymmetry for  $W$  or  $Z$  boson production, where the SM prediction is very small [141].  $W^\pm$  and  $Z^0$  production in  $p^\uparrow p$  collisions at RHIC is expected to have good sensitivity on  $\mathcal{L}_{SM} - \delta\mathcal{L}$  interference at the parton level due to strong correlation between the proton spin and the polarization of high- $x$  valence quarks, that participate in the gauge boson production [145]. This asymmetry could arise from anomalous electroweak dipole moments of quarks [141, 142, 143]. The RHIC sensitivity can improve present experimental limits by a factor  $\sim 5-10$  [143]. These limits do not approach the SM expectations, and a signal would be direct indication of new



Collider	$\sqrt{s}(\text{TeV}) L(\text{fb}^{-1})$	$\Lambda$ (TeV)	
RHIC $p \uparrow p$	0.5	1	3.3
	0.5	10	5.5
Tevatron limit	1.8	0.5	1.6
Tevatron $p\bar{a}r p$	2.0	30	5
LHC $pp$	12	100	30

Table 3: Limits on quark compositeness ( $\Lambda$ ) at 95% CL for different colliders. RHIC uses  $P=0.7$ , STAR detector acceptance, single jet production, parity violation signal with maximal parity violation for compositeness. The Tevatron and LHC use the deviation from the Standard Model for the jet inclusive cross section versus  $p_T$  [126]. **What systematic errors are assumed??**

physics.

## 2.9 Connection to eRHIC (Abhay)

Addition of a high energy high polarization lepton (electron/positron) beam facility to the existing RHIC Complex to be able to collide with its hadron beam would dramatically increase RHIC's capability to do precision QCD physics. Such a facility with 10 GeV/c polarized electron/positron has been proposed and is called eRHIC. There are many direct and indirect connections between the RHIC spin program and the eRHIC. We categorize them in to two groups:

- *Direct connections to RHIC Spin:* In these the physics observables measured by the existing RHIC spin physics program will be measured in complementary kinematic regions, or in some cases augmented to complete the understanding of the nucleon spin.
- *Indirect Connection to RHIC Spin:* These include measurements not possible with RHIC Spin, but are of significance to understanding QCD with spin in general or nucleon spin in particular.

### 2.9.1 Direct Connections

Directions connections between RHIC Spin and eRHIC are made on three principle topics. The measurement of polarized gluon distribution, the measurement of quark-anti-quark distributions, and on transverse physics measurements.

For polarized gluon distribution measurement eRHIC enables increase in the kinematic range and precision, particularly in the low  $x$ . At eRHIC the polarized gluon distribution will be measured using a) the scaling violations of spin structure function  $g_1^{p/n}$  and b) di-jet and high  $p_T$  di-hadron production in the photon gluon fusion process.[?] RHIC spin measurements discussed before will predominantly most significant in in the medium-high  $x$  range  $x > 10^{-2}$ , while eRHIC will complement them with precision on low  $x$  ( $x < 10^{-2}$ ) all the way to  $x \sim 10^{-4}$ .

RHIC Spin will for the first measure model independently the polarized quark and anti-quark

distributions using single longitudinal asymmetry measurements in pp scattering via ( $W^\pm$ ) production. Analysis of these asymmetries would give us  $\Delta u, \Delta \bar{u}, \Delta d, \Delta \bar{d}$ ???. The quark-anti-quark separation in such a way is not possible in fixed target DIS where the virtual  $\gamma$  is the propagator of the force which can not differentiate between quarks and anti-quarks. However at high enough energy-DIS at eRHIC, in addition virtual  $W^\pm$  also get exchanged. If  $\Delta q = u, \bar{u}, d, \bar{d}$  are known by early next decade from RHIC Spin, eRHIC will be able to continue this program in to explore the heavy quarks i.e. identify the spin contributions from  $\Delta c/\bar{c}$  and  $\Delta s/\bar{s}$ . Of course, traditional methods to get quark flavor distributions, semi-inclusive DIS measurements using measurements of charged and neutral pions and kaons will also continue, (quark-anti-quark unseparated) would give access to low  $x$  flavor separation in parton distributions as in presently fixed target DIS experiments.

Transversity is the last as yet unmeasured spin structure function discussed in detail in ???. The measurements at RHIC with pp scattering will be made using measurements of Collins Fragmentation Function (CFF), Interference Fragmentation Functions (IFF) and if very large luminosities are achieved, also with Drell Yan (DY) processes.[?] These measurements will be made in the center of mass energy range from 200 to 500 GeV. The eRHIC will make a complimentary set of measurements, with high precision using CFF and IFF measurements, not unlike those made by the HERMES collaboration presently.

Diffraction physics with polarized pp and ep: More connections?

## 2.9.2 Indirect Spin Connections

In addition to the measurements eRHIC will do that will extend or complement the investigation of nucleon spin with RHIC Spin, there is another class of nucleon spin and other helicity related measurements that could also be made with eRHIC. A partial list includes:

- Measurement of spin structure functions  $g_1$  of the proton and neutron and the difference between them that tests the Bjorken spin sum rule. eRHIC will do this with accuracies that will for the first time start competing and challenging the experimental systematic uncertainties at the level of 1- 2%. Low  $x$  phenomenon has been one of the most exciting aspect of the physics that developed in the unpolarized DIS measurements in the last decade, and eRHIC will probe that low  $x$  kinematics for the first time with polarized beams
- eRHIC will be the only possible facility in the foreseeable future at which QCD spin structure of the virtual photon could be explored. The process employed for this investigation is that of photon gluon fusion[?].
- Deeply virtual compton scattering (DVCS) for final state photons as well as other vector mesons measured using almost complete acceptance ( $4\pi$ ) detectors has been suggested as a preliminary requirement toward the measurement of the Generalized Parton Distributions (GPDs). A series of different GPD measurements may be required eventually to extract the orbital angular momentum of the partons. This is the last part of the nucleon spin puzzle which we may have to address after the spin of the gluon is understood. Although the theoretical formulation is not yet ready, it is expected that by the time the eRHIC comes on line, there will be a formalism available to take the measured GPDs and determine the orbital

angular momentum of partons. These measurements at eRHIC will be complementary, at much higher energy scales, to those being planned at Jefferson Laboratory with its 12 GeV upgrade plan.

- Drell-Hern Gerasimov spin rule measurements presently underway at Jefferson laboratory [?] and at MAMI [?] are mostly at low value of  $\nu$  [?]. While the significance of the contribution the spin sum rule from high  $\nu$  is small, absolutely no measurements exist beyond the value of  $\nu > \approx 1$  GeV. eRHIC will extend direct measurements of the high  $\nu$  components to up to 500 GeV.
- Precessions measurements of spin structure functions in very high  $x \sim 0.9$  region could be part of the eRHIC physics program with specially designed detectors as has been discussed in [?].

In summary, while the physics programs with polarized proton beams at RHIC and eRHIC have much in the way of complementarity of physics measurements, the way to success at eRHIC passes through a successful RHIC spin program not only at 200 GeV in center of mass but also at 500 GeV in center of mass.

### 3 Accelerator performance (Mei & Wolfram)

Polarized proton beams were accelerated, stored and collided in RHIC at a proton energy of 100 GeV. The average store luminosity reached  $4 \times 10^{30} \text{cm}^{-2} \text{s}^{-1}$ , and the average store polarization 40% (see Tab. 4). Over the next 4 years we aim to reach the Enhanced Luminosity goal for polarized protons, consisting of an average store luminosity of

- **$60 \times 10^{30} \text{cm}^{-2} \text{s}^{-1}$  for 100 GeV** proton energy, and
- **$150 \times 10^{30} \text{cm}^{-2} \text{s}^{-1}$  for 250 GeV** proton energy,

both with an **average store polarization of 70%**. Tab. 4 gives a projection of the luminosity and polarization evolution through FY2008. Luminosity numbers are given for 100 GeV proton energy and one interaction point, with collisions at two interaction points. For operation with more than two experiments, the luminosity per interaction point is reduced due to an increased beam-beam interaction. For each year the maximum achievable luminosity and polarization is projected. Projections over several years are not very reliable and should only be seen as guidance for the average annual machine improvements needed to reach the goal. We assume that 10 weeks of physics running are scheduled every year to allow for commissioning of the improvements and development of the machine performance.

In Fig. 23 the integrated luminosity delivered to one experiment is shown through FY2012 for two scenarios: 10 weeks of physics operation per year, and 10 weeks of physics operation every other year. For every projected year shown in Fig. 23 the weekly luminosity starts at 25% of the final value, and increases linearly in time to the final value in 8 weeks. During the remaining weeks the weekly luminosity is assumed to be constant. For the maximum projection the values in Tab. 4 are used as final values until FY2008. For later years the FY2008 values are assumed with no further improvement. The minimum projection is one third of the maximum projection, based on past experience in projecting heavy ion luminosities [146].

Table 4: Maximum projected RHIC polarized proton luminosities through FY2008. Delivered luminosity numbers are given for 100 GeV proton energy and one interaction point, with collisions at two interaction points. 10 weeks of physics operation per year are assumed.

Fiscal year		2002A	2003A	2004A	2005E	2006E	2007E	2008E
No of bunches	...	55	55	56	79	79	100	112
Protons/bunch, initial	$10^{11}$	0.7	0.7	0.7	1.0	1.4	2.0	2.0
$\beta^*$	m	3	1	1	1	1	1	1
Peak luminosity	$10^{30}\text{cm}^{-2}\text{s}^{-1}$	2	6	6	16	31	80	89
Average luminosity	$10^{30}\text{cm}^{-2}\text{s}^{-1}$	1.5	3	4	9	21	53	60
Time in store	%	30	41	41	50	53	56	60
Max luminosity/week	$\text{pb}^{-1}$	0.2	0.6	0.9	2.8	6.6	18.0	21.6
Max integrated luminosity	$\text{pb}^{-1}$	0.5	1.6	3	20	46	126	151
Average store polarization	%	15	30	40	45	65	70	70
Max $\text{LP}^4/\text{week}$	$\text{nb}^{-1}$	0.1	5	23	120	1180	4330	5190

For the scenario with 10 weeks of physics operation per year, the assumed proton energy is 100 GeV until FY2008, and 250 GeV thereafter. For the scenario with 10 weeks every other year, the assumed proton energy is 100 GeV throughout the entire period to reach the physics goal.

For the scenario with 10 weeks of physics operation every other year, the final values are not increased in years without proton operation, since no time is available to develop the machine performance. Thus in our projections we reach the Enhanced Luminosity goal in FY2008 with 10 week physics operation per year, but need until FY2011 with 10 weeks of physics operation every other year. For operation at 250 GeV proton energy, the luminosity projections in Tab. 4 need to be multiplied by 2.5. We expect no significant reduction in the averages store polarization after full commissioning of polarized proton ramps to 250 GeV.

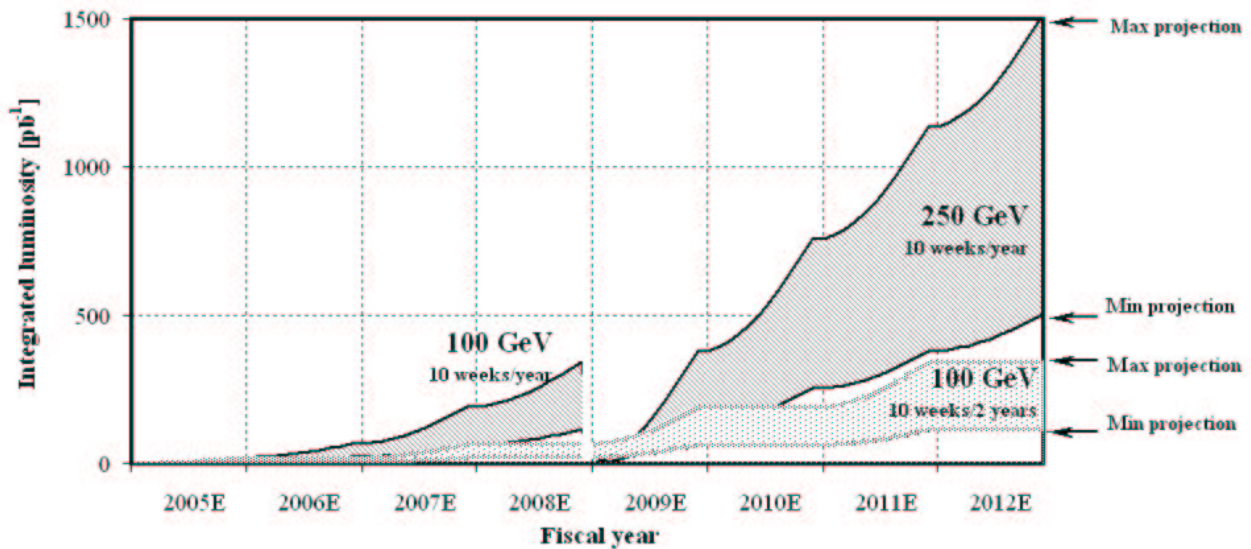


Figure 23: Minimum and Maximum projected integrated luminosity through FY2012. Delivered luminosity numbers are given for one interaction point, with collisions at two interaction points. For the scenario with 10 weeks of physics operation per year, the assumed proton energy is 100 GeV until FY2008, and 250 GeV thereafter. For the scenario with 10 weeks every other year, the assumed proton energy is 100 GeV throughout the entire period.

### 3.1 Polarization limitations

The RHIC beam polarization at 100 GeV is currently limited by the AGS beam polarization transmission efficiency of about 70%, and the source polarization. With the installation of a new solenoid in FY2005, the source polarization is expected to increase from 80% to 85%. The existing AGS polarized proton setup includes a 5% warm helical snake for overcoming imperfection spin depolarizing resonances and an RF dipole for overcoming 4 strong intrinsic spin resonances. This setup has two drawbacks:

1. All the weak intrinsic spin resonances are crossed with no correction and result in a total depolarization of about 16%.
2. Operation with the RF dipole still leads to about 15% depolarization.

In addition, the AGS has shown a dependence of the beam polarization on the bunch intensity. These shortcomings can be overcome with the installation of a new AGS cold snake, to be initially commissioned in 2005. With a scheme that combines the AGS cold snake of 15%, and the AGS warm snake of 5%, depolarizations at all imperfection and all intrinsic spin resonances should be eliminated, making the AGS spin transparent with the exception of some mismatch at injection and extraction [147].

Obtaining 70% beam polarization in RHIC at 250 GeV is challenging because of strong intrinsic and imperfection resonances beyond 100 GeV. Betatron tunes and orbit distortions have to be controlled precisely to avoid depolarization due to snake resonances. Simulations show that orbit distortions have to be corrected to less than 0.3 mm rms. Orbit errors are introduced due to misalignments and remain if the orbit cannot be corrected completely. A realignment of the entire ring is scheduled for the 2005 summer shutdown. Efforts continue to improve the existing beam position monitor system, and the orbit correction techniques. A beam-based alignment technique is under development. With the existing hardware and software, orbit distortions of 1 mm rms were achieved, as measured by the beam position monitors. Acceleration of polarized proton beams beyond 100 GeV is planned in 2005. The result of this machine development effort will provide guidance for the tolerable levels of machine misalignments and orbit errors.

### 3.2 Luminosity limitations

A number of effects limit the achievable luminosity. Currently the bunch intensity is limited to about  $1 \times 10^{11}$  to maintain maximum polarization in the AGS. This restriction should be removed with the AGS cold snake. With intense bunches the beam-beam interaction will limit the luminosity lifetime. With bunches of  $2 \times 10^{11}$  protons and 2 interaction points, the total beam-beam induced tune spread will reach 0.015. Operation with more than two collision will significantly reduce the luminosity lifetime. High intensity beams also lead to a vacuum breakdown, caused by electron clouds. In the warm sections, NEG coated beam pipes are installed, that have a lower secondary electron yield, and provide linear pumping. In the cold regions, additional pumps are installed to improve the vacuum to an average value of  $10^{-5}$  Torr before the cool-down starts. With the PHENIX and STAR detector upgrades, the vacuum system in the experimental regions will also be improved.

Time in store can be gained through faster machine set-up, a reduction in system failures, and

the injection of multiple bunches in each AGS cycle. We project that the time in store can be increased to about 100 hours per week, or 60% of calendar time.

### 3.3 Polarimetry

Beam polarization measurements in RHIC provide immediate information for performance monitoring, and absolute polarization to normalize the experimental asymmetry results. Two types of polarimeters are used. Both are based on small angle elastic scattering, where the sensitivity to the proton beam polarization comes from the interference between the electromagnetic spin-flip amplitude that generates the proton anomalous magnetic moment and the hadronic spin non-flip amplitude, and possibly a hadronic spin-flip term.

One type of polarimeter uses a micro-ribbon carbon target, and provides fast relative polarization measurements. The other type uses a polarized atomic hydrogen gas target, and provides slow absolute polarization measurements. In addition, both PHENIX and STAR have developed local polarimeters that measure the residual transverse polarization at their interaction points. These polarimeters are used to tune and monitor the spin rotators that provide longitudinal polarization for the experiments. They polarimeters are discussed in the Experiments section.

The fast proton-carbon polarimeter was first developed at the IUCF and the AGS [148]. It measures the polarization in RHIC to  $\Delta P = \pm 0.02$  in 30 seconds. Measurements taken during a typical store in 2004 are shown in Fig. 24. A carbon ribbon target is introduced into the beam, and the left-right scattering asymmetry of recoil carbon ions is observed with silicon detectors inside the vacuum. The silicon detectors observe the energy and time of flight of the recoil particles near  $90^\circ$  [149]. The detector selects carbon ions with a momentum transfer in the coulomb-nuclear interference (CNI) region,  $-t = 0.005 - 0.02 \text{ (GeV/c)}^2$ . In this region, the interference of the electromagnetic spin flip amplitude and the hadronic non-flip amplitude produces a calculable  $t$ -dependent asymmetry of 0.03 to 0.02. The cross section is large, so that the sensitivity to polarization is large. A term from a hadronic spin flip amplitude is also possible and is reported in Ref. [148]. This contribution is not calculable, so that this polarimeter must be calibrated using a beam of a known polarization.

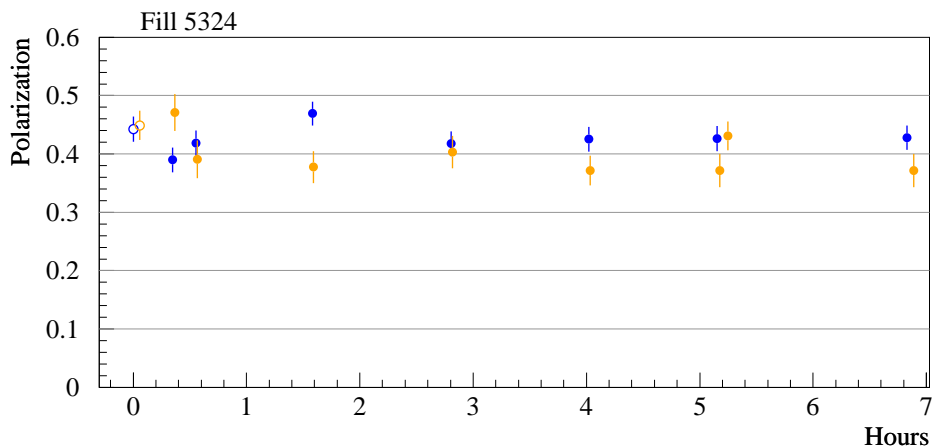


Figure 24: Measured polarization during one store of RHIC in 2004.

A polarized atomic hydrogen gas jet target was used for the first time in RHIC in 2004 [150].

The atoms are polarized with the Stern-Gehrlach process to give electronic polarization, with rf transition to select proton polarization. The atoms are focused in the RHIC beam region to 6 mm FWHM using the atomic hydrogen magnetic moment. A Breit-Rabi polarimeter after the RHIC beam measures the polarization by cycling through rf transition states. The polarization was determined to be  $0.92 \pm 0.02$ , including correction for the measured 2% molecular fraction (4% nuclear fraction) that is unpolarized. Silicon detectors observe a left-right asymmetry for proton-proton elastic scattering in the CNI region, similar to the p-carbon polarimeters. By measuring the asymmetry with respect to the target polarization sign, flipped every 8 minutes in 2004 by changing rf transitions, we measure the analyzing power for proton-proton elastic scattering. This is shown in Fig. 25. This (preliminary) result from 2004 provides the most sensitive measurement of  $A_N$ , as can be seen in the figure. By then measuring the left-right asymmetry with respect to the beam polarization sign, flipping each bunch (every 200 ns), we obtain the absolute beam polarization. The absolute beam polarization was measured to about  $\Delta P/P = 7\%$  in 2004 (preliminary).

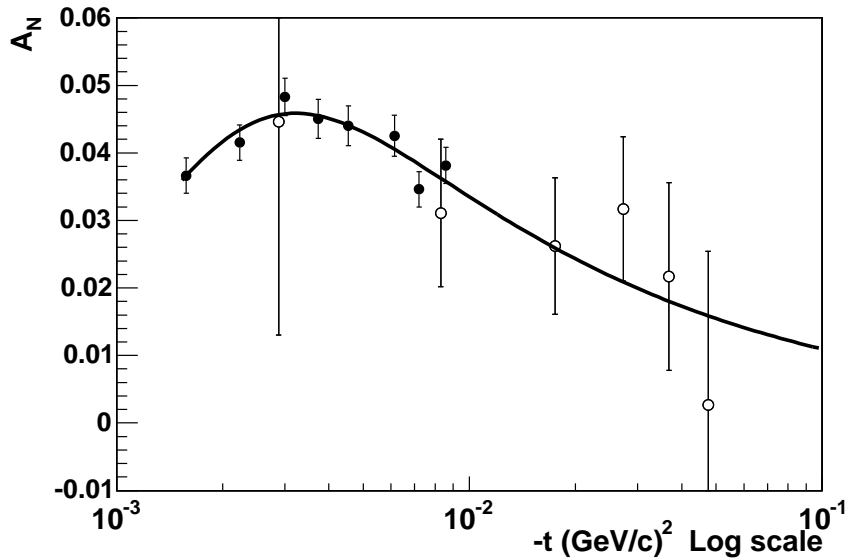


Figure 25:  $A_N$  for proton-proton elastic scattering in the CNI region, measured using the polarized atomic hydrogen jet target in RHIC [150]. The open circles are data from E704 at Fermilab [151].

A remaining issue is whether the carbon polarimeter calibration can be used for different detectors, from year to year, or whether it will be necessary to recalibrate each year using the jet target. We can also choose to use the jet target as the RHIC polarimeter, with the carbon polarimeter used for corrections, for example for different polarization of the bunches and for a polarization profile of the beams.

### 3.4 Long-term perspective

A number of ideas are pursued for long-term improvements of the machine performance. RHIC II aims at increasing the heavy ion luminosity by an order of magnitude through electron cooling. For protons, cooling at store is not practical but pre-cooling at injection might be beneficial. A

further reduction of  $\beta^*$ , especially at 250 GeV proton energy appears possible. Some benefits may also come from stochastic cooling, currently developed for heavy ions. We expect a luminosity improvement of a factor 2-5 for polarized protons for RHIC II.

With a new interaction region design, the final focusing quadrupoles can be moved closer to the interaction point, thus allowing to squeeze  $\beta^*$  further. This, however, makes some space unavailable for the detectors. Additional increases in the luminosity may come from a further increase in the number of bunches, to close to 360, as is planned for eRHIC, or operation with very long bunches. The latter requires a substantial R&D effort, as well as a new timing system for the detectors.

## 4 Experiments (Brahms, PHENIX, and STAR)

### 4.1 PHENIX

RHIC has made great strides towards providing high luminosity beams of highly polarized protons. To make statistically sensitive asymmetry measurements with low systematics requires well understood detectors; clean, highly selective triggers, reliable measurements of beam luminosity and polarization, and the ability to take and analyze data at high rates. In this section we discuss the current and proposed capabilities of the PHENIX detector in the context of meeting the challenges of the spin program.

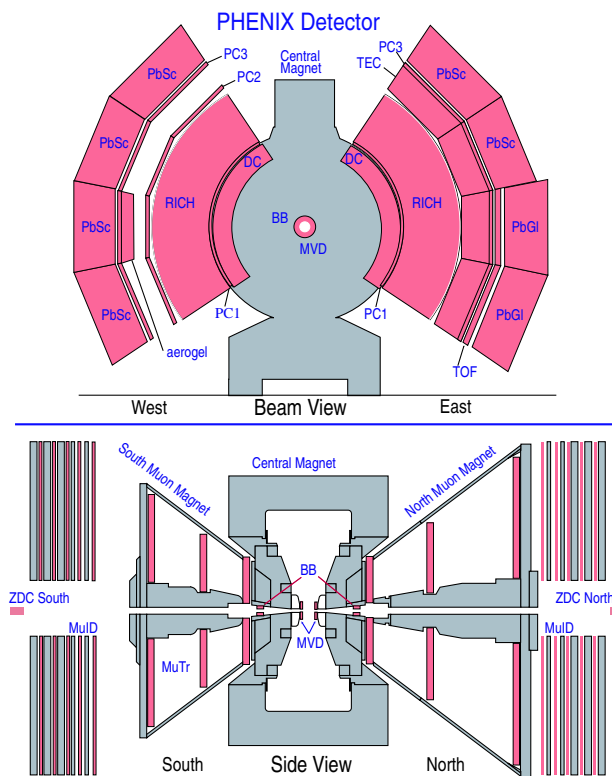


Figure 26: Plan view and side views of the PHENIX detector.



Figure 27: The  $\pi^0$  mass spectrum in  $p_T$  bins 1-2 GeV/c, 2-3 GeV/c, 3-4 GeV/c and 4-5 GeV/c. Events are collected using the high  $p_T$  photon trigger of the EMCal. The combinatorial background is  $\sim 30\%$  for a  $p_T$  range from 1 to 2 GeV/c, and  $\sim 5\%$  for  $p_T > 5$  GeV/c. The two-photon invariant mass resolution is 8.5% in the first  $p_T$  bin and 6.4% in the last  $p_T$  bin.

As shown in Fig. 26, the PHENIX detector comprises four instrumented spectrometers (arms) and three global detectors. The east and west central arms are located at central rapidity and instrumented to detect electrons, photons, and charged hadrons. The north and south forward arms have full azimuthal coverage to detect muons. In addition, the zero degree calorimeters (ZDCs) and beam-beam counters (BBCs) measure the time and position of the collision vertex.

#### 4.1.1 PHENIX Central Arms

The PHENIX central arms consist of tracking systems for charged particles and electromagnetic calorimetry. We require a calorimeter with the ability to distinguish isolated photons from those from  $\pi^0$  decays over a large  $p_T$  range. A thorough understanding of the calorimeter and associated triggers is vital for these measurements.

The calorimeter (EMCal) is the outermost subsystem of the central arms, located at a radial distance of  $\sim 5$  m from the beam line. Each arm covers a pseudorapidity range of  $|\eta| < 0.35$  and an azimuthal angle interval of  $\Delta\phi \approx 90^\circ$ , and is divided into sectors containing a lead scintillator (PbSc) calorimeter or lead glass (PbGl) calorimeter. Each calorimeter tower subtends a solid angle  $\Delta\phi \times \Delta\eta \sim 0.01 \times 0.01$ , ensuring the two photons from  $\pi^0$  decay are resolved up to a  $p_T$  of 12 GeV/c. Shower profile analysis can extend this  $p_T$  range beyond 20 GeV/c. The energy calibration used the position of the two photon invariant mass peak from  $\pi^0$  decay, the energy deposit from minimum ionizing charged particles traversing the EMCal (PbSc), and the momentum determined by the tracking detectors of electrons and positrons identified by the ring-imaging Čerenkov detector. These studies show that the accuracy of the energy measurement was within 1.5%. At a  $p_T$  of  $\sim 11$  GeV/c, this uncertainty translates into a systematic error on the  $\pi^0$  cross-section of  $\sim 12\%$ . The effective energy resolution was deduced by comparing the measured energy and momentum for identified electrons and positrons and from the widths of the  $\pi^0$  invariant mass peaks as shown in Fig.27. Their widths varied with  $p_T$  from 7% to 10% (PbSc) and 12% to 13% (PbGl).

The number of recorded high- $p_T$   $\pi^0$ 's is enhanced by a high- $p_T$  trigger which uses threshold discrimination applied to sums of the analog signals from  $2 \times 2$  groupings (tiles) of adjacent EMCal towers. A plot of the trigger efficiency as a function of deposited energy is shown in Fig. 29. The efficiency reached a plateau of  $0.78 \pm 0.03$  at  $\sim 3$  GeV, which is consistent with the geometrical acceptance of the active trigger tiles, and was reproduced by Monte Carlo calculations. Charged particle contamination in the photon sample was minimized by using information from the PHENIX ring-imaging Čerenkov and tracking detectors [?].

The calorimeter and trigger performance have enabled PHENIX to make many significant measurements within the first few years of running. Measurements have been made of the cross-section and double-helicity asymmetry for  $\pi^0$  production (see Figures. ??, ??). The prompt

Figure 28: The decomposed nonphotonic spectrum extracted using the converter method with statistical uncertainties corresponding to  $\sim 20 \text{ pb}^{-1}$  and one central arm.

Figure 29: The normalized efficiency of the high- $p_T$  trigger a function of energy. The red line shows the predictions of a Monte Carlo simulation.

photon production cross section in pp collisions has also been measured ([161], [162]) and the NLO pQCD calculation is in good agreement with the data ???. In Ref. [162], a photon isolation cut was applied as a first step towards a spin asymmetry measurement. The cut reduces the level of background photons diluting the analyzing power. With increased luminosity we expect improved precision on these measurements, and the first measurements of the double spin asymmetry  $A_{LL}^{pp \rightarrow \gamma X}$ .

The EMCAL will also be used for measurements of inclusive electron asymmetries from semi-leptonic decays of charm and beauty produced mainly by gluon-gluon fusion in  $pp$  scattering. Electrons in the central arms are identified by the RICH detector (Čerenkov threshold for  $\pi^\pm \approx 4.9 \text{ GeV}/c$ ) and the EMCAL. The yield of electrons can be categorized into nonphotonic electrons mainly from semi-leptonic decays of charm and beauty (see Fig.28), and photonic electrons mainly from gamma conversion and Dalitz decays of neutral mesons such as  $\pi^0$  and  $\eta$  [155].

*The transverse single-spin asymmetries of neutral pions and non-identified charged hadrons, shown in Fig.21 (page 28 of the combined report), have been measured at mid-rapidity ( $x_F \approx 0$ ). The asymmetries seen in this previously unexplored kinematic region are consistent with zero within statistical errors of a few percent. The dominant partonic processes in both  $\pi^0$  and charged hadron production in the current kinematic region are gluon-gluon and gluon-quark scattering. This gluon dominance suggests that any potential contribution from mechanisms involving transversity [152] should be significantly suppressed, and the current measurement is probing gluon-sensitive models such as that given in [153, 154].*

*Ref. to Fig.4, page 13 of the combined report.*

#### 4.1.2 Muon Arms

The systematic study of  $J/\psi$  production at Relativistic Heavy Ion Collider (RHIC) energies with wide  $p_T$  and rapidity coverage should provide crucial tests of  $J/\psi$  production models. In addition, the RHIC proton-proton results provide a baseline for studying cold and hot nuclear matter in proton-nucleus and nucleus-nucleus collisions using  $J/\psi$  yields as a probe. PHENIX has two forward spectrometers devoted to the characterization of single and di-muon events in the forward rapidity regions. The central magnet poles act as a hadron absorber in front of a radial field magnet with acceptance from  $1.2 < \eta < 2.2$  (2.4) in the South (North) spectrometer. Inside the magnetic field, there are three high resolution cathode strip tracking chambers capable of determining space point position to  $< 100$  microns. Downstream of each spectrometer magnet is a Muon Identifier (MuId) which covers the same rapidity region. They consist of five layers of steel

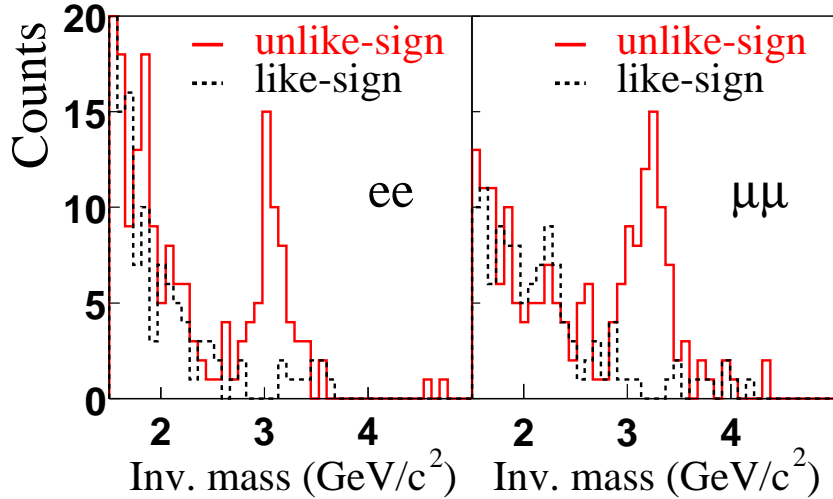


Figure 30:

absorber sandwiching both horizontal and vertical proportional tubes, with the total thickness of the absorber material of 60cm. The minimum muon momentum able to penetrate all 5 gaps is 2.7 GeV/c, and the pion rejection factor at 3 GeV/c is  $2.5 \times 10^{-3}$ . The MuID is also used as trigger counter as well as identifying the muon. It uses full hit information of the detector, 9 cm in horizontal and vertical direction for each gap, and determines whether a muon candidate road exists for each beam crossing. Triggers on single and double tracks with sufficient depth in the MuID are passed to the global level-1 trigger of PHENIX.  $J/\psi$  yields in the muon arm were obtained by reconstructing  $\mu^+ - \mu^-$  pairs. Muon tracks were reconstructed by finding a track seed in the MuID and matching it to clusters of hits in each of the three MuTr stations. The momentum was determined by fitting, with a correction for energy loss, the MuID and MuTr hit positions and the vertex position.  $J/\psi$  mass resolution of 160 MeV/c<sup>2</sup> in  $p - p$  collisions has been achieved as shown in Fig.30. Together with the di-electron measurement in the central arm, PHENIX has published the  $p_T$ , rapidity and total cross-sections for  $J/\psi$  at  $\sqrt{s} = 200$  GeV/c shown in Fig.31.

#### 4.1.3 PHENIX Local Polarimetry and Relative Luminosity Detectors

Local polarimeters, sensitive to the transverse polarization at collision, were used to set up the spin rotators, and to monitor the beam polarization direction at the PHENIX experiment. The local polarimeters utilized a transverse single spin asymmetry in neutron production in  $p-p$  collisions at  $\sqrt{s} = 200$  GeV [156]. For vertically polarized beam a left-right asymmetry is observed for neutrons produced at very forward angles, with no asymmetry for production at very backward angles. A fully longitudinally polarized beam produces no asymmetry.

Neutrons with  $E_n > 20$  GeV and production angle  $0.3 < \theta_n < 2.5$  mrad were observed by two hadronic calorimeters located  $\pm 18$  meters from the interaction point (ZDC or Zero Degree Calorimeter [157]). Scintillator hodoscopes at 1.7 interaction length provided the neutron position at the ZDC, and thus the neutron production angle and azimuthal angle  $\phi = \arctan(x/y)$  with  $\hat{y}$  vertically upward. The  $\hat{x}$  axis forms a right handed coordinate system with the  $\hat{z}$  axis

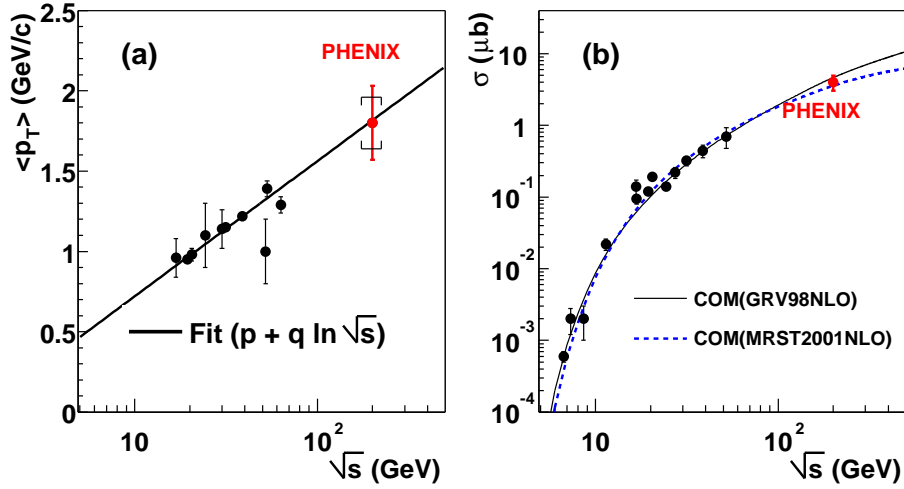


Figure 31:

Figure 32: The raw asymmetry normalized by the beam polarization,  $\epsilon/P$ , as a function of azimuthal angle  $\phi$ , for forward neutron production. The solid points and curve correspond to the spin rotators off (transverse polarization) and the open points and dashed curve correspond to the spin rotators on (longitudinal polarization). Curves are sine function fits to the data, representing possible transverse polarization. The data are for special runs used to set up the spin rotators, where the blue (yellow) polarization was 0.24 and 0.33 (0.08 and 0.28), for spin rotators off and on, correspondingly.

defined by the beam direction for forward production. Figure 32 shows the observed asymmetry, for the spin rotators off and on, for the blue and yellow beams. With the spin rotators off, a left-right asymmetry is observed from the vertically polarized beam. With the spin rotators on, the measured transverse polarization, averaged over the run, was  $\langle P_{Bx} \rangle = 0.033 \pm 0.019$ ,  $\langle P_{By} \rangle = 0.008 \pm 0.020$ ,  $\langle P_{Yx} \rangle = -0.020 \pm 0.013$  and  $\langle P_{Yy} \rangle = 0.054 \pm 0.017$ , out of  $\langle P \rangle = 0.27$ . The double spin transverse polarization was  $\langle P_{Bx} P_{Yx} \rangle = (0.4 \pm 1.1) \cdot 10^{-3}$  and  $\langle P_{By} P_{Yy} \rangle = (-0.2 \pm 0.8) \cdot 10^{-3}$ , compared to  $\langle P_B P_Y \rangle = 0.07$ . Therefore, with the spin rotators on, the transverse asymmetry is greatly reduced, indicating a high degree of longitudinal polarization: the longitudinal fraction of the beam polarization was 0.99 and 0.98 for the blue and yellow beams, respectively. A separate run with the spin rotators set to give radial polarization confirmed the direction of the polarization for each beam.

In addition to the polarization of the beams, we require information on the intensities and possibly the profiles of the colliding bunches. This knowledge is necessary because the spin structure information we seek is manifested in correlations between the rate or angular distribution of specific final states and the spin direction(s) of the colliding protons. However, spin correlated differences in the production rate of particular final states may appear even in the absence of a physics asymmetry simply because the luminosities of the colliding bunches are different. This necessitates measurements of the relative luminosities of the colliding bunches which are

insensitive to the beam polarization to greater precision than the smallest physics asymmetry to be measured. PHENIX is currently equipped with two forward detectors, the BBCs and ZDCs [157, 158], which are primarily sensitive to the  $pp$  inelastic and double-diffractive cross-section respectively. They have demonstrated an insensitivity to the colliding bunch polarization at the level of  $2 \times 10^{-3}$  and have a high rejection of backgrounds. Scalars attached to these detectors which can count a single event per crossing form the successful foundation of the relative luminosity measurements suitable for the current  $pp$  luminosity. As RHIC approaches its design luminosity,  $2 \times 10^{32} \text{ cm}^{-2}\text{s}^{-1}$ , there will be multiple  $pp$  interactions per bunch crossing, and ambiguities in determining whether the event vertices lay within the PHENIX acceptance. We believe these complications may be overcome by incorporating additional information from the detectors which is linear in the rate such as phototube charge and multiplicity. Bunch profile information from existing RHIC instrumentation, new analysis techniques and trigger logic will be used to minimize the effects of vertex ambiguities on the determination of relative luminosity. Also, a dedicated low cost, small acceptance detector is being considered to address these issues.

#### 4.1.4 PHENIX DAQ and Computing

The PHENIX DAQ has been designed from inception as a parallel pipelined buffered system capable of very high rates of nearly deadtime-less data-taking. In this kind of design, data is sent from each detector element in multiple parallel streams, buffered at each stage in the chain to smooth out fluctuations in rate, and then uses simultaneous read and write for the highest possible throughput with existing technology. At present, PHENIX has achieved data rates of over 4 kHz, and with improvements in noise reduction PHENIX should be able to approach the peak design interaction trigger rate of 12.5 kHz. Such high DAQ rates are crucial for providing the capability and flexibility to record the many different kinds of interesting rare events at RHIC.

In addition to the RHIC Computing Facility (RCF) at BNL, PHENIX has regional computing centers in the world. The biggest one is the RIKEN CC-J, Computing Center in Japan. The CC-J has comparable computing resources to the PHENIX part of the RCF, CPU power and data storage capability with the High Performance Storage System (HPSS). The main missions of the CC-J for the PHENIX experiment are the primary simulation center, an Asian regional computing center, and a computing center for the spin physics. In run5, it will be used for the reconstructed data production of all the polarized proton collision data. Raw data are sent from PHENIX to the CC-J as much as possible with using WAN connection in parallel to the RCF HPSS. The sustained transfer rate of WAN connection between BNL and RIKEN was confirmed about 10 MB/s and recently is reaching up to 60 MB/s while sustained PHENIX DAQ rate is expected to be 60 - 100 MB/s. Remaining data are sent after the DAQ period through the WAN, and with tape transfer on plains as a backup plan. A bottleneck of the WAN was upgraded very recently, so the transfer rate may reach up to 100 MB/s.

## 5 Detector upgrades

*physics goals and table of physics for upgrades to be inserted ...*

### 5.0.5 Muon trigger

The flavor separation of quark and anti-quark polarizations for up- and down-quarks, requires separate high statistics measurements of inclusive lepton counting rate asymmetries:  $A_L^{W^+ \rightarrow \mu^+}(p_T)$  and  $A_L^{W^- \rightarrow \mu^-}(p_T)$ . These measurements translate into the following experimental requirements for the PHENIX muon arms: (a) superior event selection capability in order to reduce the 10MHz collision rate to the data archiving bandwidth available in PHENIX (b) the ability to assign the correct proton polarization (that is bunch crossing number) to a given W-event candidate, (c) tracking resolution to correctly determine the lepton charge sign and (d) good signal to background ratios in the off-line analysis.

Extensive Monte Carlo simulations including a full GEANT simulation of the muon arms show that the existing muon spectrometers are capable of defining a clean sample of W events for the off-line analysis: a requirement of  $p_T > 25$  GeV on the transverse momentum of the final state decay muon will remove most of the collision and beam related backgrounds; we expect a signal to background ratio of about 2:1.

A new first level muon trigger is required to improve the online performance of the present first level muon trigger. Rejection factors achieved in the present PHENIX muon trigger, based on information from the existing muon identifier system are about  $R=250$ . Measurements at the luminosities needed for the W-physics program will require rejection factors of  $R>5000$ .

The new first level muon trigger in PHENIX will be based on three fast trigger stations which will be added to each of the PHENIX muon spectrometers. The triggers stations will use Resistive Plate Chamber (RPC) technology developed for the muon trigger in the CMS experiment at LHC. In addition new front end electronics for the existing muon tracker chambers will make it possible to introduce muon arm tracking information in the future muon trigger. Information from the three RPC stations and the muon tracker will be processed in standard PHENIX first level trigger processor boards. The boards carry large Xilinx Fast Programmable Gate Arrays (FPGAs) and can carry out a fast online momentum measurement based on the tracking information from the RPCs and the muon trackers. In addition a timing cut will be applied in the RPC front-end electronics to remove beam backgrounds.

Detailed beam background measurements and beam-loss Monte Carlo simulations were carried out to confirm that the substantial steel absorbers in PHENIX introduce a large asymmetry in the incoming and outgoing beam backgrounds which can be exploited for triggering purposes. Overall the expected rejection power of the new muon trigger is expected to be well above the required level of  $R>10000$ .

### 5.0.6 Silicon VTX

PHENIX Collaboration proposes to construct a Silicon Vertex Tracker (VTX) in the next few years. The VTX will substantially enhance the physics capabilities of the PHENIX central arm spectrometer. Our prime motivation is to provide precision measurements of heavy-quark production (charm and beauty) in A+A and p(d)+A collisions, and polarized p+p collisions. In addition, addition of a large acceptance central detector capable of monitoring multiplicities of hadronic final states along with their directions, will enhance PHENIX's capability to study Jets

in hadron-hadron collisions. These are key measurements for future RHIC program, both for heavy ion physics which intends to study the properties of dense nuclear medium created in their collisions, and for the exploration of the nucleon spin-structure through polarized pp collisions. While the detailed list of physics measurements possible with the VTX detector are discussed elsewhere [1], the the principle measurements associated with polarized pp program are:

- $\Delta G/G$  from charm and beauty production in polarized pp scatterin
- x dependence of  $\Delta G/G$  from  $\gamma$ -Jet correlations

The PHENIX detector has been described before in Section???. The heavy quark production has been measured by PHENIX only indirectly through the observation of inclusive (decay) electrons. These measurements are limited in accuracy by the systematic uncertainties resulting from possible large electron backgrounds originating from Dalitz Decays and photon conversionsaThe measurements are statistical in nature, and one uses different models to distinguish between charm and beauty contributions. The VTX detector will provide tracking with a resolution of  $< 50\mu\text{m}$  over a large coverate both in rapidity  $|\eta| < 1.2$  and in azimuthal angle ( $\Delta\phi \sim 2\pi$ ). A significantly improved measurement of heavy quarks in pp collisions is deemed possible over a wide kinematic range with the VTX.

The proposed VTX detector will have four tracking layers. For the inner two lateres we propose to use silicon pixel devices with  $50 \times 425 \mu\text{m}$  channels that were developed for the ALICE experiment at CERN/LHC. Our preferred technology for outer two detector layers is a silicon strip detector developed by the BNL instrumentation division which consists of  $80\mu\text{m} \times 3 \text{ cm}$  strips layed to achieve an effective pixel size of  $80 \times 1000 \mu\text{m}$ . We plan to use SVX4 readout chip developed at FNAL for the strip readout. The main aim in using ready technology has been to shorten the cost and the time for the R&D that for such a project could ordinarily be rather high and long, respectively.

PHENIX anticipates that the project will be mainly funded by two agencies: the DOE Office of Nuclear Physics and RIKEN Institute of Japan. While RIKEN funding has been available since 2002, it is anticipated that the construction funds for the Strip Layers will be available from DOE starting FY06 and the project will get constructed and commissioned in the RHIC - Run 8 which presently is expected to be a long Au+Au run.

### 5.0.7 Nosecone calorimeter

The PHENIX detector at RHIC has been designed to study hadronic and leptonic signatures of the new states of matter in heavy ion collisions and polarized proton collisions. The baseline detector measures muons in two muon spectrometers located forward and backward of mid-rapidity, and measures hadrons, electrons, and photons in two central spectrometer arms each of which covers 90 degrees in azimuth and  $\pm 0.35$  unit of rapidity where the existing electromagnetic calorimeters are installed. Further progress requires extending rapidity coverage for hadronic and electromagnetic signatures beyond the limits set by already built central spectrometer, in particular upgrading the functionality of the PHENIX forward spectrometers to include photon and jet measurement capabilities.

Figure 33: Longitudinal structure of a single NCC tower.

A forward spectrometer upgrade is being proposed with the objective of introducing new detector capabilities and greatly enhancing present capabilities for PHENIX in the forward direction. When completed it will result in a nearly ten-fold increase to its rapidity coverage for photons and to some extent for hadrons, jet detection and better triggering capabilities. Newly acquired access to forward production of inclusive jets, direct photons or Drell-Yan pairs at large  $x_F$  in nucleon-ion collisions at RHIC will provide a new window for the observation of saturation phenomena expected at high parton number densities and its importance in the evolution of the partonic distribution functions.

The PHENIX Forward Upgrade is constrained by the existing muon spectrometer configuration including its wire chambers, hadron absorber walls and magnet yokes. The core element of the proposed upgrade are compact tungsten calorimeters with silicon pixel readout and fine transverse and longitudinal segmentation built to identify and measure forward electromagnetic activity and provide jet identification and coarse jet energy measurements. The principal performance aspect of the NCC is its ability to run in the unassisted mode (without upstream tracking).

The NCC is extremely dense sampling calorimeter using tungsten absorber interleaved with silicon readout layers. Geometrical constraints of the PHENIX detector call for a very nontraditional and challenging design. Tungsten has a very short radiation length and a large absorption/radiation length ratio. The electromagnetic shower develops in the very first few cm of the calorimeter depth thus allowing the implementation of both electromagnetic and shallow hadronic compartments within the available 20 cm of space. To further suppress the hadronic contribution to the energy seen in the electromagnetic compartment the electromagnetic calorimeter will be only  $\sim 10$  radiation length deep. The tungsten in the first 16 layers has a thickness of 2.5 mm ( $\sim 0.7 X_0$ ), and 1.6 cm in the remaining 6 layers serving as hadron rejecter - shower tail catcher (Fig.33).

Limiting the depth of the electromagnetic compartment to  $\sim 10$   $L_{rad}$  serves to improve the em/hadron shower discrimination but will also result in the loss of resolution for high energy showers. To minimize the potential negative impact of this decision on the performance of the energy measurements the same lateral granularity will be retained in both electromagnetic and hadronic compartments ( $1.5 \times 1.5$  cm<sup>2</sup> pixels). Measurements in both compartments will combine to recover the resolution.

*plan for high luminosity (relative luminosity, trigger rates, bandwidth, backgrounds, crossing ambiguities, vertex, ... to be inserted ...*

*text for funding issue to be inserted ...*

### 5.0.8 Projection for future measurements

In the PHENIX, single electrons from semi-leptonic decays from charm and beauty meson are measured in mid-rapidity region. These 2 sources will be decomposed by VTX upgrade (looking



at DCA distribution). This picture shows the ALL error of electrons from charm and beauty. Each points shows ALL error of the pT region above pTmin.

Ref. to Fig.8, page 19 of the combined report.

Ref.[160]

## 5.1 Star (Steve)

RHIC Spin Report for DOE: Outline of STAR Detector Section 4.2 (each major heading represents 1 paragraph)

### A. Overview of STAR detector and collaboration

1. Figure: cross section of STAR, emphasizing subsystems already added with spin program as primary driver. 2. Brief description of BBC's and FPD's and their use for spin program: Figure of BBC asymmetries vs. CNJ asymmetries, with STAR rotators on and off. 3. Status of barrel and endcap EMCs; timeline to complete BEMC readout. 4. Use of EMCs in p+p triggers for jets, photons, ( $0$ , W, J/ $\psi$ ). 5. Recent expansions of collaboration interests in spin program.

### B. Performance of STAR EMC's

1. Figure: photo of insertion of last BEMC module; photo of completed EEMC. 2. Figure: event display of dijet with TPC and BEMC; jet neutral/total ET spectrum from BEMC + TPC in 2004 p+p run. 3. Figure: typical SMD profile and ( $0$  invariant mass spectrum from EEMC for 2004 p+p run. 4. Brief description of ongoing algorithm development for ( $0$  and ( $\psi$  ID.

### C. Motivation for STAR upgrade needs for spin program

1. Improved forward tracking: TPC resolution limits at 40 GeV/c, especially in endcap region; need for W charge sign discrimination, improved e/h discrimination for W program; fast tracking minimizes TPC pileup ambiguities. 2. Figure: charge sign discrimination improvements with model forward tracking vs. TPC alone. 3. Forward extension of calorimetry: primary motivation from studying low-x gluons in nuclei; benefits to spin program in low-x and large ( $\sqrt{s}$ ) access. 4. Benefits to spin from planned STAR upgrades driven by other physics: TOF pion ID for interference fragmentation studies of transversity (?); DAQ upgrades, rate capability, space-saving for forward tracker; Heavy Flavor Tracker for improved ID of open charm, beauty, sensitivity to quark mass terms in QCD, etc.

### D. Plan for forward tracking improvements

1. Figure: schematic illustrations of inner silicon barrels and disks, and of endcap GEM tracker under consideration. 2. Envisioned timeline (rough), staging and integration with other STAR upgrades. 3. Organization of efforts and institutions involved; R&D activities under way. 4. Rough estimate of resources needed to design/construct. 5. Open issues to address: optimum tradeoffs between coverage and cost; resolution impact of material at endcap of TPC; others?

### E. Plan for Forward Meson Spectrometer

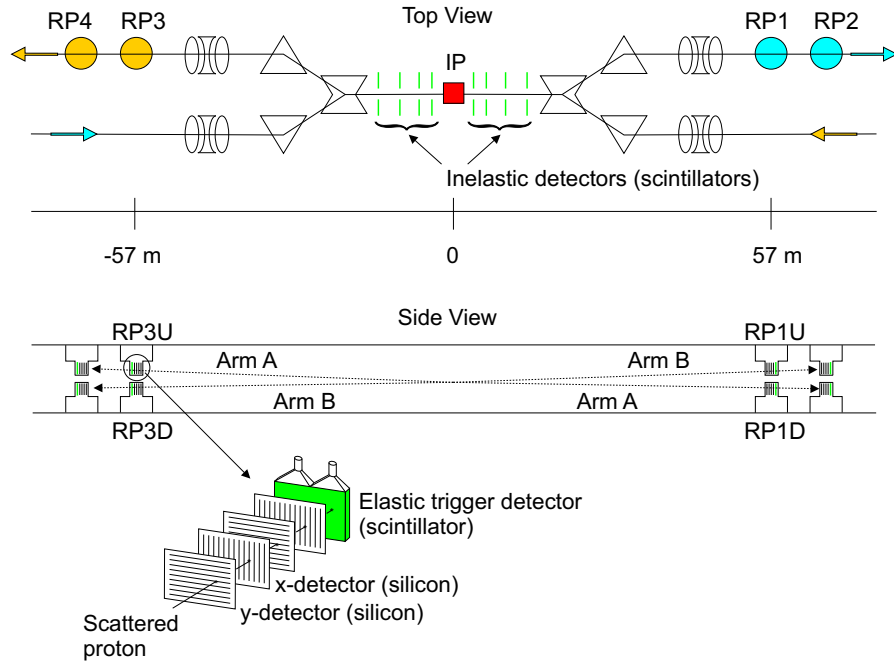


Figure 34: Layout of the pp2pp experiment. Note the detector pairs RP1, RP2 and RP3, RP4 lie in different RHIC rings. Scattering is detected in either one of two arms: Arm A is formed from RP3U and RP1D. Conversely, Arm B is formed from RP3D and RP1U.

1. Figure: transverse profile of proposed calorimeter, and location within STAR.
2. Institutions involved, cost estimate, source of materials and funding, MRI proposal submitted to NSF.
3. Timeline driven by d+Au gluon saturation studies.
4. Open issues to address?

## 5.2 Other experiments

### 5.2.1 PP2PP running with the current setup

With a small modification requiring rotation of RP2 and RP4 to horizontal orientation, the present experimental setup, see Fig. ?? is suitable for additional measurements in an extended  $|t|$ -range. At  $\sqrt{S} = 200$  GeV one can use the capacity of existing power supplies to run with the accelerator optics of  $\beta^* = 20$  m. The  $\beta^* = 20$  m tune at  $\sqrt{S} = 200$  GeV makes it possible to extend the kinematic coverage to a lower  $|t|$  of  $0.003 < |t| < 0.020$  (GeV/c)<sup>2</sup>. At  $\sqrt{S} = 500$  GeV the optics with  $\beta^* = 10$  m will be used, allowing measurements up to  $|t| \approx 0.12$  (GeV/c)<sup>2</sup>.

The result obtained in Run 2003 is shown in Fig. ?. With the modification of the setup described above one will be able to improve the  $A_N$  measurements, measure  $A_N N$ . This will certainly help resolve the issue of the presence of the hadronic spin flip amplitude at high energies.

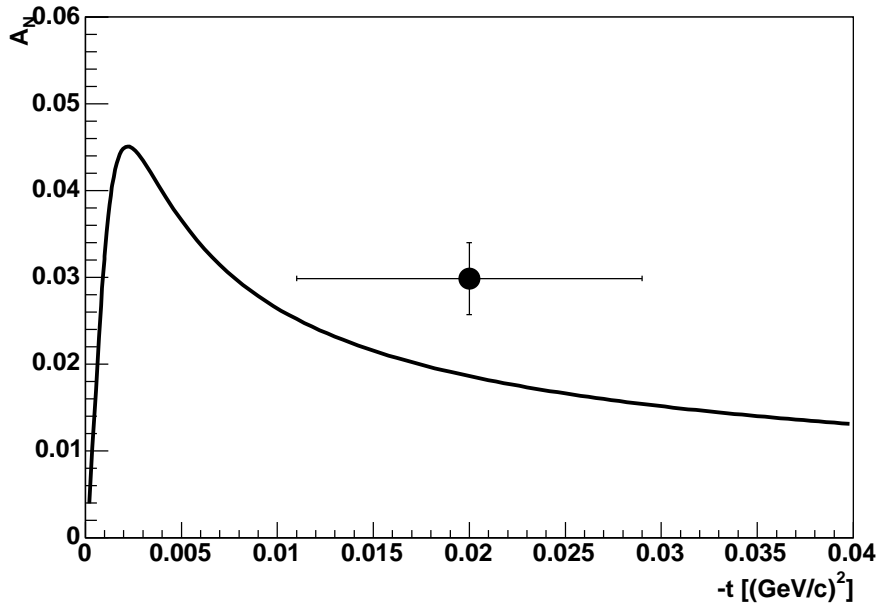


Figure 35: The single spin analyzing power  $A_N$  for the full interval. Vertical error bars show statistical errors, horizontal error bars show the  $|t|$ -range. Solid curve corresponds to theoretical calculations without hadronic spin flip[?].

### 5.2.2 Brahms

The BRAHMS detector is well suited to explore the  $x_f$  and  $p_T$  dependence of the single spin asymmetries for identified charged hadrons. The forward spectrometer is operated at  $2.3^\circ$  and  $4.0^\circ$  for these measurements. The spectrometer has a total bending power of 7.2 Tm and a momentum resolution of  $\delta p/p \approx 1 - 2\%$ . The particle identification in the current setup using a Ring Imaging Cherenkov (RICH) detector allows for  $\pi^\pm$  identification for momenta up to 35 GeV/c. Operating the RICH at a lower pressure of the radiative gas of  $C_4F_{10}$  will allow for  $\pi$  identification up to  $\approx 50 \text{ GeV}/c$ . Identification of kaons is possible up to a somewhat lower momentum than  $\pi$ s due to the lower yields. During Run-4 a small sample of  $\pi^+$  and  $\pi^-$  data were taken. Preliminary data are shown in section XX. The coverage in  $p_T$  vs  $x_f$  is shown in Fig. yy. Future measurements in Run-5 and possible Run-6 will extend this coverage towards larger  $x_f$  and  $p_T$ . The required delivered luminosity for such measurements are  $2 - 4 \text{ pb}^{-1}$ .

- jet (Sandro)
- New detector

## 6 Spin plan schedule (Gerry)

In the charge, we were requested to consider two running schedules: 10 and 5 physics weeks on spin per year. These follow, showing *example* plans. We emphasize that we expect that the actual run plan will be developed from the experiment beam use proposals. Our consideration of these scenarios should not suggest that we advocate a change to this successful approach.

A key issue is the completion of experiment hardware to run the W physics program. The required hardware are the muon trigger improvements for PHENIX, and a forward tracker for STAR. The PHENIX improvements are being proposed to NSF (\$1.8M for resistive plate chambers) and to the Japan Society for Physical Sciences (\$1.0M for muon tracking readout electronics), with a planned completion for the 2008 RHIC run. The STAR tracker is planned to be proposed to DOE (estimated \$5M) in 2006, and to be complete for the 2010 run.

The example plan below for the 10 physics week/year case is "technically driven". The plan assumes that the funding is received, and the work is completed as planned. For the 5 week plan, the delay in reaching luminosity goals for  $\sqrt{s}=200$  GeV delays the start of the W running considerably, by greater than three years. An early completion of the W hardware is less of an issue for this case.

A second key issue is machine performance. We assume that we reach the polarization goal of 70% in 2006. For luminosity, we assume in the example plan that we reach two thirds of the "maximum" luminosity (see section 3). This assumption is discussed there.

A third key issue is experiment availability, in which we include up time, live time, and the fraction of the collision vertex accepted by the experiment. This results in "recorded luminosity" for each experiment. We have taken the up time to be 70% for each experiment, as has been achieved. The live time for PHENIX is 90%, due to multi-event buffering; the live time for STAR is 50%. The online data selection adjusts thresholds, for example the lower  $p_T$  requirement, to reach these live time levels. The PHENIX vertex acceptance for the 200 GeV running is 60%, requiring the vertex to be within 20 cm of the IP. We have used this acceptance also for 500 GeV. The STAR vertex acceptance contains all collisions. The overall factor for recorded/delivered luminosity for both experiments is 35%. The physics sensitivities shown in section 2 also include apparatus acceptance and event selection acceptance.

### 6.1 10 physics weeks

Table 6 shows the example spin plan for 10 physics weeks per year, with a *technically driven* schedule. The 200 GeV running continues through 2008, with a total of  $300 \text{ pb}^{-1}$  delivered, and  $100 \text{ pb}^{-1}$  recorded luminosity by both PHENIX and STAR. By the year 2009, the PHENIX muon triggering improvements are complete, and the STAR forward tracking is partially in place, and complete for the 2010 run. The year 2009 is considered an engineering run, for both the accelerator and the experiments. By the completion of the year 2012, for 500 GeV,  $800 \text{ pb}^{-1}$  luminosity is delivered, and  $300 \text{ pb}^{-1}$  recorded by each experiment. These luminosities and polarizations provide the physics sensitivities presented in section 2.

Table 5: RHIC spin example schedule, 10 physics weeks per year, technically driven.

Fiscal year	Spin Weeks	CME(GeV)	P	L(pb <sup>-1</sup> )	Remarks
2002	8	200	0.15		First pol. pp collisions! Transverse spin
2003	10	200	0.27		Spin rotators commissioned, first helicity measurements
2004	1	200	0.4		New betatron tune developed, first jet absolute meas. P
2005	9	200	0.5	10-20	$A_{LL}(\pi^0, jet)$ , also 500 GeV studies
2006	10	200	0.7		AGS Cold Snake commissioned, NEG vacuum coating complete
2007	0				
2008	20	200	0.7		Direct $\gamma$ , completes goal for 200 GeV running
2009	10	500	0.7		PHENIX muon arm trigger installed, eng. run
2010	10	500	0.7		STAR forward tracker installed, W physics
2011	10	500	0.7		
2012	10	500	0.7		Completes 500 GeV goal

## 6.2 5 physics weeks

Table ?? gives the example spin plan for 5 physics weeks per year, which we have interpreted to mean 10 physics weeks each two years to reduce the end effects. As has been presented in section 3, the delay in the RHIC spin physics results is actually greater than a factor of two, compared to 10 physics weeks each year. This is due to an assumed "turn-on" period of reaching the instantaneous luminosity maximum that is based on our experience, from the heavy ion program. In any case, the programs are stretched out to over 6 years for the gluon polarization measurements at 200 GeV, and an additional 6 years or more for the W physics program. The proposed measurements would be completed in 2018 or later.

Table 5.2 RHIC spin example schedule, 5 physics weeks per year.

## 7 Summary (Gerry)

In this document we have described the RHIC spin research plan, responding to the request by the Department of Energy Office of Nuclear Physics. We were requested to cover 1) the science, 2) the requirements for the accelerator, 3) the resources that are needed and timelines, and 4) the impact of a constant effort budget to the program.

Table 6: RHIC spin example schedule, 10 physics weeks per year.

Fiscal year	Spin Weeks	CME(GeV)	P	L(pb <sup>-1</sup> )	Remarks
2005	9	200	0.5	10-20	$A_{LL}(\pi^0, jet)$ , also 500 GeV studies
2006-2007	10	200	0.7		AGS Cold Snake commissioned, NEG vacuum coating complete
2008-2009	10	200	0.7		Direct $\gamma$
2010-11	10	200	0.7		completes goal for 200 GeV running
20012-13	10	500	0.7		PHENIX muon arm trigger installed, eng. run
2014-2015	10	500	0.7		STAR forward tracker installed, W physics
2016-2017	10	500	0.7		
2018-2019	10	500	0.7		Completes 500 GeV goal

1) The science is presented in section 2. Here we have emphasized measuring gluon polarization and anti-quark polarization in the proton. RHIC will provide the first sensitive measurements of each. We believe this is an exciting program, which addresses the structure of matter.

2) The accelerator requirements are presented in section 3. We are well along in reaching the polarization requirement of 70%, and anticipate reaching this goal in 2006, for 200 GeV running. To reach this goal for 500 GeV running will require releveling the machine, which is planned. Reaching the luminosity goal will be challenging. We must store  $2 \times 10^{11}$  polarized protons in 110 rf bunches in each RHIC ring and collide them. Limits of betatron tune shift and of electron cloud formation will be tested. For the physics sensitivities presented, we have used a luminosity of 2/3 of the calculated maximum.

3) The required experiment resources are presented in section 4. The PHENIX and STAR detectors are complete for the gluon polarization program. Both need improvements to be ready for the W physics program. These are described in the section. For a "technically driven" program, where the improvements are funded and completed as proposed, the PHENIX detector will be ready for W physics in 2009, and the STAR detector in 2010.

There are also important planned upgrades for the heavy ion and spin programs that greatly extend the range of spin physics, and these are also described in section 4.

4) The impact of a constant effort budget is presented in section 5, where we compare the two plans, as requested in the charge to the RHIC Spinplan Group:

*"I ask that you consider two RHIC Spin running scenarios: 1) 5 spin physics data taking weeks per year (averaged over two years using the combined fiscal year concept); 2) 10 spin physics data taking weeks per year. These two scenarios will give appropriate indications of the physic goals that can be met over a period of years without involving the Group in difficult funding and cost scenarios that are not central to the calculation of physics accomplishments*

over time.” (Appendix A)

The plan with 10 spin physics weeks per year, the technically driven plan, completes the gluon polarization measurements and the W physics measurements by 2012.

The plan with 5 spin physics weeks per year completes this program in 2019 or later. With this plan RHIC runs 25% of the year on average (we assume 10 spin physics weeks per two year cycle).

## Acknowledgments

## References

- [1] I. Estermann, R. Frisch, O. Stern, *Nature* **132** (1933) 169;  
see also: O. Stern, “The Method of Molecular Rays”, Nobel lecture 1946,  
<http://nobelprize.org/physics/laureates/1943/stern-lecture.pdf>.
- [2] M. Gell-Mann, *Phys. Lett.* **8** (1964) 214; G. Zweig, CERN-TH-412.
- [3] O. W. Greenberg, *Phys. Rev. Lett.* **13** (1964) 598; M. Y. Han and Y. Nambu, *Phys. Rev.* **139** (1965) B1006.
- [4] E. D. Bloom *et al.*, *Phys. Rev. Lett.* **23**, 930 (1969); *ibid.* 935. For review see, for example: J. I. Friedman, H. W. Kendall, *Ann. Rev. Nucl. Part. Sci.* **22** (1972) 203; see also: H.W. Kendall, “Deep Inelastic Scattering: Experiments on the Proton and the Observation of Scaling”, Nobel lecture 1990, <http://nobelprize.org/physics/laureates/1990/kendall-lecture.pdf>.
- [5] J. D. Bjorken, *Phys. Rev.* **179**, 1547 (1969); R. P. Feynman, *Phys. Rev. Lett.* **23** (1969) 1415; J. D. Bjorken and E. A. Paschos, *Phys. Rev.* **185**, 1975 (1969).
- [6] C. G. . Callan and D. J. Gross, *Phys. Rev. Lett.* **22** (1969) 156.
- [7] J. G. H. de Groot *et al.*, *Phys. Lett. B* **82**, 292 (1979); *ibid.* 456; *Z. Phys. C* **1**, 143 (1979).
- [8] R. Brandelik *et al.* [TASSO Collaboration], *Phys. Lett. B* **86**, 243 (1979); C. Berger *et al.* [PLUTO Collaboration], *Phys. Lett. B* **86**, 418 (1979); W. Bartel *et al.* [JADE Collaboration], *Phys. Lett. B* **91**, 142 (1980).
- [9] R. Brandelik *et al.* [TASSO Collaboration], *Phys. Lett. B* **97**, 453 (1980); J. R. Ellis and I. Karliner, *Nucl. Phys. B* **148**, 141 (1979).
- [10] C. G. . Callan and D. J. Gross, *Phys. Rev. D* **8** (1973) 4383.
- [11] H. Fritzsch, M. Gell-Mann and H. Leutwyler, *Phys. Lett. B* **47** (1973) 365; D. J. Gross and F. Wilczek, *Phys. Rev. D* **8**, 3633 (1973); S. Weinberg, *Phys. Rev. Lett.* **31**, 494 (1973).

- [12] D. J. Gross, F. Wilczek, Phys. Rev. Lett. **30**, 1343 (1973); H. D. Politzer, *ibid.* 1346.
- [13] H. Georgi and H. D. Politzer, Phys. Rev. D **9** (1974) 416; Phys. Rev. D **14**, 1829 (1976).
- [14] S. D. Drell and T. M. Yan, Phys. Rev. Lett. **25**, 316 (1970) [Erratum-*ibid.* **25**, 902 (1970)].
- [15] S. M. Berman and M. Jacob, Phys. Rev. Lett. **25**, 1683 (1970); S. M. Berman, J. D. Bjorken and J. B. Kogut, Phys. Rev. D **4**, 3388 (1971); R. L. Jaffe, Phys. Rev. D **5**, 2622 (1972); R. P. Feynman, R. D. Field and G. C. Fox, Phys. Rev. D **18**, 3320 (1978).
- [16] S.B. Libby and G. Sterman, Phys. Rev. **D18**, 3252 (1978); R.K. Ellis, H. Georgi, M. Machacek, H.D. Politzer, and G.G. Ross, Phys. Lett. **78B**, 281 (1978); Nucl. Phys. **B152**, 285 (1979); D. Amati, R. Petronzio, and G. Veneziano, Nucl. Phys. **B140**, 54 (1980); Nucl. Phys. **B146**, 29 (1978); G. Curci, W. Furmanski, and R. Petronzio, Nucl. Phys. **B175**, 27 (1980); J.C. Collins, D.E. Soper, and G. Sterman, Phys. Lett. **B134**, 263 (1984); Nucl. Phys. **B261**, 104 (1985); J.C. Collins, Nucl. Phys. **B394**, 169 (1993).
- [17] G. Arnison *et al.* [UA1 Collaboration], Phys. Lett. B **122**, 103 (1983); G. Arnison *et al.* [UA1 Collaboration], Phys. Lett. B **126**, 398 (1983); M. Banner *et al.* [UA2 Collaboration], Phys. Lett. B **122**, 476 (1983); P. Bagnaia *et al.* [UA2 Collaboration], Phys. Lett. B **129**, 130 (1983).
- [18] C. Y. Prescott *et al.*, SLAC-PROPOSAL-E-095.
- [19] M. J. Alguard *et al.*, Phys. Rev. Lett. **37**, 1261 (1976).
- [20] J. Ashman *et al.* [European Muon Collaboration], Phys. Lett. B **206**, 364 (1988); Nucl. Phys. B **328**, 1 (1989); for review, see: E. W. Hughes and R. Voss, Ann. Rev. Nucl. Part. Sci. **49**, 303 (1999).
- [21] see: D.L. Adams *et al.* [FNAL E704 Collaboration], Phys. Lett. B **261**, 201 (1991); K. Krueger *et al.*, Phys. Lett. B **459**, 412 (1999), and references therein.
- [22] For review, see: G. Bunce, N. Saito, J. Soffer and W. Vogelsang, Ann. Rev. Nucl. Part. Sci. **50**, 525 (2000) [arXiv:hep-ph/0007218].
- [23] U. Stösslein, Acta Phys. Polon. **B33**, 2813 (2002).
- [24] S. Kretzer, Phys. Rev. **D62** 054001 (2000); B. Kniehl, G. Kramer and B. Pötter, Nucl. Phys. **B582** 514 (2000); Nucl. Phys. **B597** 337 (2001); L. Bourhis, M. Fontannaz, J.P. Guillet, M. Werlen, Eur. Phys. J. **C19** 89 (2001); S. Kretzer, E. Leader, E. Christova, Eur. Phys. J. **C22**, 269 (2001).
- [25] C. Bourrely and J. Soffer, hep-ph/0311110.
- [26] PHENIX Collaboration (S.S. Adler *et al.*), Phys. Rev. Lett. **91**, 241803 (2003); STAR Collaboration (J. Adams *et al.*), Phys. Rev. Lett. **92**, 171801 (2004).
- [27] B. Jäger, A. Schäfer, M. Stratmann and W. Vogelsang, Phys. Rev. **D67**, 054005 (2003).
- [28] OPAL Collaboration (G. Abbiendi *et al.*), Eur. Phys. J. **C37**, 25 (2004).



- [29] B. E. Bonner *et al.*, Phys. Rev. Lett. **61**, 1918 (1988); A. Bravar *et al.*, *ibid.* **77**, 2626 (1996); D.L. Adams *et al.*, Phys. Lett. B **261**, 201 (1991); **264**, 462 (1991); Z. Phys. C **56**, 181 (1992).
- [30] G. L. Kane, J. Pumplin, and W. Repko, Phys. Rev. Lett. **41** 1689 (1978).
- [31] K. Krueger *et al.*, Phys. Lett. B **459**, 412 (1999); C. E. Allgower *et al.*, Phys. Rev. D **65**, 092008 (2002).
- [32] A. Airapetian *et al.*, Phys. Rev. Lett. **84**, 4047 (2000); Phys. Lett. B **535**, 85 (2002); **562**, 182 (2003).
- [33] A. Bravar *et al.*, Nucl. Phys. Proc. Suppl. **79**, 520 (1999).
- [34] J. Adams *et al.*, Phys. Rev. Lett. **92** (2004) 171801; A. Ogawa, 16th International spin physics symposium (SPIN2004) proceedings hep-ex/0412035.
- [35] D. W. Sivers, Phys. Rev. **D41** 83 (1990)
- [36] J. C. Collins, Nucl. Phys. **B396** 161 (1993); J. C. Collins, S. F. Heppelmann, G. A. Ladinsky, Nucl. Phys. **B396** 161 (1993);
- [37] D. Boer, AIP Conf. Proc. **675** 479-483 (2003).
- [38] J. Qiu and G. Sterman, Phys. Rev. D **59**, 014004 (1999).
- [39] Y. Koike, AIP Conf. Proc. **675**, 449 (2003).
- [40] M. Anselmino, M. Boglione, and F. Murgia, Phys. Rev. D **60**, 054027 (1999); M. Boglione and E. Leader, Phys. Rev. D **61**, 114001 (2000).
- [41] M. Anselmino, M. Boglione, and F. Murgia, Phys. Lett. B **362**, 164 (1995); M. Anselmino and F. Murgia, *ibid.* **442**, 470 (1998); U. D'Alesio and F. Murgia, AIP Conf. Proc. **675** 469 (2003).
- [42] M. Anselmino *et. al.* **hep-ph/0408356**; U. D'Alesio, Proceedings of Spin2004
- [43] M. Boglione, E. Leader, Phys. Rev. **D61** 114001 (2000).
- [44] J. Soffer, Phys. Rev. Lett. **74** 1292 (1995).
- [45] D. Boer, W. Vogelsang, Phys. Rev. **D69** 094025 (2004).
- [46] B. Jaffe *et al.*, Phys. Rev. **bf D57** 5920 (1998); J. Tang, hep-ph/9807560 and J. Tang, Thesis, MIT (1999).
- [47] X. Artru, J. Collins, Z. Phys. **C69** 277 (1996); D. Boer, R. Jakob, P. J. Mulders, Phys. Lett. **B424** 143 (1998).
- [48] M. Grosse Perdekamp, A. Ogawa, K. Hasuko, S. Lange, V. Siegle, Nucl. Phys. **A711** 69 (2002).
- [49] A. Mukherjee, M. Stratmann and W. Vogelsang, Phys. Rev. **D67** 114006 (2003).

- [50] M. Anselmino, U. D'Alesio, F. Murgia, Phys. Rev. **D67** 074010 (2003).
- [51] M. Anselmino, V. Barone, A. Drago, N. N. Nikolaev, Phys. Lett. **B594** 97 (2004).
- [52] M. Anselmino, M. Boglione, U. D'Alesio, E. Leader, F. Murgia, Phys. Rev. **D70** 074025 (2004)  
M. Anselmino, V. Barone, A. Drago, N. N. Nikolaev, Phys. Lett. **B594** 97 (2004).
- [53] G.L. Kane, J. Pumplin, and W. Repko, Phys. Rev. Lett. **41**, 1689 (1978).
- [54] B. E. Bonner *et al.*, Phys. Rev. Lett. **61**, 1918 (1988); A. Bravar *et al.*, *ibid.* **77**, 2626 (1996); D.L. Adams *et al.*, Phys. Lett. B **261**, 201 (1991); **264**, 462 (1991); Z. Phys. C **56**, 181 (1992).
- [55] K. Krueger *et al.*, Phys. Lett. B **459**, 412 (1999); C.E. Allgower *et al.*, Phys. Rev. D **65**, 092008 (2002).
- [56] A. Airapetian *et al.*, Phys. Rev. Lett. **84**, 4047 (2000); Phys. Lett. B **535**, 85 (2002); **562**, 182 (2003).
- [57] A. Bravar *et al.*, Nucl. Phys. Proc. Suppl. **79**, 520 (1999).
- [58] J. Adamset *et al.*, Phys. Rev. Lett. **92** (2004) 171801; A. Ogawa, 16th International spin physics symposium (SPIN2004) proceedings hep-ex/0412035.
- [59] D. W. Sivers, Phys. Rev. **D41** 83 (1990)
- [60] J. C. Collins, Nucl. Phys. **B396** 161 (1993); J. C. Collins, S. F. Heppelmann, G. A. Ladinsky, Nucl. Phys. **B396** 161 (1993);
- [61] D. Boer, AIP Conf. Proc. **675** 479-483 (2003).
- [62] J. Qiu and G. Sterman, Phys. Rev. D59, 014004 (1999).
- [63] Y. Koike, AIP Conf. Proc. **675**, 449 (2003).
- [64] M. Anselmino, M. Boglione, and F. Murgia, Phys. Rev. D **60**, 054027 (1999); M. Boglione and E. Leader, Phys. Rev. D **61**, 114001 (2000).
- [65] M. Anselmino, M. Boglione, and F. Murgia, Phys. Lett. B **362**, 164 (1995); M. Anselmino and F. Murgia, *ibid.* **442**, 470 (1998); U. D'Alesio and F. Murgia, AIP Conf. Proc. **675** 469 (2003).
- [66] M. Anselmino *et. al.* **hep-ph/0408356**; U. D'Alesio, Proceedings of Spin2004
- [67] M. Boglione, E. Leader, Phys. Rev. **D61** 114001 (2000).
- [68] J. Soffer, Phys. Rev. Lett. **74** 1292 (1995).
- [69] D. Boer, W. Vogelsang, Phys. Rev. **D69** 094025 (2004).
- [70] B. Jaffe *et al.*, Phys. Rev. bf D57 5920 (1998); J. Tang, hep-ph/9807560 and J. Tang, Thesis, MIT (1999).

- [71] X. Artru, J. Collins, Z. Phys. **C69** 277 (1996); D. Boer, R. Jakob, P. J. Mulders, Phys. Lett. **B424** 143 (1998).
- [72] M. Grosse Perdekamp, A. Ogawa, K. Hasuko, S. Lange, V. Siegle, Nucl. Phys. **A711** 69 (2002).
- [73] A. Mukherjee, M. Stratmann and W. Vogelsang, Phys. Rev. **D67** 114006 (2003).
- [74] M. Anselmino, U. D'Alesio, F. Murgia, Phys. Rev. **D67** 074010 (2003).
- [75] M. Anselmino, V. Barone, A. Drago, N. N. Nikolaev, Phys. Lett. **B594** 97 (2004).
- [76] M. Anselmino, M. Boglione, U. D'Alesio, E. Leader, F. Murgia, Phys. Rev. **D70** 074025 (2004)  
M. Anselmino, V. Barone, A. Drago, N. N. Nikolaev, Phys. Lett. **B594** 97 (2004).
- [77] J. P. Ralston and D. E. Soper, Nucl. Phys. B **152**, 109 (1979).
- [78] R. L. Jaffe and X. D. Ji, Phys. Rev. Lett. **67**, 552 (1991).
- [79] K. Chen, G. R. Goldstein, R. L. Jaffe and X. D. Ji, Nucl. Phys. B **445**, 380 (1995) [arXiv:hep-ph/9410337].
- [80] V. Barone, Phys. Lett. B **409**, 499 (1997) [arXiv:hep-ph/9703343].
- [81] W. Vogelsang, Phys. Rev. D **57**, 1886 (1998) [arXiv:hep-ph/9706511].
- [82] A. Hayashigaki, Y. Kanazawa and Y. Koike, Phys. Rev. D **56**, 7350 (1997) [arXiv:hep-ph/9707208].
- [83] B. L. G. Bakker, E. Leader and T. L. Trueman, Phys. Rev. D **70**, 114001 (2004) [arXiv:hep-ph/0406139].
- [84] J. Soffer, Phys. Rev. Lett. **74** 1292 (1995).
- [85] J. C. Collins, Nucl. Phys. **B396** 161 (1993); J. C. Collins, S. F. Heppelmann, G. A. Ladinsky, Nucl. Phys. **B396** 161 (1993);
- [86] B. E. Bonner *et al.*, Phys. Rev. Lett. **61**, 1918 (1988); A. Bravar *et al.*, *ibid.* **77**, 2626 (1996); D.L. Adams *et al.*, Phys. Lett. B **261**, 201 (1991); **264**, 462 (1991); Z. Phys. C **56**, 181 (1992).
- [87] K. Krueger *et al.*, Phys. Lett. B **459**, 412 (1999); C. E. Allgower *et al.*, Phys. Rev. D **65**, 092008 (2002).
- [88] A. Airapetian *et al.*, Phys. Rev. Lett. **84**, 4047 (2000); Phys. Lett. B **535**, 85 (2002); **562**, 182 (2003).
- [89] A. Bravar *et al.*, Nucl. Phys. Proc. Suppl. **79**, 520 (1999).
- [90] J. Adamset *et al.*, Phys. Rev. Lett. **92** (2004) 171801; A. Ogawa, 16th International spin physics symposium (SPIN2004) proceedings hep-ex/0412035.

- [91] G. L. Kane, J. Pumplin, and W. Repko, Phys. Rev. Lett. **41**, 1689 (1978).
- [92] A. V. Efremov and O. V. Teryaev, Phys. Lett. B **150**, 383 (1985); Sov. J. Nucl. Phys. **36**, 140 (1982) [Yad. Fiz. **36**, 242 (1982)]; Yad. Fiz. **39**, 1517 (1984).
- [93] J. W. Qiu and G. Sterman, Phys. Rev. Lett. **67**, 2264 (1991); Nucl. Phys. B **378**, 52 (1992); Phys. Rev. D **59**, 014004 (1999).
- [94] Y. Koike, AIP Conf. Proc. **675**, 449 (2003).
- [95] D. W. Sivers, Phys. Rev. **D41** 83 (1990); Phys. Rev. D **43**, 261 (1991).
- [96] M. Burkardt, Phys. Rev. D **69**, 091501 (2004).
- [97] D. Boer and W. Vogelsang, Phys. Rev. D **69**, 094025 (2004).
- [98] X. d. Ji and F. Yuan, Phys. Lett. B **543**, 66 (2002).
- [99] A. V. Belitsky, X. d. Ji and F. Yuan, Phys. Rev. D **69**, 074014 (2004).
- [100] D. Boer, AIP Conf. Proc. **675** 479-483 (2003).
- [101] J. C. Collins and A. Metz, Phys. Rev. Lett. **93**, 252001 (2004) [arXiv:hep-ph/0408249].
- [102] X. d. Ji, J. p. Ma and F. Yuan, arXiv:hep-ph/0404183. Phys. Lett. B **597**, 299 (2004) [arXiv:hep-ph/0405085].
- [103] M. Anselmino, M. Boglione and F. Murgia, Phys. Lett. B **362**, 164 (1995); M. Anselmino and F. Murgia, Phys. Lett. B **442**, 470 (1998); U. D'Alesio and F. Murgia, AIP Conf. Proc. **675**, 469 (2003).
- [104] M. Anselmino, M. Boglione and F. Murgia, Phys. Rev. D **60**, 054027 (1999); M. Boglione and E. Leader, Phys. Rev. D **61**, 114001 (2000).
- [105] M. Anselmino, M. Boglione, U. D'Alesio, E. Leader and F. Murgia, Phys. Rev. D **71**, 014002 (2005) [arXiv:hep-ph/0408356].
- [106] J. Adams *et al.* [STAR Collaboration], Phys. Rev. Lett. **92**, 171801 (2004) [arXiv:hep-ex/0310058].
- [107] D. W. Sivers, Phys. Rev. **D41** 83 (1990)
- [108] J. Qiu and G. Sterman, Phys. Rev. D **59**, 014004 (1999).
- [109] M. Anselmino, M. Boglione, and F. Murgia, Phys. Rev. D **60**, 054027 (1999); M. Boglione and E. Leader, Phys. Rev. D **61**, 114001 (2000).
- [110] M. Anselmino, M. Boglione, and F. Murgia, Phys. Lett. B **362**, 164 (1995); M. Anselmino and F. Murgia, *ibid.* **442**, 470 (1998); U. D'Alesio and F. Murgia, AIP Conf. Proc. **675** 469 (2003).
- [111] M. Anselmino *et al.* **hep-ph/0408356**; U. D'Alesio, Proceedings of Spin2004
- [112] M. Boglione, E. Leader, Phys. Rev. **D61** 114001 (2000).

- [113] D. Boer, W. Vogelsang, *Phys. Rev.* **D69** 094025 (2004).
- [114] B. Jaffe *et al.*, *Phys. Rev.* **D57** 5920 (1998); J. Tang, hep-ph/9807560 and J. Tang, Thesis, MIT (1999).
- [115] X. Artru, J. Collins, *Z. Phys.* **C69** 277 (1996); D. Boer, R. Jakob, P. J. Mulders, *Phys. Lett.* **B424** 143 (1998).
- [116] M. Grosse Perdekamp, A. Ogawa, K. Hasuko, S. Lange, V. Siegle, *Nucl. Phys.* **A711** 69 (2002).
- [117] A. Mukherjee, M. Stratmann and W. Vogelsang, *Phys. Rev.* **D67** 114006 (2003).
- [118] M. Anselmino, U. D'Alesio, F. Murgia, *Phys. Rev.* **D67** 074010 (2003).
- [119] M. Anselmino, V. Barone, A. Drago, N. N. Nikolaev, *Phys. Lett.* **B594** 97 (2004).
- [120] M. Anselmino, M. Boglione, U. D'Alesio, E. Leader, F. Murgia, *Phys. Rev.* **D70** 074025 (2004)  
M. Anselmino, V. Barone, A. Drago, N. N. Nikolaev, *Phys. Lett.* **B594** 97 (2004).
- [121] F. Paige and M. J. Tannenbaum, cited in R. Ruckl, *J. de Phys.* **46**, C2-55 (1985) and T. L. Trueman, *ibid.*, C2-721.
- [122] E. J. Eichten, K. D. Lane and M. E. Peskin, *Phys. Rev. Lett.* **50**, 811 (1983).
- [123] CDF Collaboration, F. Abe, *et al.*, *Phys. Rev. Lett.* **68**, 1104 (1992); *ibid.* **77**, 438 (1996). See also New York Times, Feb 8, 1996.
- [124] J.-M. Virey, in *Beyond the Desert 1997, Proceedings of 1st International Conference on Particle Physics Beyond the Standard Model*, 8-14 Jun 1997, Castle Ringberg, Germany, hep-ph/9707470. See also, J. Soffer, *Acta Phys. Polon.* **B29**, 1303 (1998).
- [125] P. Taxil and J. M. Virey, *Phys. Rev.* **D 55**, 4480 (1997); *Phys. Lett.* **B522**, 89 (2001).
- [126] P. Taxil, J. M. Virey, *Phys. Lett.* **B364** (1995) 181; *Phys. Rev.* **D55** (1997) 4480.
- [127] P. Taxil, J. M. Virey, *Phys. Lett.* **B383** (1996) 355; *Phys. Lett.* **B441** (1998) 376.
- [128] P. Taxil, E. Tugcu, J. M. Virey, *Eur. Phys. J.* **C24** (2002) 149.
- [129] C. Bourelly, *et al.*, *Phys. Rep.* **177** (1989) 319; P. Taxil, *Polarized Collider Workshop, AIP Conf. Proc.* **223**, ed. J. Collins, S. F. Heppelmann, R. W. Robinett, p. 169 (1991); M. J. Tannenbaum, *Polarized Collider Workshop, AIP Conf. Proc.* **223**, ed. J. Collins, S. F. Heppelmann, R. W. Robinett, p. 201 (1991).
- [130] B. Abott, *et al.* (DØ Collaboration), *Phys. Rev. Lett.* **82** (1999) 2457.
- [131] J. D. Lykken, *Snowmass 1996*, ed. D. G. Cassel, L. Trindle Gennari, R. H. Siemann, p. 891; J. L. Lopez, D. V. Nanopoulos, *Phys. Rev.* **D55** (1997) 397; K. S. Babu, C. Kolda, J. March-Russell, *Phys. Rev.* **D54** (1996) 4635; A. E. Fraggi, M. Masip, *Phys. Lett.* **B388** (1996) 524.

- [132] K. Agashe, M. Graesser, I. Hinchliffe, M. Suzuki, *Phys. Lett.* **B385** (1996) 218; H. Georgi, S. L. Glashow, *Phys. Lett.* **B387** (1996) 341.
- [133] M. Cvetič, et al., *Phys. Rev.* **D56** (1997) 2861.
- [134] E. Courant, *Proc. of the RIKEN-BNL Research Center Workshop*, April 1998, BNL Report 65615, p. 275.
- [135] T. Gehrmann, D. Maître, D. Wyler, *Nucl. Phys.* **B703** (2004) 147.
- [136] B. Abott, et al. (DØ Collaboration), *Phys. Rev. Lett.* **83** (1999) 4937; T. Affolder, et al. (CDF Collaboration), *Phys. Rev. Lett.* **88** (2002) 041801.
- [137] P. Steinberg et al., “Expression of Interest for a Comprehensive New Detector at RHIC II”, Presentation to the BNL PAC, BNL, September 8, 2004 (available at [http://www.bnl.gov/HENP/docs/pac0904/bellwied\\_eoi\\_r1.pdf](http://www.bnl.gov/HENP/docs/pac0904/bellwied_eoi_r1.pdf), unpublished).
- [138] G. Bozzi, B. Fuks, M. Klasen, *Preprint LPSC 04-091; hep-ph/0411318*.
- [139] C. Bourelly, J. Soffer, *Phys. Lett.* **B314** (1993) 132; *Nucl. Phys.* **B423** (1994) 329; P. Chiappetta, J. Soffer, *Phys. Lett.* **B152** (1985) 126.
- [140] D. Boer, *Phys. Rev.* **D62** (2000) 094029.
- [141] S. Kovalenko, I. Schmidt, J. Soffer, *Phys. Lett.* **B503** (2001) 313.
- [142] G. L. Kane, G. A. Ladinsky, C.-P. Yuan, *Phys. Rev.* **D45** (1992) 124.
- [143] A. Ogawa, V. L. Rykov, N. Saito, *Proc. of the 14th Int. Symp. on Spin Physics, AIP Conf. Proc* **570**, ed. T. Nakamura, p. 379 (2000); V. L. Rykov, *hep-ex/9908050*.
- [144] R. Escrivano, E. Masso, *Nucl. Phys.* **B429** (1994) 19.
- [145] J. Soffer, *Nucl. Phys. (Proc. Suppl.)* **64** (1998) 143.
- [146] T. Roser, W. Fischer, M. Bai, F. Pilat, “RHIC Collider Projections (FY2005-FY2008)”, <http://www.rhichome.bnl.gov/RHIC/Runs/RhicProjections/pdf> (Last update on 16 August 2004).
- [147] T. Roser et al., “Acceleration of Polarized Beam Using Multiple Strong Partial Siberian Snakes.”, *Proceeding of European Particle Accelerator Conference, Lucerne, Switzerland, 2004*.
- [148] J. Tojo et al., *Phys. Rev. Lett.* **89**, 052302 (2002).
- [149] O. Jinnouchi et al., *RHIC/CAD Acc. Phys. Note 171* (2004),
- [150] T. Wise et al., and H. Okada et al., *Spin2004 Proceedings, Trieste, Italy, to be published; and talks in* <http://www.ts.infn.it/events/SPIN2004/>.
- [151] N. Akchurin et al., *Phys. Rev.* **D48**, 3026 (1993).
- [152] J. C. Collins, *Nucl. Phys.* **B396**, 161 (1993).

- [153] *D. W. Sivers, Phys. Rev. D* **41**, 83 (1990).
- [154] *D. W. Sivers, Phys. Rev. D* **43**, 261 (1991).
- [155] *S. S. Adler et al. [PHENIX Collaboration], nucl-ex/0409028.*
- [156] *A. Bazilevsky et al., AIP Conf. Proc.* 675: 584-588, 2003.
- [157] *C. Adler et al., Nucl. Instrum. Methods* **A470**, 488 (2001).
- [158] *M. Allen et al., Nucl. Instrum. Methods* **A499**, 549 (2003).
- [159] *he PHENIX Silicon Vertex Tracker Proposal*
- [160] *M. Togawa [PHENIX Collaboration], hep-ex/0501047.*
- [161] *From Run2pp to be submitted to PRD Rapid Communication*
- [162] *From Run3pp hep-ex/0501066*